CHAPTER 5

Development of PNIPAAm Grafted 3D NWF Scaffolds

-Published in 1) Journal of Thermal Analysis and Calorimetry; 2) Biotechnology and Bioengineering; and 3) Colloids and Surfaces A: Interfaces and Engineering aspects

5.1 Introduction

Although the conventional cell culture method based on the use of tissue-culture polystyrene (TCPS) trays is convenient for use in routine work, it is well-known that this method is highly tedious, prone to contamination, and sometimes inaccurate. Due to the constraints and limitations of conventional 2D cell culture (refer to **Section 1.2** for a detailed discussion), researchers, developers, and manufacturers alike, are now turning to 3D cultures for a more physiological representation of mammalian cells. When grown on 3D surfaces, cells maintain more of their native characteristics like phenotype, differentiated state, and other biological functions (Justice et al., 2009). Another major concern with the conventional cell culture method is that enzymes are routinely used to release confluent cells, which damages critical cell surface proteins, growth factor receptors, and cell-to-cell gap junction proteins (Yamato et al., 2007). There thus is a need for a 3D scaffold capable of non-destructive cell release.

The requirements for the ideal cell culture scaffold are as follows:

- It should display a porous structure with open pores to enable cell-cell interactions, oxygenation, nutrient supply to cells, and removal of waste products
- It should display a 3D structure to support cell growth in 3D as opposed to 2D monolayer cultures
- It should enable cells to be released spontaneously from its surface without requiring enzymes or other destructive cell release methods
- It should be low-cost
- It should be cytocompatible to cells without inducing any toxic effects
- It should enable high-density cell culture with ease

Poly(*N*-isopropylacrylamide) (PNIPAAm), a temperature responsive polymer, has revolutionised the cell culture fraternity by providing a non-invasive means of harvesting adherent cells, whereby confluent cells can be spontaneously released by simply cooling the cell culture medium and without requiring enzymes. PNIPAAm is a thermoresponsive polymer that switches its properties reversibly between hydrophobic (cell adhesive) and hydrophilic (non-cell adhesive) states at temperatures higher and lower than its lower critical solution temperature (LCST) (~32 °C) respectively (Schild, 1992). PNIPAAm provides a unique means of harvesting adherent cells, whereby confluent cells can be spontaneously released by simply cooling the cell culture medium (Okano et al., 1995). However majority of the studies which have been conducted to date has focussed on the use of 2D PNIPAAm surfaces, which lack 3D structural support to cells.

The Council for Scientific and Industrial Research (CSIR) is developing a thermoresponsive 3D (T3D) cell culture device consisting of a smart thermoresponsive 3D scaffold housed in a perfused bioreactor, whereby the manual cell culturing steps are automated, and cells are released non-invasively by changing the temperature of the cell culture media, and without requiring enzymes.

This chapter deals with development of the 3D PNIPAAm grafted scaffolds for use in the T3D bioreactor.

5.1.1 Choice of 3D scaffold

When cells are cultured *in vitro*, the scaffold plays a critical role in directing cellular behaviour and performance. The choice of scaffold and scaffold architecture is very important since it is known that a change in environment for cells translate into a change in function and capacity for growth and differentiation. The scaffold should therefore as far as possible resemble the *in vivo* 3D environment of native tissue. Some of the important characteristics of the scaffold include porosity, pore size, pore interconnectivity, surface chemistry, and mechanical properties amongst others (Chang et al., 2011). The porous structure would enable cell-cell interactions and allow diffusion of nutrients and oxygen to the cells. Additionally the 3D structure of the scaffolds would support cell growth in 3D which is known to be superior to 2D cell culture (see detailed discussion in Section 2.).

In this study, a number of different 3D scaffold architectures were considered including hydrogels, foams, porous films, beads, and fibres. PNIPAAm hydrogels based on PNIPAAm were studied in detail (see Chapter 4); however the hydrogels were found to be unsuitable for use in a robust system such as a bioreactor due to their slow response time, poor stability, unsuitable porous structure, dense surface layer at 37°C, and high cost. An initial study was conducted using polyurethane foams as the base scaffold onto which PNIPAAm was attached (unreported). However difficulties were experienced with respect to manufacture of open celled foams and the foams were relatively dense with low free volume. Foams typically display lower open volume compared to non-woven fibers, also reduced interconnectivity of pores. Microbeads are currently quite common for cell culture, however these were excluded in this study, since the surface of microbeads is typically 2D and does not provide cells with the 3D architecture of the ECM; additional they are difficult to handle especially during washing steps. However a fibre-based scaffold whereby the fibres are

bonded into a non-woven fabric (NWF) matrix was found to be the ideal scaffold for cell culture.

A NWF is a scaffold comprised of a sheet or web structure whereby fibers or filaments are bonded together by entangling which can be achieved by various methods such as mechanical, thermal or chemical treatment (Singha et al., 2012) (**Figure 5.1a**). To enable spontaneous cell release from the 3D NWF, (**Figure 5.1b)** the fiber surface was grafted with a layer of PNIPAAm.

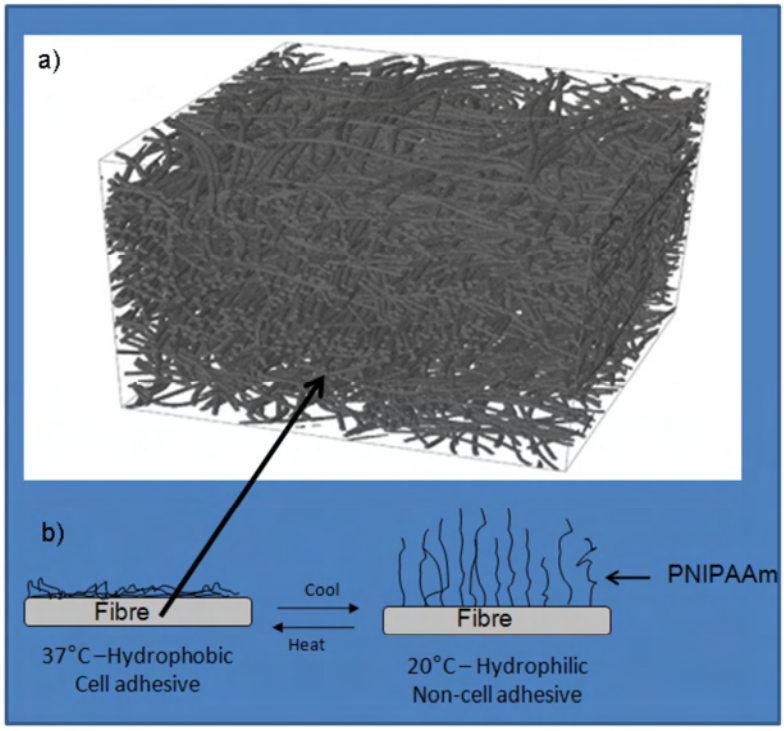

Figure 5.1: (a) 3D image showing morphology of a typical non-woven fabric (Jaganathan et al., 2009) and (b) schematic showing the thermoresponsive behaviour of a single fibre contained in the NWF when the surface is grafted with PNIPAAm.

NWF scaffolds display a number of advantages over other scaffold types, which includes:

- Porous 3D structure
- High porosity content
- High volume of open interconnected pores
- High surface area per volume ratio
- Ease of manipulation of scaffold structure and mechanical properties
- Non-woven manufacture is an industrial method
- Scaffolds can be cut into any size or shape and readily used as a cell culture insert

The NWF scaffolds were manufactured using polypropylene (PP), poly(ethylene)terephthalate) (PET) and nylon 6.6 (nylon) since they can be easily processed into fibres, they are cytocompatible to cells, and have been used for various biomedical applications (Mark, 1999). PP and PET which belong to the polyolefin and polyester polymer classes respectively, are known for low cost, good chemical resistance and mechanical properties (Mark, 1999). Nylon is a polyamide which contains polar groups; it is hydrophilic and displays a similar chemical structure to PNIPAAm which would be desirable for grafting in an aqueous medium.

5.1.2 Graft polymerisation method-OAGP

Techniques reported in literature to graft PNIPAAm onto polymer surfaces include electron-beam radiation, gamma radiation, plasma radiation; UV-irradiation; ozonation; corona-discharge; chemical treatment, and controlled radical polymerisation techniques (Bucio et al., 2005; Contreras-Garcıa et al., 2008; Wan et al., 2009). A major concern with the high energy radiation techniques is unwanted side reactions. Some of these include cross-linking, chain scission, post-irradiation degradation, discolouration, and limited long-term stability of the radiated products (Clough, 2001).

In this study, oxyfluorination-assisted graft polymerisation (OAGP) technique was used to synthesise the PNIPAAm grafted NWF scaffolds. This method is based on surface functionalisation of the NWF using oxyfluorination (or direct fluorination), followed by free-radical graft polymerisation in solution. Oxyfluorination is a polymer surface modification technique which involves treatment of a polymer surface with a F_2:O_2 gas mixture. For direct fluorination, typically a F_2:N_2 gas mixture is used. However it has been reported that oxyfluorination always accompanies direct fluorination due to the presence of oxygen in technical grade nitrogen gas (Kharitonov, 2008). In this study both oxyfluorination and direct fluorination were investigated to functionalise the NWF surfaces. (A detailed discussion on the fluorination process was presented in **Chapter 2**).

Oxyfluorination was preferred over the radiation techniques, since it is dry technology which is simple to perform and it is less invasive than some of the other radiation based surface modification methods. Additionally the main elementary stage of the process is highly exothermic and proceeds spontaneously at room temperature without requiring initiation or catalysts (Kharitonov and Kharitonova, 2009; Lee et al., 2003). The spontaneity of the oxyfluorination process is due to the high electronegativity of fluorine.

It has been reported that when oxygen groups are introduced onto a polymeric surface during oxyfluorination, the surface wettability and adhesion properties are increased. Oxyfluorination is known to form reactive polar groups on polymer surfaces, which can serve as active centres for grafting (Jeong et al., 2011). The main functional groups which have been reported previously include CF, CF_2, CF_3, C(=O)F, C(=O)OH, CO-O$^{\bullet}$ (peroxyradicals), CO-OH (peroxides) (Jeong et al., 2011; Kharitonov, 2008; Lee et al., 2003; Park et al., 2005 ; Woo et al., 2005). The formation of reactive peroxide groups (ROOH; ROOR) and long-lived trapped peroxyradicals (ROO$^{\bullet}$) on oxyfluorinated polymer surfaces have been shown to form active sites for graft polymerisation (Jeong et al., 2011). However, to our knowledge, the use of oxyfluorination as a pre-treatment for graft polymerisation has not been widely reported.

In this study, an oxyfluorination-assisted graft polymerisation (OAGP) method was employed to synthesise the PNIPAAm grafted 3D NWF scaffolds. Development of the 3D PNIPAAm grafted NWF scaffolds involved the following steps:

1) *NWF manufacture:*
   Highly porous NWF scaffolds based on PP, PET and nylon were manufactured using a needle-punching technology

2) *Functionalisation:*
   Oxyfluorination and direct fluorination were investigated as functionalisation techniques to modify the surface of the NWF scaffolds with reactive groups which could then serve as active sites for graft polymerisation.

3) *Graft polymerisation*:
   The NWF (either pre-functionalised or pure) were treated by graft polymerisation in an aqueous NIPAAm solution using ammonium persulphate (APS) as the initiator to produce the PNIPAAm grafted NWF scaffolds.

The NWF scaffolds have been characterised using capillary flow porometer, attenuated total reflectance Fourier transform infrared (ATR-FTIR), X-ray photo electron spectroscopy (XPS), scanning electron microscopy (SEM), static water contact angle, X-ray diffraction (XRD), differential scanning calorimetry (DSC), electron spin resonance (ESR), and UV-VIS spectroscopy.

5.2 Experimental

5.2.1 Materials

PP, PET, and nylon fibres were purchased from FiberVision (Denmark). PP and PET fibres of linear density of 6.7 dtex and fibre staple length of 60 mm were used, while the nylon fibres displayed a linear density of 3.3 dtex and 50 mm fibre staple length. *N*-isopropylacrylamide (NIPAAm) (97%), PNIPAAm (Mw 20 000 g/mol) and ammonium persulphate (APS) (> 98%, ACS reagent) were obtained from Sigma Aldrich and used without further purification. Ethanol, benzene (anhydrous 99.8%), and 2,2-Diphenyl-1-1-picrylhydrazyl were also obtained from Sigma Aldrich. High purity (99.99%) argon and nitrogen gas were obtained from Air Products.

5.2.2 Manufacture of NWF scaffolds

PP, PET, and nylon NWF were manufactured using the needle-punching technology. Manufacture of the NWF was conducted at CSIR Material Science and Manufacturing in Port Elizabeth by Boguslavsky *et al* (Boguslavsky, 2009; Boguslavsky and Anandjiwala, 2007; Boguslavsky et al., 2008). Briefly for the needle-punching process, fibres were either opened (by carding) or unopened and the resulting web was cross-lapped and then needle-punched on the Dilo needle-punching machine (Boguslavsky, 2010). Needle punching involved mechanical intertwining of fibres using needles. To improve the mechanical integrity of the NWF, some of the needle-punched scaffolds were post-treated by a thermo bonding process in an oven with varying conveyor speeds. Five trials were conducted whereby the following parameters were varied, i.e. needling arrangement; depth of needle penetration; speed of needling; and thermo bonding temperature to produce NWF scaffolds with varying morphologies (Boguslavsky, 2009; Boguslavsky and Anandjiwala, 2007; Boguslavsky et al., 2008).

5.2.3 Graft polymerisation of PNIPAAm onto the NWF

Graft polymerisation of PNIPAAm onto the NWF scaffolds was performed on the pre-functionalised NWF scaffolds with the use of APS as the chemical initiator. To verify if grafting could be initiated by the surface peroxy groups, graft polymerisation was also conducted without any chemical initiation. For the latter NWF scaffolds were heated to activate the free radicals. Grafting was also conducted on the pure non-functionalised NWF scaffolds which served as controls.

5.2.3.1 Step 1: Surface functionalisation of NWF

Prior to surface functionalisation, PP, PET and nylon NWF were washed in ethanol to remove impurities, followed by water and then the NWF scaffolds were dried in an oven. Washed NWF scaffolds were treated at Pelchem Pty. Ltd. (SA) by a proprietary method which involved either oxyfluorination or direct fluorination (Louw and Carstens, 2006). The NWF scaffolds were loaded into a reaction vessel and the treatment protocols were as follows:

- *Oxyfluorination*: The reaction vessel was purged with air and partially evacuated, and then a 20:80 (vol%) F_2:N_2 gas mixture at 5 kPa was introduced into the vessel at room temperature for 30 minutes to allow the oxyfluorination reaction to proceed. The gas mixture was then cycle purged from the vessel with air at 25 kPa to complete the oxyfluorination process. The oxygen present in the reactor during the oxyfluorination treatment was from air which was introduced during both the partial evacuation and the cycle purging steps in air.
- *Direct fluorination*: The reaction vessel was fully evacuated and a 5:95 (vol%) F_2:N_2 gas mixture was introduced into the vessel for a given time.

5.2.3.2 Step 2: Graft polymerisation

1) Use of chemical initiation

The experimental set-up which was used for graft polymerisation is shown in **Figure 5.2**. Briefly aqueous solutions of 10 wt% NIPAAm and 10 wt% APS were prepared in deionised water. Oxyfluorinated and direct fluorinated PP, PET, and nylon NWF (prepared as described above) were cut into disks (1.5 cm x 0.7 mm) and each disk was immersed in 10 ml of the APS solution in round bottom flasks and left to swell to saturation at 23 ºC for 16 hrs. Prior to grafting, the solutions were degassed for 30 mins by continuously flowing high purity argon gas into the flasks. The APS solution was decanted, and 10 ml of the NIPAAm (previously degassed) was added into each reaction vessel containing the swollen fluorinated NWF scaffolds. The reaction vessels were immediately capped and graft polymerisation was conducted by immersing the flasks in an oil bath at 70 $^{\circ}$C for 7 hrs. The grafted NWF disks were washed in copious amounts of cold deionised water for 72 hrs with regular water changes to remove PNIPAAm homopolymer or residual monomer. Control grafting experiments were performed using pure non-functionalised NWF scaffolds.

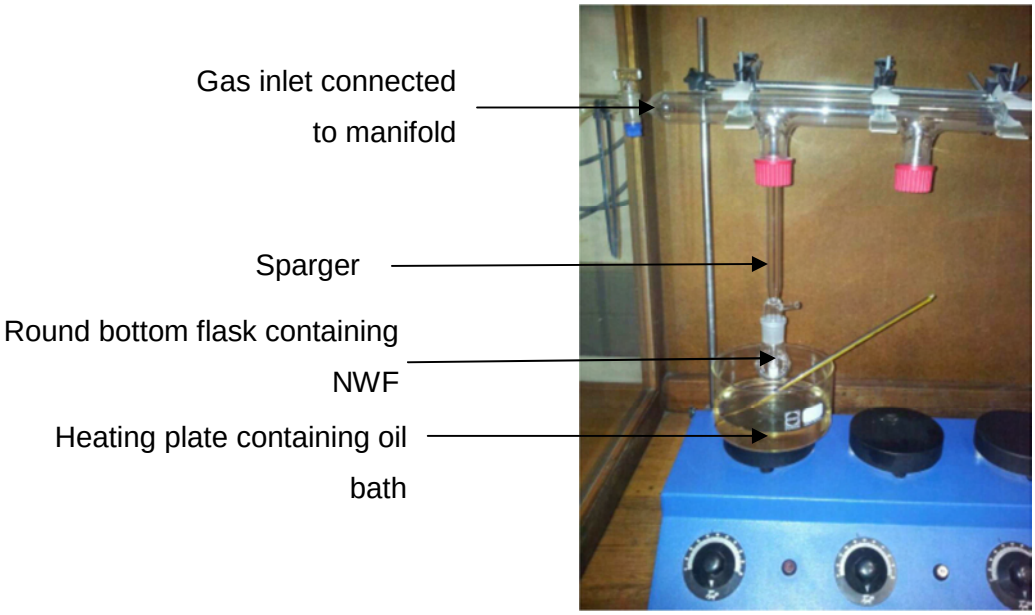

Figure 5.2: Photo showing experimental set-up used for graft polymerisation of PNIPAAm onto NWF scaffolds.

2) Without chemical initiator

Graft polymerisation was also conducted as described above, except the fluorinated samples were swollen directly in 10 wt% aqueous NIPAAm solution overnight and no APS was used. Samples were degassed as above, and then placed in an oil bath at 70 ^{o}C for 7 hrs to enable grafting. The grafted NWF scaffolds were then washed as described previously.

5.2.4 Characterisation of pure and functionalised NWF

5.2.4.1 Physical properties of pure NWF

The pure NWF scaffolds were characterised by Ms Lydia Boguslavsky at CSIR MSM in Pretoria for thickness, mean are weight, pore size distribution, water permeability, and tensile strength (Boguslavsky, 2009; Boguslavsky and Anandjiwala, 2007; Boguslavsky et al., 2008). A capillary flow porometer was employed to determine the pore size distribution and the mean flow pores (MFP) according to the 6212005-134 Test of the ASTM E 1294 Method.

5.2.4.2 Attenuated-total reflectance Fourier transform infrared spectroscopy

A Spectrum 100 FTIR spectrometer was used, with a diamond crystal for attenuated-total reflectance Fourier transform infrared (ATR-FTIR) analysis. For each measurement, 16 scans were taken, with a resolution of 4 cm^{-1} and an average of 8 spots were taken per sample to get representative data. To see the stability of the new functional groups following oxyfluorination, oxyfluorinated PP NWF scaffolds were incubated in water either at 25 °C for 3 hrs or at 70 ºC for 10 mins. Samples were thereafter dried and re-analysed by ATR-FTIR.

Determination of graft yield by ATR-FTIR

A stock solution of 0.8 g/L of PNIPAAm was prepared in ethanol. A serial dilution of the stock PNIPAAm solution was prepared such that the new solutions had the following concentrations: 0.4 g/L, 0.24 g/L, 0.12g/L, 0.04 g/L and 0.002 g/L. A commercially available polypropylene sheet (obtained from a hardware store) was cut into disks of 27 mm diameter and 0.7 mm thickness and weighed. The disks were soaked in 3 ml of PNIPAAm solution each in capped 25 ml beakers for 16 hrs. The ethanol was then evaporated in the oven at 50 ^{o}C. The dried disks were then weighed and characterised by ATR-FTIR. For the peak area ratio determination, the ratio of the carbonyl peak at 1644 cm^{-1} and the methyl group at 1455 cm^{-1} was measured. In the absorbance mode, peaks were first normalised before the peak areas were measured. Using Lamberts-Beer law a calibration graph was constructed by plotting the absorption ratios with the known PNIPAAm concentrations and a linear relationship was predicted between peak intensity and concentration as follows (Skoog et al., 1996):

$$A = \varepsilon c \ell \qquad \text{(Eq 5.1)}$$

whereby A is the absorbance; ε is the molar absorptivity (extinction coefficient) of the absorber, c is the concentration of absorbing species in the material and ℓ is the distance the light travels through the material (i.e. the path length). A trendline was added through the data points and an equation was determined relating peak area ratios to PNIPAAm mass which was used to calculate the graft yield on the scaffolds (µg/cm^2). Statistics was performed using the Anova Single Factor test with α=0.05.

5.2.4.3 X-ray photoelectron spectroscopy

X-ray photoelectron spectroscopy (XPS) was performed to determine the elemental composition of the surface of the NWF scaffolds. A Quantum 2000 (Physical Electronic) scanning XPS was used. The XPS was equipped with an Al K α (1486 eV) X-ray source (20 W), and a beam diameter of 100 µm. Both wide and high-resolution scans for the F1s, O1s, N1s, and the C1s binding energies were performed for all the NWF scaffolds.

5.2.4.4 Contact Angle

The water contact angle of the NWF scaffolds was determined using the Kruss DSA 100. 4 µl of pure deionised water was dispensed onto the surface of the NWF disks using a needle. The contact angle was measured every second with a total drop age of 10 seconds using either the circle or sessile-drop fitting. When measurements were taken at 40 ℃, a heated stage was used, and samples were equilibrated at 40 ℃ in an oven for 1 hr prior to analysis. Measurements were performed in triplicates for each time point.

5.2.4.5 Percent swelling

The pure and oxyfluorinated NWF scaffolds were cut into small pieces with masses ranging between 0.02-0.03 g. The dry mass was taken at time 0 by equilibrating the scaffolds in an oven at 50 ºC for 2 hrs. Scaffolds were placed in 5 ml of water in polytops, and the wet masses were taken after 2, 4, 6, and 24 hrs. Wet NWF scaffolds were gently dabbed between tissue paper. The percent swelling of the NWF scaffolds in water was calculated as follows:

$$\%\ \text{swelling} = \frac{\text{Ww}-\text{Wd}}{\text{Wd}} * 100 \qquad \text{(Eq. 5.2)}$$

where Ww is the weight of the wet NWF, while Wd is the initial weight of the dried NWF.

5.2.4.6 Scanning electron microscopy

Scanning electron microscopy (SEM) was performed to determine the surface morphology of the NWF scaffolds. A LEO 1525 field emission SEM with Oxford's INCA system was used. All samples were sputter coated with carbon prior to imaging.

5.2.4.7 X-ray diffraction

An X'PertPro wide angle X-ray diffraction (XRD) system was used to determine the crystal structure of the NWF scaffolds. A Ni filtered CuKα source was used with radiation of λ= 0.154 nm, with operating conditions of 40 mA, 45 kV, and exposure time of 12 minutes. For the WAXS measurements, 2 theta (2θ) was measured from 5°to 60°for all samples.

5.2.4.8 Differential scanning calorimetry

Differential scanning calorimetry (DSC) was used to measure the heat flux in the NWF scaffolds. A Tzero™ (DSC-Q2000) and a micro DSC (MicroDSCIII apparatus (SETARAM)) were used for determining the melting crystallisation peaks of the NWF scaffolds and the LCST of PNIPAAm on the grafted NWF scaffolds respectively. For the melting and crystallisation curves, NWF scaffolds of mass ranging between 2-5 mg were weighed and pressed in Tzero™ pans and Tzero™ Hermetic lids. Samples were heated from 50 ℃ to 220 ℃ at a heating rate of 20 ℃/min under nitroge n gas. This was followed by an isothermal step at 220 ℃ for 1 min; then a cooling cycle from 220 ℃ to 50 ℃ at 20 ℃ /min; and a final isothermal step at 50 ℃ for 1 minute. Quantitative analysis for melting was obtained from the second heating cycle. The degree of crystallisation was estimated from heat of fusion measurements from the melting thermogram according to:

$$\%\ \text{crystallisation} = \left(\frac{\Delta H_f^*}{\Delta H_f}\right) * 100 \qquad \text{(Eq. 5.3)}$$

where ΔH_f^* is the measured heat of fusion of the sample; and ΔH_f is the heat of fusion of 100% crystalline polymer, which was taken as 146.5 J/g in the case of PP (Huda et al., 1985). For the LCST determination of the PNIPAAm grafted PP NWF scaffolds, 20 mg of dry grafted sample was placed in contact with 500 µL of deionised water and kept at 10 ℃ for 2 hours to obtain equilibrium. The samples were heated from 0 ℃ to 80 ℃ at a heating rate of 0.5 ℃ / min (László et al., 2004).

5.2.4.9 Electron spin resonance

Electron spin resonance (ESR) of the oxyfluorinated PP NWF was conducted using a Bruker Elexsys 500 spectrometer operating at X-band frequencies of ~9–10 GHz, 100 kHz modulation frequency and 1G modulation amplitude. Spectra were recorded as first

derivatives of microwave absorption at ambient temperature, using 2 mW microwave power. Spectra were recorded both at room temperature and at 70 °C.

5.2.4.10 Determination of peroxides using DPPH method

It is well-known that 2,2-diphenyl-l-picrylhydrazyl (DPPH) is a stable free-radical which can be used as radical scavenger to determine peroxide content (Fargere et al., 1995; Ionita, 2005; Jeong et al., 2011). For the DPPH- radical scavenger method, firstly 20 ppm stock solution of DPPH was prepared in benzene, and serial dilutions of 10 ppm, 5 ppm, 2 ppm, and 1 ppm were prepared in volumetric flasks. A calibration graph of absorbance versus concentration was constructed by measuring the UV-VIS absorbance of each DPPH solution at 520 nm using a Lambda 35 UV-VIS spectrometer (Perkin Elmer). The amount of peroxides on the oxyfluorinated PP NWF scaffolds was determined by incubating 1.5 cm NWF disks in 10 ml of 20 ppm DPPH solution in a glass reaction vessel, at 70 ºC for 7 hrs. The control experiments consisted of pure PP NWF, and a blank control (DPPH solution treated as above but without any sample). The moles of peroxide present on the oxyfluorinated PP were determined as follows:

$$\frac{\text{Moles peroxide}}{\text{Surface area of NWF}}\ (\text{Mol.cm}^2) = \frac{(C_0 - C) * V}{2A} \qquad \text{(Eq 5.4)}$$

Where Co is the initial DPPH concentration which was determined from the absorbance of the blank control, C is the concentration of DPPH remaining in solution which was measured after reaction with the oxyfluorinated PP NWF, and V is the volume of the DPPH solution. It is assumed that the molar ratio of peroxide: DPPH is 1:2 (Fargere et al., 1995) .

5.3 Results and discussion

In this study NWF scaffolds based on PP, PET, and nylon were prepared using the needle-punching technology. Two surface functionalisation treatments were investigated to improve the reactivity of the NWF scaffolds towards graft polymerisation. This included direct fluorination and oxyfluorination treatments. Direct fluorination involved exposure of the NWF scaffolds with 5:95 F_2:N_2 gas mixture; while for oxyfluorination a 20:80 F_2:N_2 gas mixture was used, and air was introduced during the partial evacuation and cycle purging steps. The NWF scaffolds were graft polymerised with PNIPAAm in an aqueous medium for use in cell culture. This chapter deals with the synthesis and physicochemical properties of the synthesised NWF scaffolds.

5.3.1 Physical properties of pure NWF scaffolds

Using the needle-punching technique, PP, PET, and nylon NWF scaffolds were produced as shown in **Figure 5.3**. A number of different trials (T1-4) were conducted to manufacture the NWF scaffolds. The processing parameters and physical properties of the scaffolds which were selected for functionalisation appear in **Table 5.1**.

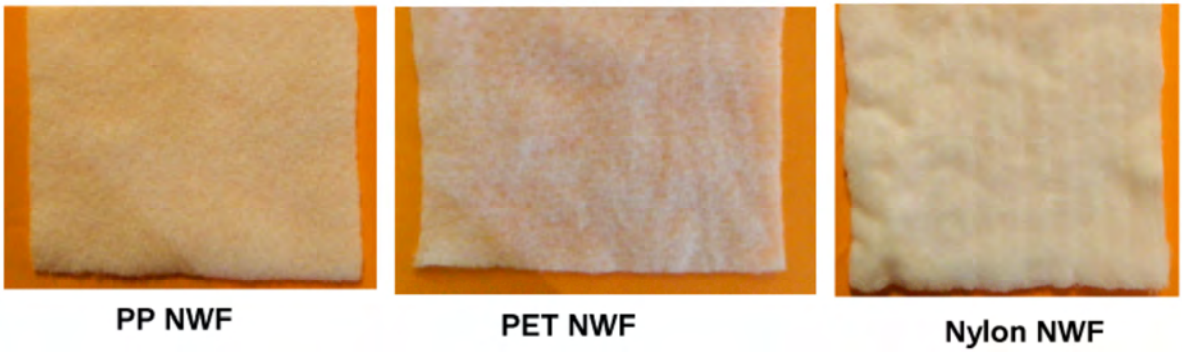

Figure 5.3: Images of PP T2-N6(1), PET T2-N7(1), and nylon T3-N8 developed by needle-punching.

The main criteria for selection of the NWF scaffolds were pore size, porosity, and mechanical integrity. In literature various optimal pore sizes have been reported to encourage cell migration and proliferation (Chang et al., 2011). These include sub-micron pores (1-10 µm) for sub-cellular interactions and for providing oxygenation and nutrient transport as well as larger micron sized pores (100-1000µm) for multiple cellular interactions (Chang et al., 2011). Since pore size also influences the structural stability of NWF scaffolds, in this study, we selected 100-300 µm as the optimal mean pore sizes for the scaffolds. Capillary flow porometry was used to measure the minimum, mean and maximum pore sizes of the NWF scaffolds. A wide range in pore sizes was reported for the manufactured NWF scaffolds (**Table 5.1**), with the MFP diameters for the PP and PET NWF ranging between 100-200 µm which was within the desired range. However for the nylon NWF, the MFP was ~60 µm, which was substantially lower. The smaller pore sizes in the nylon NWF scaffolds were attributed to the lower linear density of the fibres used (i.e. 3.3 dtex compared to 6.7 dtex for PP and PET fibres respectively). To improve the structural stability of the NWF scaffolds, the fibers were thermobonded but pore size was slightly reduced (Boguslavsky and Anandjiwala, 2007; Boguslavsky et al., 2008). The PP and PET NWF showed higher water permeability than the nylon NWF due to the higher pore size of the former (data not shown) (Boguslavsky and Anandjiwala, 2007; Boguslavsky et al., 2008). A higher depth of needle punching and needling from both sides resulted in more intense interlocking of fibres, resulting in more stable structures.

Table 5.1: Processing parameters and physical properties of NWF scaffolds produced by needle-punching technology.

NWF	Batch*	Fibre linear density / dtex	Machine processing parameters			Thermobonding temperature / ºC	Area weight / g.m^{-2}	Thickness / mm	Pore size / µm		
			Needling Arrangement	Feeding speed / m.min^{-1}	Depth of Needling / mm				Min	Mean MFP	Max
PP	T2- N6(1)	6.7	Opened	1.6	10	145	130	3.21	7.74	127.44	247.46
	T4-N11	6.7	Unopened single	0.55	10	-	202	5.1	7.69	101.37	195.6
	T4-N12	6.7	Unopened single	0.55	15	-	95	3.2	7.18	156.84	572.84
	T4-N13	6.7	Unopened double	0.55	6	-	98	3.3	7.68	199.38	411.09
PET	T2-N7(1)	6.7	Opened single	1.6	10	180	150	3.14	7.55	142.55	263.80
Nylon 6.6	T3-N7	3.3	Unopened single	0.25	10	190	195	2.84	6.97	59.37	123.87
	T3 - N8	3.3	Opened	0.25	10	-	103	1.86	7.47	78.82	152.24

(*T refers to the trial number, and N is the NWF number)

5.3.2 Analysis of NWF by ATR-FTIR

ATR-FTIR was used to determine the functional groups on the surface of pure and fluorinated NWF scaffolds (**Section 5.3.2.1**), and PNIPAAm grafted NWF scaffolds (**Section 5.3.2.2**).

5.3.2.1 Assessment of functional groups on NWF before and after fluorination

The functional groups on the NWF scaffolds were assessed before and after fluorination using ATR-FTIR to determine the efficiency of the fluorination process.

1) Pure and fluorinated PP NWF

The chemical structures for pure PP, PET, nylon, and PNIPAAm appear in **Figure 5.4**. Pure PP NWF was characterised by four distinctive absorption bands between 3000-2800 cm^{-1} which were due to the C-H asymmetric and C-H symmetric stretches of the methyl (2950 cm^{-1}; 2868 cm^{-1}) and methylene groups (2917 cm^{-1}; and 2838 cm^{-1}) respectively (**Figure 5.5a**), and two strongly absorbing bands at 1455 cm^{-1}, and 1375 cm^{-1}, which were assigned to the bending vibration of the methylene and isopropyl groups respectively.

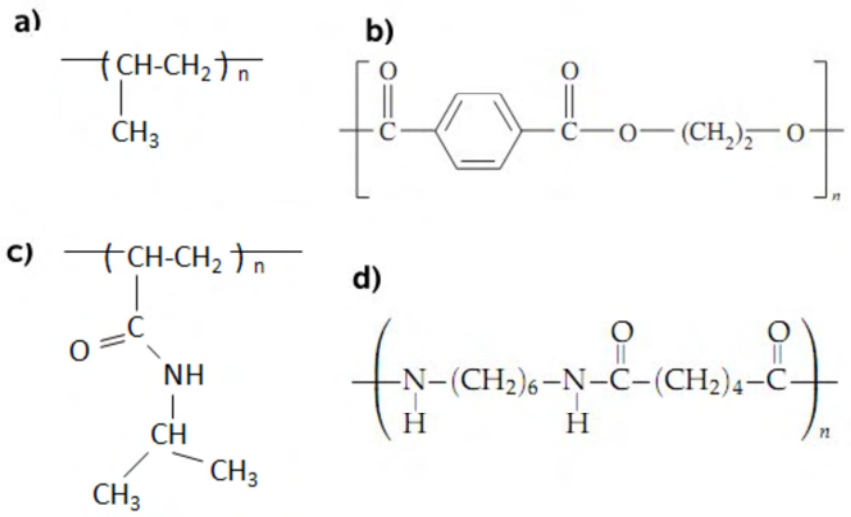

Figure 5.4: Chemical structures of (a) PP; (b) PET; (c) PNIPAAm and (d) nylon.

After the direct fluorination treatment (**Figure 5.5b**), slight changes were observed to the absorption bands of the fluorinated PP. A new broad band appeared at 3100-3550 cm^{-1} which was assigned to the O-H stretching vibration. Additionally at 900-1300 cm^{-1} a declining baseline was observed which could be indicative of a C-F stretching vibration. For the oxyfluorinated PP surface, the changes were more clearly discernible.

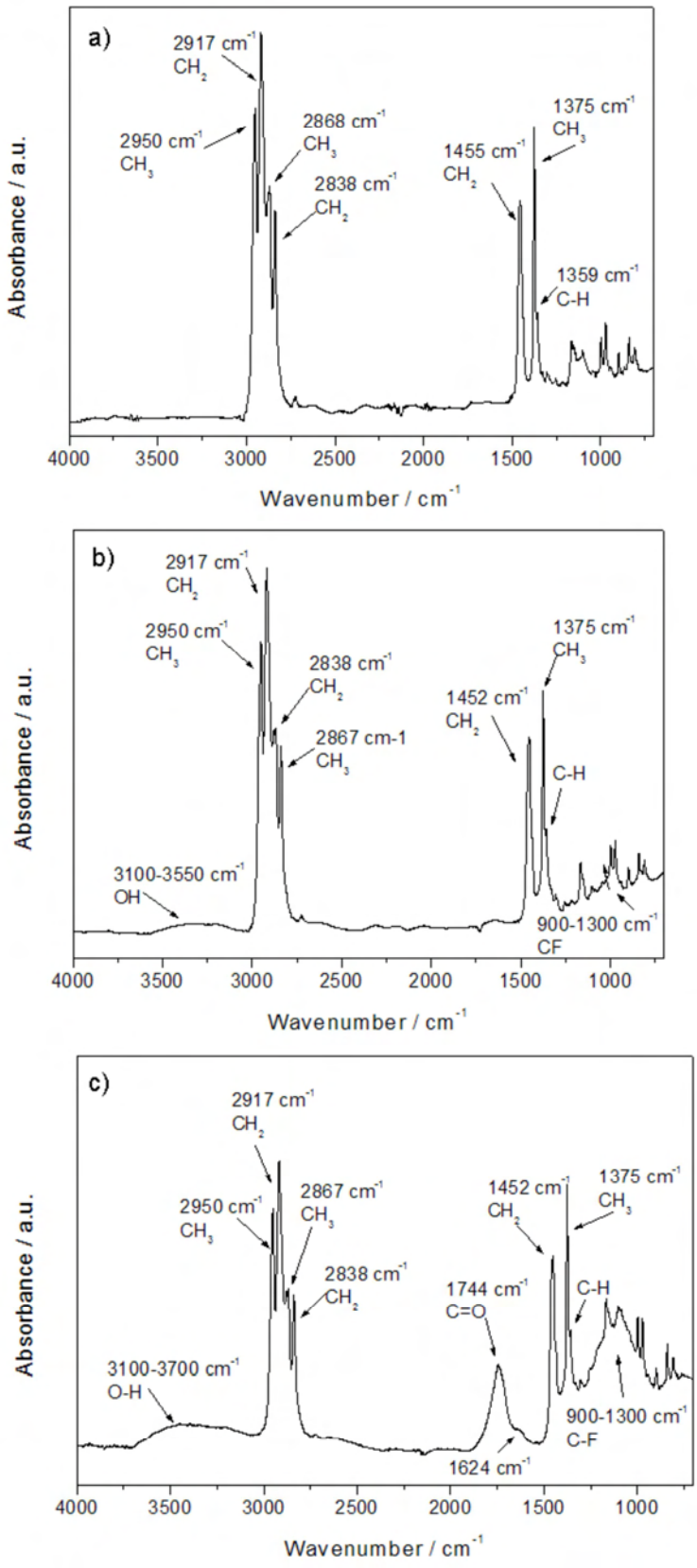

Figure 5.5: ATR-FTIR spectra of (a) pure PP NWF (control) prior to surface functionalisation, and PP NWF after (b) direct fluorination and c) oxyfluorination treatments.

A broad O-H stretching band and a distinctive C=O peak appeared at 3100-3700 cm^{-1} and 1744 cm^{-1} respectively. A small shoulder peak was also observed at 1624 cm^{-1}. Finally a broad diffuse band occurred at 900-1300 cm^{-1} which was attributed to the stretching vibration of the C-F group (Kharitonov and Kharitonova, 2009). It could also be seen that under the present processing conditions, oxyfluorination was more effective than direct fluorination in adding new functionality to the surface of PP NWF scaffolds.

It has been reported previously that direct fluorination of polymers results in replacement of H atoms with F (Kharitonov, 2008). It has also been reported that in the presence of oxygen, acid fluorides, carboxylic acids, peroxy radicals ($RO_2^{\bullet}$) and peroxide groups (ROOH, ROOR) also form on oxyfluorinated surfaces (Jeong et al., 2011; Kharitonov, 2008; Park et al., 2005). Many authors have also shown that the acid fluoride groups (-COF) which display an absorbance peak at 1850 cm^{-1} easily hydrolyse by moisture to the corresponding carboxylic acid which displays an absorbance peak at 1750 cm^{-1} (du Toit and Sanderson, 1999; Kharitonov et al., 2005; Lee et al., 2003). Only trace levels of COF was seen on the PP NWF scaffolds following oxyfluorination.

Due to the presence of the C=O and OH peaks on the oxyfluorinated PP NWF scaffolds, it can be assumed that the acid fluoride groups may have already hydrolysed to the corresponding carboxylic acid. The band at 1744 cm^{-1} could possibly indicate a carboxylic acid (CHF-(C=O)OH; α-fluoroester –CHF–(C=O)–O–; α-fluoroaldehyde –CHF–(C=O)H; or a α-fluoroketone $–CH_2–(C=O)–CHF–$ (Kharitonov and Kharitonova, 2009). A weak shoulder band at 1624 cm^{-1} has been reported previously following oxyfluorination of low-density polyethylene and it was attributed to both C=O vibration in the enol form of the β-diketones –(C=O)–CF=C(OH)– or the double bond C=C (e.g. –FC=CH–) stretching vibration (Kharitonov and Kharitonova, 2009). A summary of the main adsorption bands for pure PP appear in **Table 5.2**. For the C-F stretching vibration for the oxyfluorinated PP, peak maximum was observed at ~ 1160 cm^{-1} and 1150 cm^{-1} which was attributing to CF, CF_2 and CF_3 groups (Kharitonov and Kharitonova, 2009). After oxyfluorination, the CH_3, CH_2, and CH PP peaks were still present indicating that PP was only partially fluorinated. According to Kharitonov, the formation of a totally fluorinated polymer having a Teflon-like structure $(–CF_2–CF_2–)_n$ is not common by fluorination, since the latter needs a duration exceeding several weeks or even months at conditions exceeding industrially acceptable limits (Kharitonov and Kharitonova, 2009).

Hydrolysis post-treatment of the oxyfluorinated PP NWF revealed a decrease in peak intensities of the newly formed functional groups as shown in **Figure 5.6**.

Table 5.2: Assignment of FTIR peaks for pure PP NWF scaffolds (Mark, 1999; Socrates, 2001).

Functional group	Wavenumber / cm^{-1}	Peak assignment
Methyl (CH_3)	2950	CH_3 asymmetric stretch
	2868	CH_3 symmetric stretch
	1455	CH_3 asymmetric bend
	1375	Isopropyl
Methylene (CH_2)	2917	CH_2 asymmetric stretch
	2838	CH_2 symmetric stretch
	1455	CH_2 bend
Methyne (CH)	1359	C-H bend
	1300-700	C-C vibrations

Changes were observed to all of the newly formed functional groups, i.e. O-H, C=O and the C-F groups on the oxyfluorinated PP NWF when samples were treated in water at either room temperature or at elevated temperatures. It is likely that the lower ATR-FTIR peak intensities can be attributed to direct hydrolysis of the new functional groups. Studies have indicated that fluorinated esters are very unstable due to the high electronegativity of the fluorine group and can undergo rapid hydrolysis even under neutral conditions (Uchimaru et al., 2003). It can be postulated that oxyfluorination resulted in a fluorine substituted ester, which degrade due to hydrolysis.

Additionally the lower ATR-FTIR peak intensities can be attributed to a reduction in the Lewis basicity of the oxyfluorinated PP surface during hydrolysis due to conversion of the pure carbonyl group of the acid fluoride to carboxylic acid (Tu et al., [1997]). According to Tu et al., during hydrolysis, an inter-hydrogen bonded conjugated structure occurs in oxyfluorinated PP between two neighbouring COOH groups. This inter-hydrogen bonded structure could likely reduce the net dipole on the carbonyl peak and neighbouring C-F peaks, which would account for the reduced peak intensities of the newly formed oxyfluorinated groups after hydrolysis. Also after hydrolysis, the shoulder peak at ~1623 cm^{-1} grew in intensity. Absorption at 1620-1623 cm^{-1} was also reported by Kharitonov *et al* following hydrolysis of oxyfluorinated low density polyethylene which was attributed to C=O vibration in the enol form of the β-diketone or the double bond C=C stretching vibration (e.g. FC=CH) (Kharitonov, 2008). Further investigations are required to confirm the structural changes on oxyfluorinated PP upon hydrolysis.

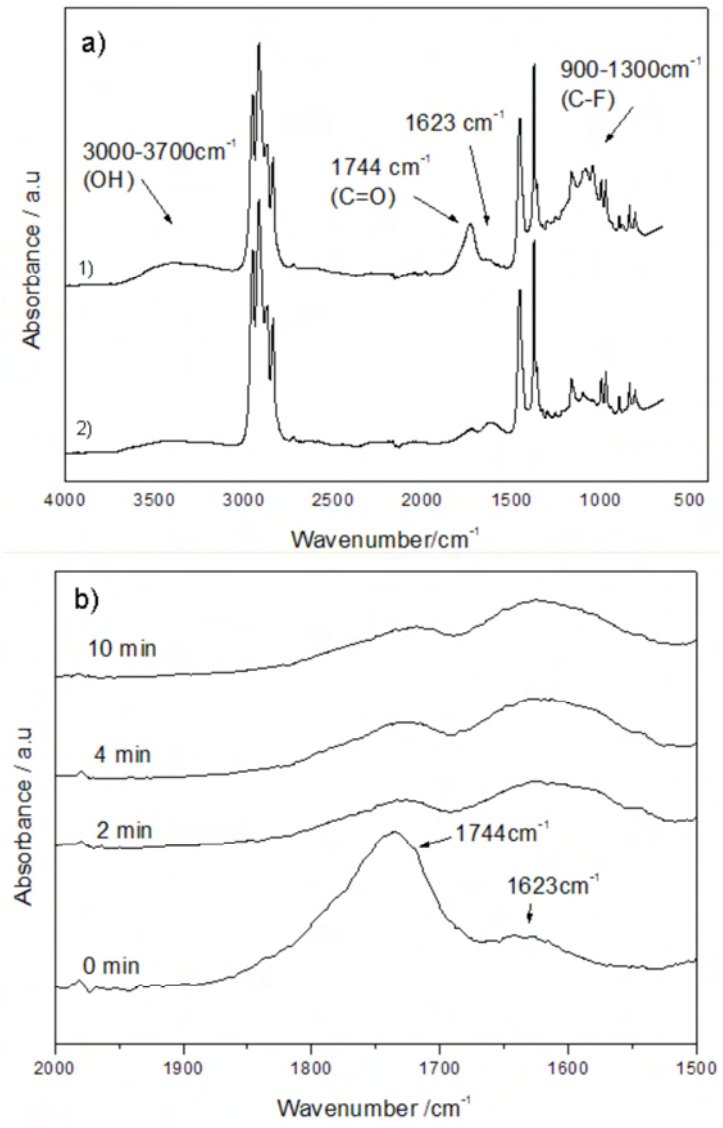

Figure 5.6: ATR-FTIR spectra of hydrolysis post-treatment of oxyfluorinated PP (a) at 25 °C (1) before hydrolysis and (2) after hydrolysis; and (b) treatment at 70 ºC for 0-10 minutes.

2) Pure and fluorinated nylon and PET NWF

The ATR-FTIR spectra for pure and functionalised nylon appear in **Figure 5.7** and a summary of the peaks is given in **Table 5.3**. For nylon 6.6 the main absorption bands were due to methylene and amide groups in the polymer backbone. For the amide group, the peak assignments were as follows: 3295 cm^{-1}; 1632 cm^{-1}; and 1532 cm^{-1} which were assigned to amide II N-H stretch, amide I C=O stretch, and the N-H bend/C-N stretch respectively (Mark, 1999).

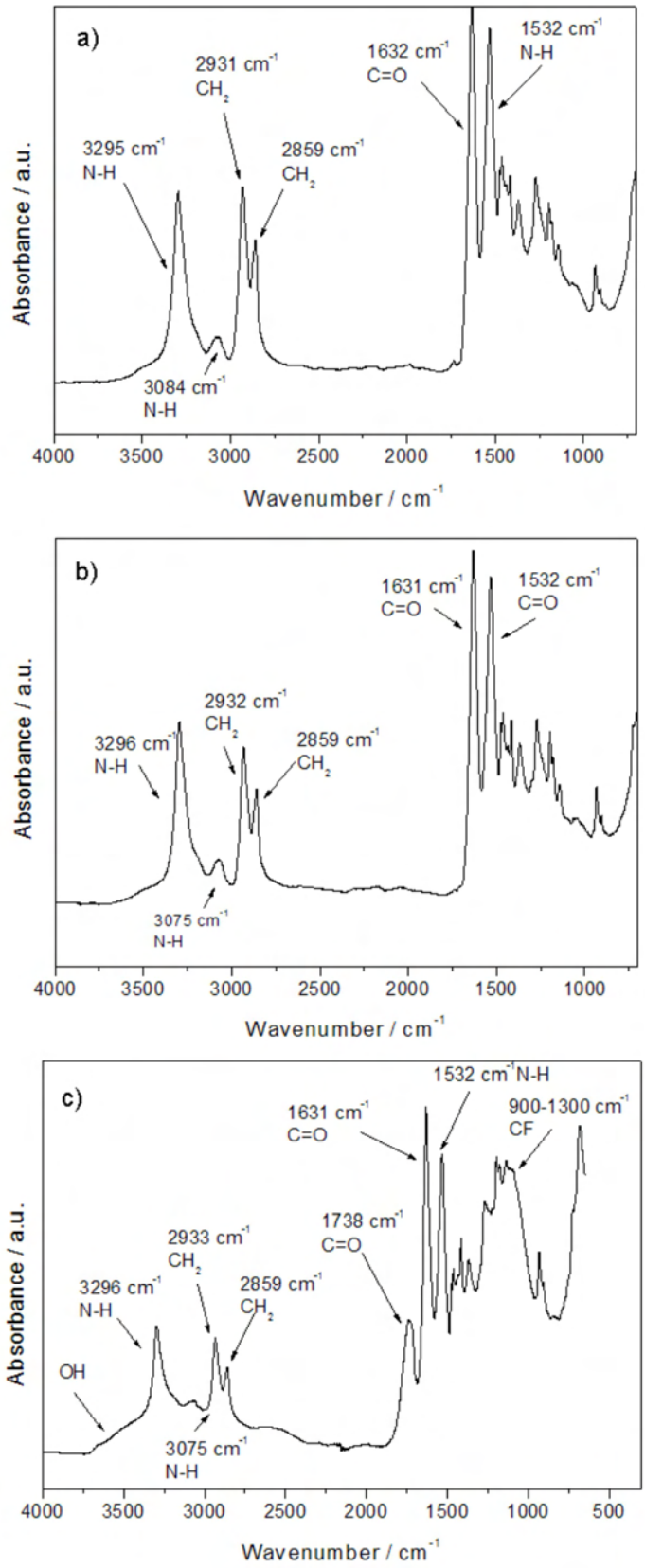

Figure 5.7: ATR-FTIR spectra of (a) pure nylon NWF (control) prior to surface functionalisation, and following (b) direct fluorination and (c) oxyfluorination treatments.

Table 5.3: Assignment of FTIR peaks for pure nylon 6.6. and PET NWF scaffolds (Mark, 1999; Socrates, 2001).

Functional group	Wavenumber / cm^{-1}	Peak assignment
Nylon		
Methylene	2931	CH_2 asymmetric stretch
	2859	CH_2 symmetric stretch
	1460	CH_2 symmetric scissors deformation
	1440	CH_2 symmetric scissors deformation – (CH_2 next to N)
	1420	CH_2 symmetric scissors deformation – (CH_2 next to C=O
	1370	CH_2 wag
	722	CH_2 rock
Amide	3295	Amide II N-H stretch
	3084	NH bend overtone
	1632	Amide I C=O stretch
	1532	N-H bend/C-N stretch
	1200	N-C=O skeletal vibration
	1170	N-C=O skeletal vibration
	700	N-H wag (broad)
PET		
Carbonyl	1712	C=O stretch
Aromatic ester	1242	Asymmetric stretching of C-O-C due to aromatic ester
	1095	Symmetric stretching of C-O-C due to aromatic ester
	722	Aromatic ring out of plane deformation

The CH_2 asymmetric and symmetric stretch appeared at 2931 cm^{-1} and 2859 cm^{-1} respectively, and between 1500-700 cm^{-1} numerous smaller peaks were present due to the amide I, II and CH_2 bond interactions. After direct fluorination, changes to the chemical structure of nylon could not be clearly distinguishable from that of pure nylon. However oxyfluorination was successful in introducing new surface groups on the nylon NWF. A new absorption peak was identified at 1738 cm^{-1} and a broad diffuse band appeared at 900-1300 cm^{-1} which corresponded to C=O and C-F stretching vibrations respectively. On careful examination, a broad O-H shoulder peak was also discernible at around 3500-3700 cm^{-1}.

For the PET NWF scaffolds (**Figure 5.8**), many adsorption bands were seen in the IR region.

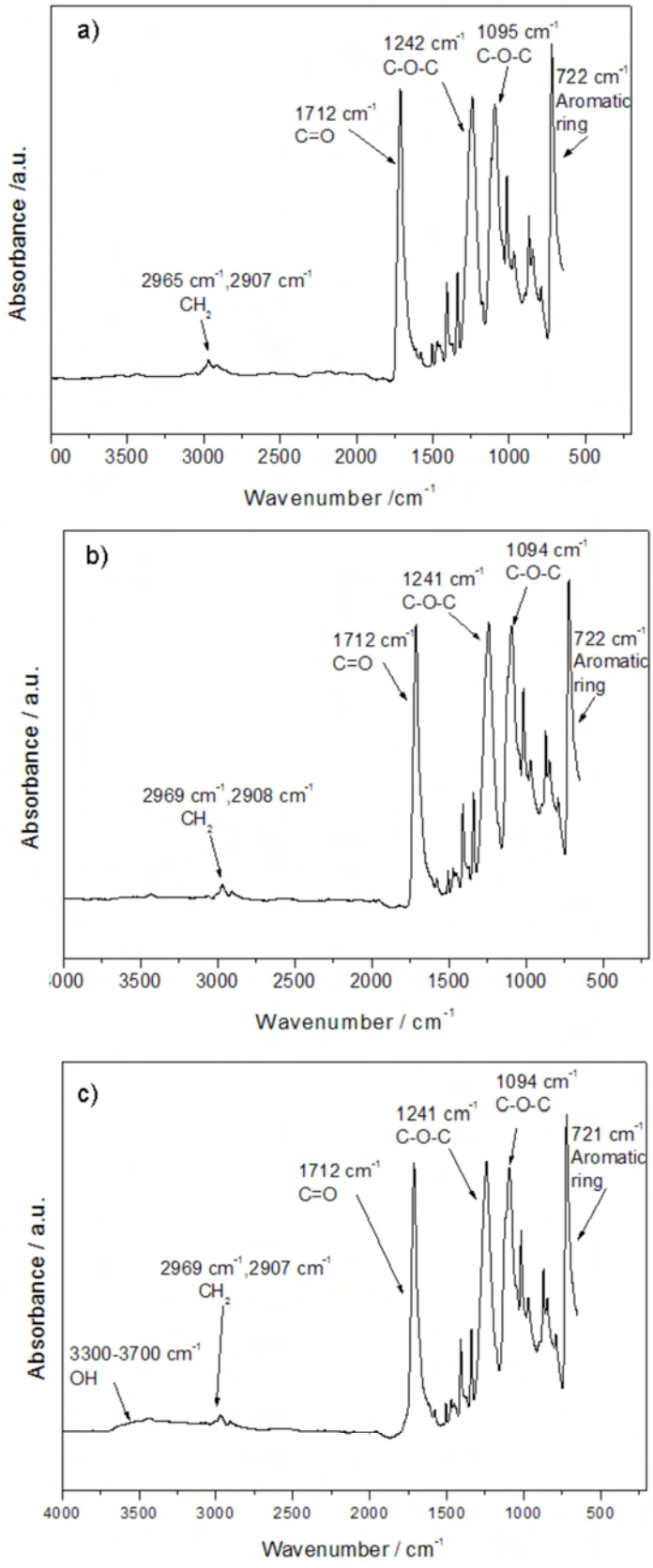

Figure 5.8: ATR-FTIR spectra of (a) pure PET NWF (control) prior to surface functionalisation, and following (b) direct fluorination and c) oxyfluorination treatments.

The most distinctive peaks for PET occurred at 1712 cm^{-1}; 1242 cm^{-1}; 1095 cm^{-1}; and 722 cm^{-1} which were due to the C=O of the ester group, the asymmetric and symmetric stretching respectively of the C-O-C group, and the out-of plan deformation of the benzene ring respectively (Socrates, 2001). After direct fluorination, no new functionality could be detected on the PET surface by ATR-FTIR while after oxyfluorination a slight OH peak could be seen at 3500-3700 cm^{-1}. Due to overlapping IR peaks occurring in the C=O and C-F region emanating from the PET backbone, it was unclear if any further modification occurred on the PET surface, due to the oxyfluorination treatment.

For all of the NWF scaffolds investigated, oxyfluorination was superior to direct fluorination for surface modification of the NWF scaffolds. The lack of functionality following the direct fluorination treatment may be due to the low F content (5:95 F_2:N_2) which was present during the direct fluorination as compared to the oxyfluorination treatment (20:80 F_2:N_2). The low fluorine content in the former may have been insufficient to replace a significant number of H atoms on the polymer backbones. Additionally studies have previously reported that F_2/O_2 gas mixtures achieve stronger fluorination compared to when F_2 is used alone (Lee et al., 2003). It is known that fluorine requires a Lewis acid such as O_2 due to its small orientational polarizability, such that when oxygen is present, it acidifies the surface and the fluorination reaction is kinetically more favourable whereby F_2 is reduced to the basic F^- anion (Lee et al., 2003). Hence the Lewis acidity of the oxyfluorination process and the higher F content used may have contributed to improving the efficiency of oxyfluorination of the NWF scaffolds.

A summary of the main absorption bands on the oxyfluorinated NWF scaffolds is given in **Table 5.4**. Of the polymers investigated in this study, PP displayed the highest modification after oxyfluorination, which was followed by nylon and then PET. PP was easily modified by fluorination, due to the tertiary C in its structure (**Figure 5.4**). It is well-known that tertiary C-H bonds are the weakest, and that tertiary H's are abstracted at the fastest rate compared to secondary or primary hydrogens (Pryor, 1966). Hence of the polymers investigated, PP was the most susceptible to forming free radicals. Nylon was also easily modified by oxyfluorination, however due to its smaller pore size, the nylon NWF scaffolds were not preferred for cell culture. PET, on the other hand was the least susceptible to formation of free radicals due to the resonance effect of the aromatic ring. PET displayed a relatively poor propensity to form free radicals on the polymer backbone (Bhattacharya et al., 2004).

Table 5.4: Summary of new functional groups present on the NWF scaffold which was detected by ATR-FTIR after oxyfluorination.

Sample	Wavenumber / cm^{-1}	Peak Assignment
Oxyfluorinated PP	3100 - 3700 1744 1624 900-1300	O-H C=O C=O or C=C C-F
Oxyfluorinated Nylon	3500-3700 1738 900-1300	O-H C=O C-F
Oxyfluorinated PET	3300-3700	O-H

5.3.2.2 Assessment of PNIPAAm grafted NWF scaffolds

To ensure all PNIPAAm homopolymer was removed from the grafted NWF scaffolds, grafted scaffolds were thoroughly washed in cold water for several days prior to analysis. PNIPAAm homopolymer is water soluble at temperatures < 32℃. Graft polymerisation was performed on the oxyfluorinated and pure NWF scaffolds (control) with and without APS as the initiator.

1) ATR-FTIR analysis of PNIPAAm

The ATR-FTIR spectrum for PNIPAAm is given in **Figure 5.9**. The most distinctive absorption bands for PNIPAAm was the broad associated amide (N-H) stretching (~3300 cm^{-1}), triplet peaks assigned to the asymmetric and symmetric stretches of the methyl groups (at 2971 cm^{-1} and 2880 cm^{-1} respectively) and the anti-symmetric stretch of the methylene group (at 2930 cm^{-1}). Additionally sharp amide I peaks (C=O and C-N stretching) and amide II (N-H deformation bands and C-N stretching) occurred at 1639 cm^{-1} and 1529 cm^{-1} respectively. A summary of the main absorption peaks for PNIPAAm homopolymer is tabulated in **Table 5.5**.

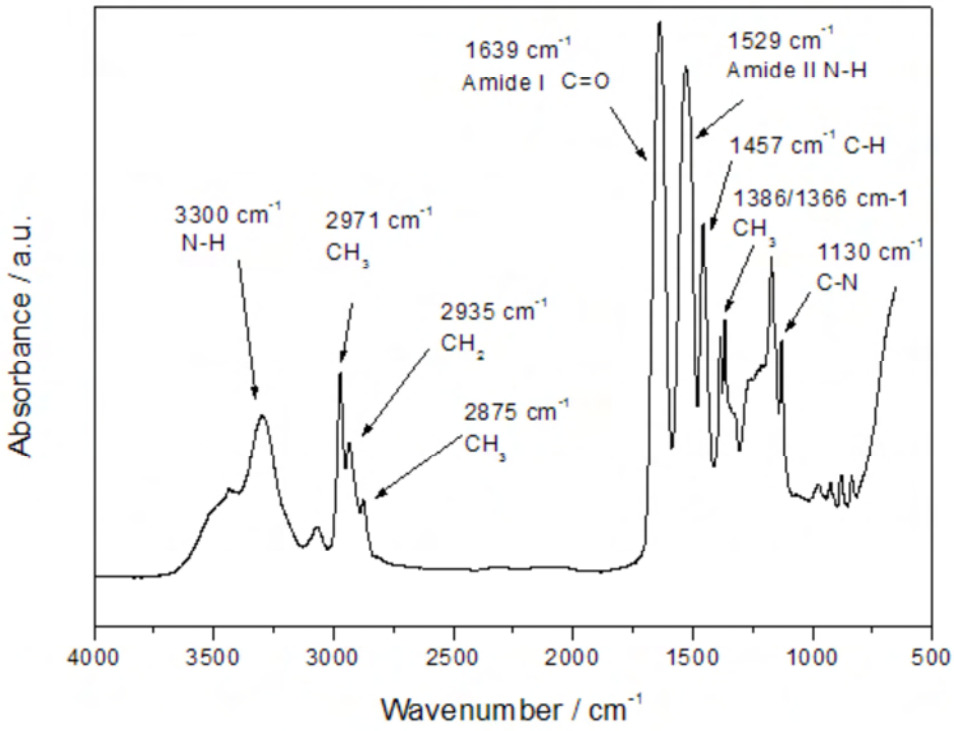

Figure 5.9: ATR-FTIR spectrum for pure PNIPAAm (Sigma).

Table 5.5: The FTIR absorption peak assignment for pure PNIPAAm homopolymer.

Functional group	Wavenumber / cm^{-1}	Assignment
Methyl CH_3	2971	C-H asymmetric stretch
	2875	C-H symmetric stretch
	1457	C-H asymmetric bend
	1386/1366	Isopropyl (doublet)
Methylene CH_2	2935	C-H asymmetric stretch
	2875	C-H symmetric stretch
	1457	C-H bend
Amide	3300-3100	Associated N-H stretch
	3065	Overtone of amide II N-H
	1639	Amide I C=O and C-N stretch
	1529	Amide II N-H in plane deformation (bend) and C-N stretch
	1130	Amide III C-N stretch and NH in plane deformation

2) ATR-FTIR spectra of PP-*g*-PNIPAAm

The ATR-FTIR spectra when graft polymerisation was performed on the functionalised PP NWF scaffolds appear in **Figure 5.10**. After graft polymerisation new peaks associated with PNIPAAm appeared on the grafted PP NWF following both the oxyfluorination and direct fluorination treatments. For the grafted PP NWF scaffolds, the new peaks occurred at 3290 cm^{-1} and 3301 cm^{-1}; 1643 cm^{-1} and 1644 cm^{-1}; and 1542 cm^{-1} respectively which were assigned to the amide (N-H) stretching vibration, amide I (C=O and C-N) stretching and amide II (N-H deformation and C-N stretching) bands respectively. The presence of PNIPAAm absorption bands in the grafted NWF scaffolds, confirmed the PNIPAAm layer on the PP-*g*-PNIPAAm NWF. The CH_3 and CH_2 peaks for pure PP were still present on both grafted samples indicating that the PP backbone was preserved during graft polymerisation. Additionally from **Figure 5.10** it was observed that the C=O peak which was present on the oxyfluorinated PP NWF prior to grafting, diminished after graft polymerisation. Also the broad C-F stretching vibration after oxyfluorination, could still be detected on the grafted NWF but it was reduced (**Figure 5.10b**). We identified the C=O peak on the oxyfluorinated NWF as a possible fluorinated ester which may have being hydrolysed during graft polymerisation.

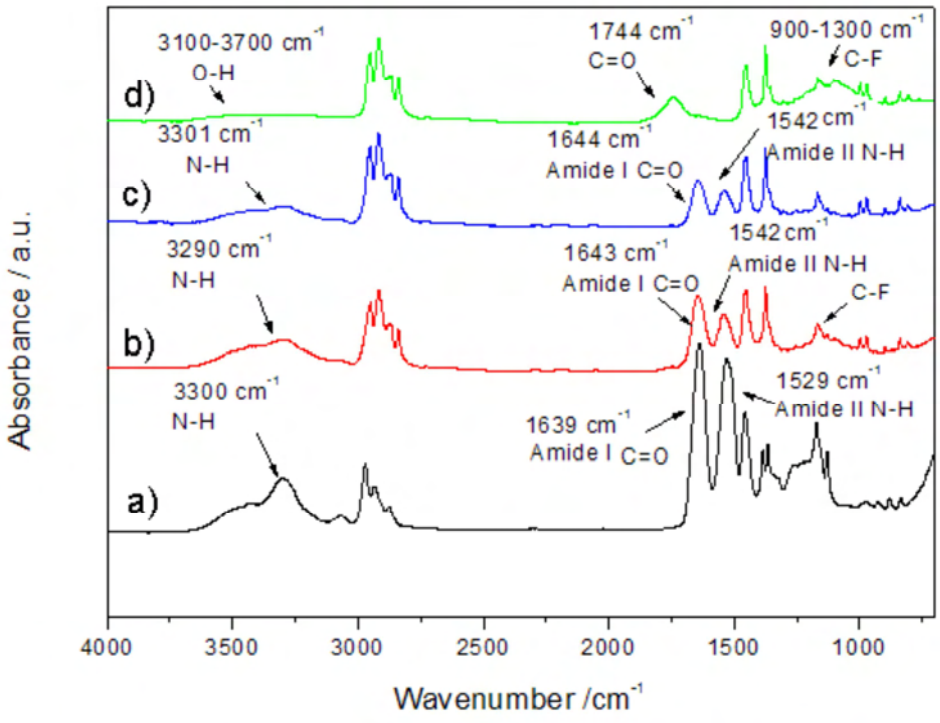

Figure 5.10: ATR-FTIR spectra of (a) PNIPAAm homopolymer control, (b) PP-*g*-PNIPAAm (grafting on oxyfluorinated PP), (c) PP-*g*-PNIPAAm (grafting on direct fluorinated PP); (d) oxyfluorinated PP control.

Interestingly shifts in the amide I and II peaks were observed for the grafted PP NWF (for both oxyfluorinated and direct fluorinated PP) compared to PNIPAAm homopolymer indicating a change in the molecular structure of the groups. For the PP-*g*-PNIPAAm NWF, the amide I and amide II bands shifted to higher wavenumbers (**Table 5.6**) after grafting which could be due to a change in H-bonding (Liu et al., 2005).

Table 5.6: FTIR absorption wavenumbers for PNIPAAm and PP-*g*-PNIPAAm on pre-oxyfluorinated surfaces.

NWF	C=0 / cm^{-1}	N-H / cm^{-1}
Pure PNIPAAm	1639	1529
PP-*g*-PNIPAAm	1643	1542

It is known that H bonding associated with the C=O group in a molecular structure can influence the position of absorption bands in the IR region. According to Lui *et al* the stronger the H bonding involving the C=O group, the lower the electron density surrounding the C=O group, hence the lower the absorption frequency and wavenumber. It is known that in PNIPAAm, intramolecular H bonding occurs between the C=O and N-H groups (**Figure 5.11**).

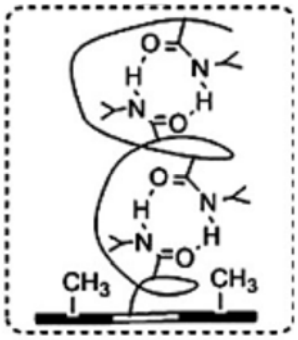

Figure 5.11: Schematic showing intramolecular H bonding between the C=O and N-H groups in PNIPAAm which can influence the absorption frequencies for the amide I and II groups (Gu et al., 2011).

It can be postulated that in the grafted structure, the placement of PNIPAAm moieties on the PP backbone is irregular therefore less H bonding is expected between the C=O and N-H groups compared to pure PNIPAAm, where the molecules are more densely packed than in the graft. Weaker H bonding would then result in a higher electron density available around the amide I and II groups which would result in higher absorption wavenumbers for both groups.

Graft polymerisation was also performed on pure non-functionalised PP as a control **(Figure 5.12)**. Results indicated that without functionalisation, PNIPAAm was still detected on the PP surface following graft polymerisation even though the PP surface was thoroughly washed following graft polymerisation. This was confirmed by the amide I and amide II peaks. It was postulated that the presence of PNIPAAm on the PP surface may be due to homopolymer adsorption rather than grafting. The PNIPAAm peak intensities on the pure grafted PP were substantially lower compared to when the scaffolds were fluorinated prior to grafting.

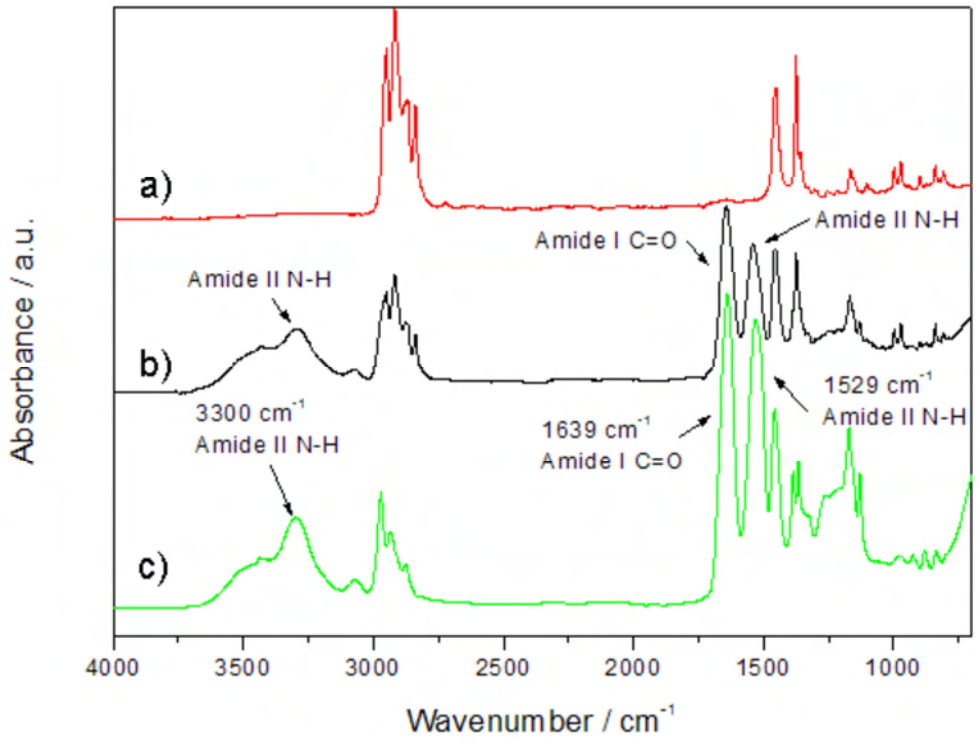

Figure 5.12: ATR-FTIR spectrum of (a) PNIPAAm homopolymer; (b) PP surface after graft polymerisation (without pre-functionalisation); and (c) pure PP.

3) ATR-FTIR spectra of PET-*g*-PNIPAAm NWF

The ATR-FTIR spectra for the grafted PET NWF scaffolds when oxyfluorinated and pure NWF scaffolds were used appear in **Figures 5.13 - 5.14**. For the grafted PET NWF scaffold, the presence of PNIPAAm peaks in the grafted scaffolds could not be clearly identified when either oxyfluorinated or direct fluorinated PET NWF scaffold was used. On closer examination, however a small amide peak was visible around 3300 cm^{-1}. This peak was more discernible when pure PET was used (**Figure 5.14**), which may be due to homopolymer formation on the pure PET surface. Additionally for both samples, the C=O peak at 1712 cm^{-1} displayed a shoulder peak which was assigned to the amide I C=O and C-

N peak of PNIPAAm. Furthermore a small peak at 1540 cm^{-1} associated with the amide II deformation peak of N-H and C-N stretch was also detected.

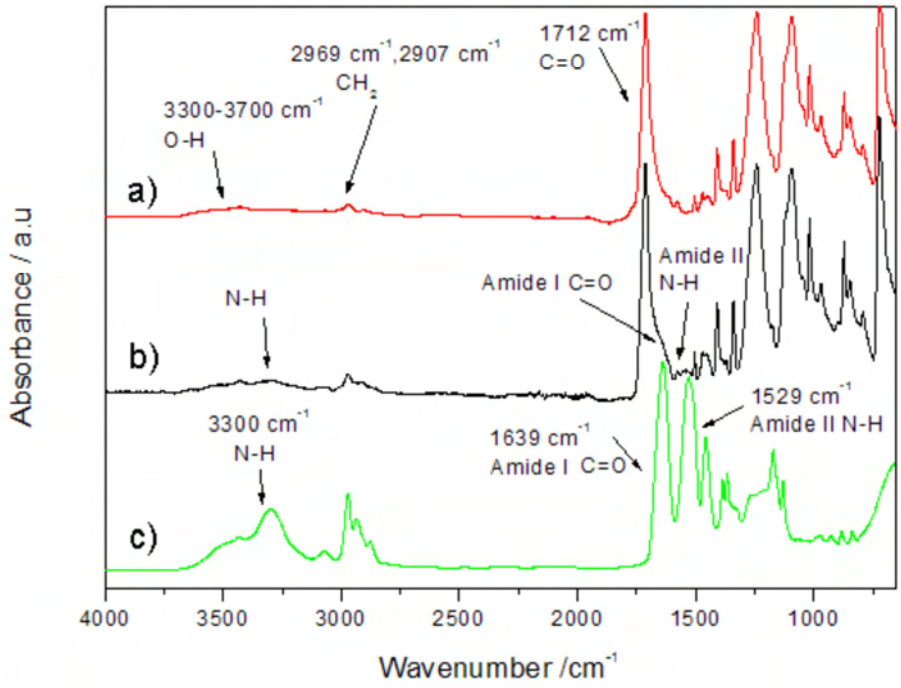

Figure 5.13: ATR-FTIR spectra of (a) pure PET NWF; (b) PET-*g*-PNIPAAm (pre-oxyfluorinated) (c) PNIPAAm control.

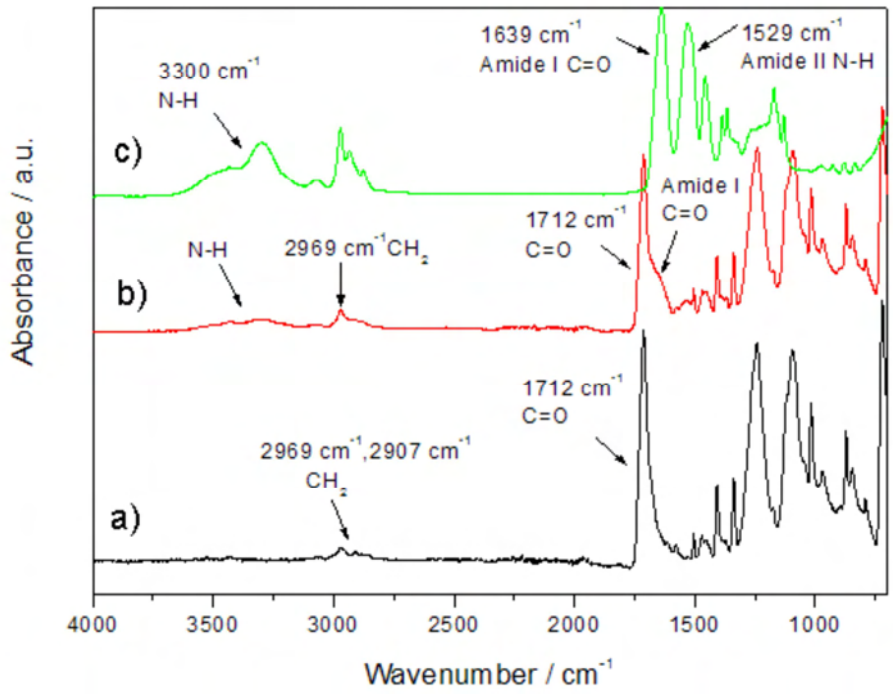

Figure 5.14: ATR-FTIR spectrum of (a) pure PET NWF; (b) PET-*g*-PNIPAAm (without pre-functionalisation); and (c) PNIPAAm.

4) ATR-FTIR spectra for nylon-*g*-PNIPAAm

The ATR-FTIR spectra for nylon-*g*-PNIPAAm when oxyfluorinated nylon was used appear in **Figure 5.15.** Detection of PNIPAAm in the nylon-*g*-PNIPAAm NWF scaffolds posed a challenge since both nylon and PNIPAAm are polyamides, and display similar functional groups and similar absorption bands are expected in the infrared region. Hence the amide I and II absorption regions could not be used for detecting PNIPAAm chains on the nylon surface. The difference in chemical composition between PNIPAAm and nylon, is that only the former contains a methyl group. Other authors have reported that the absorption band of 2970 cm^{-1} attributed to the CH_3 asymmetric stretching of PNIPAAm chains can be used to monitor the grafting of PNIPAAm onto nylon (Wang and McCord, 2007).

From **Figure 5.15**, the CH_3 stretching peak due to PNIPAAm could not be detected on the grafted nylon NWF, indicating that graft polymerisation may have been unsuccessful however due to the small intensity of the 2970 cm^{-1} peak in PNIPAAm, use of this peak was not reliable for confirming graft polymerisation on nylon.

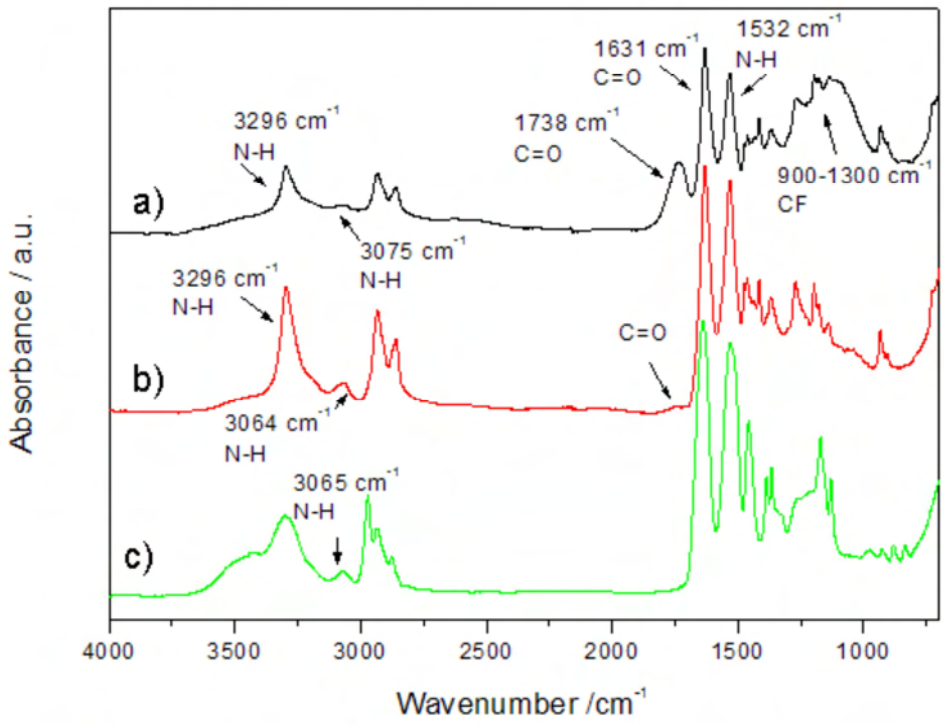

Figure 5.15: ATR-FTIR spectrum of (a) oxyfluorinated nylon NWF; (b) nylon-*g*-PNIPAAm (pre- oxyfluorinated), and (c) PNIPAAm homopolymer control.

However it was observed that the N-H overtone vibration band which appeared at 3075 cm^{-1} on the oxyfluorinated nylon shifted to 3064 cm^{-1} in the nylon-*g*-PNIPAAm spectrum, which corresponded to the N-H overtone band in pure PNIPAAm (i.e. 3065 cm^{-1}). Additionally it was also observed that the new functional groups i.e. C=O, C-F, and O-H (present after oxyfluorination) were reduced after graft polymerisation as was the case when graft polymerisation was on oxyfluorinated PP. Similar results were seen when graft polymerisation was conducted on pure nylon. However after analysis of various spots on the grafted nylon NWF, the CH_3 peak was detectable on some areas of the NWF confirming that the PNIPAAm layer was present; however the graft layer varied and was non-homogenous **(Figure 5.16).** Since no active groups were present on the pure nylon to induce grafting, it was postulated that homopolymerisation formed on pure nylon surface during graft polymerisation.

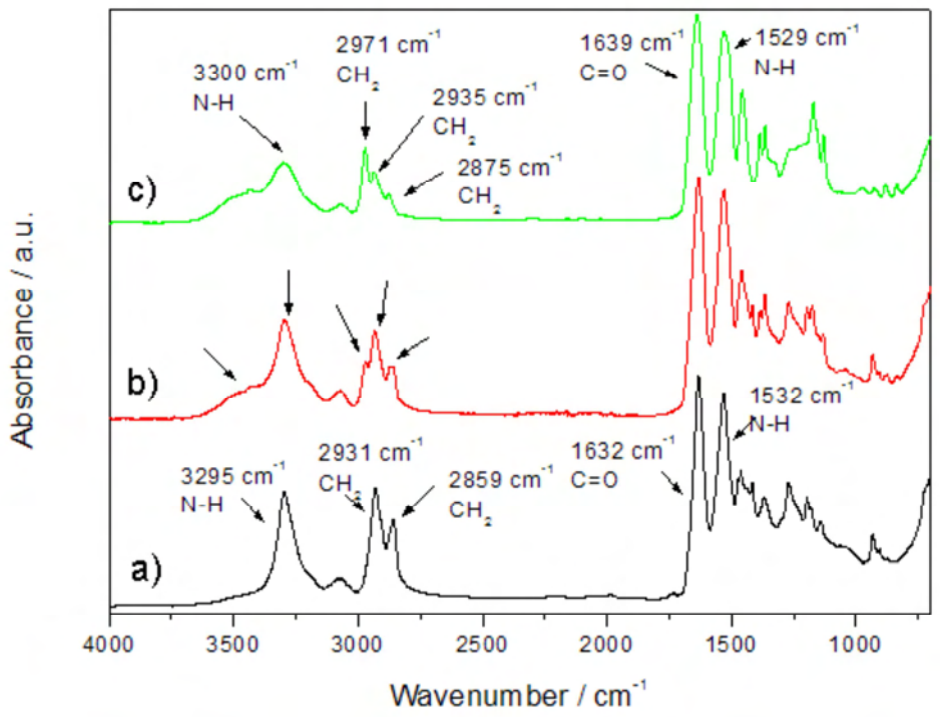

Figure 5.16: ATR-FTIR spectra of (a) pure nylon NWF; (b) nylon-*g*-PNIPAAm (without pre-functionalisation) and (c) PNIPAAm homopolymer control.

5) Graft polymerisation on the NWF in the absence of initiator

It has previously been reported that oxyfluorination produces peroxide and hydroperoxide groups on the surface of polymers which can then be used as active sites for graft polymerisation without any exogenous initiators (Jeong et al., 2011). To verify if graft

polymerisation was possible by heat activation only, grafting was attempted on oxyfluorinated and direct fluorinated NWF scaffolds without the use of a chemical initiator. Pure NWF scaffolds were used as the control.

Of all the NWF tested, the PNIPAAm graft layer was only confirmed when the oxyfluorinated PP NWF was used (**Figure 5.17**). Graft polymerisation was unsuccessful without an initiator on the direct fluorinated and pure NWF scaffolds (data not shown). This result indicates that either peroxides or trapped free radicals (peroxy, fluorine) are present on the oxyfluorinated PP NWF. Upon heating, the peroxide groups would undergo cleavage to form active peroxy radicals, or trapped radicals would diffuse out to the surface which can then induce initiation of the graft polymerisation reaction without requiring an exogenous initiator.

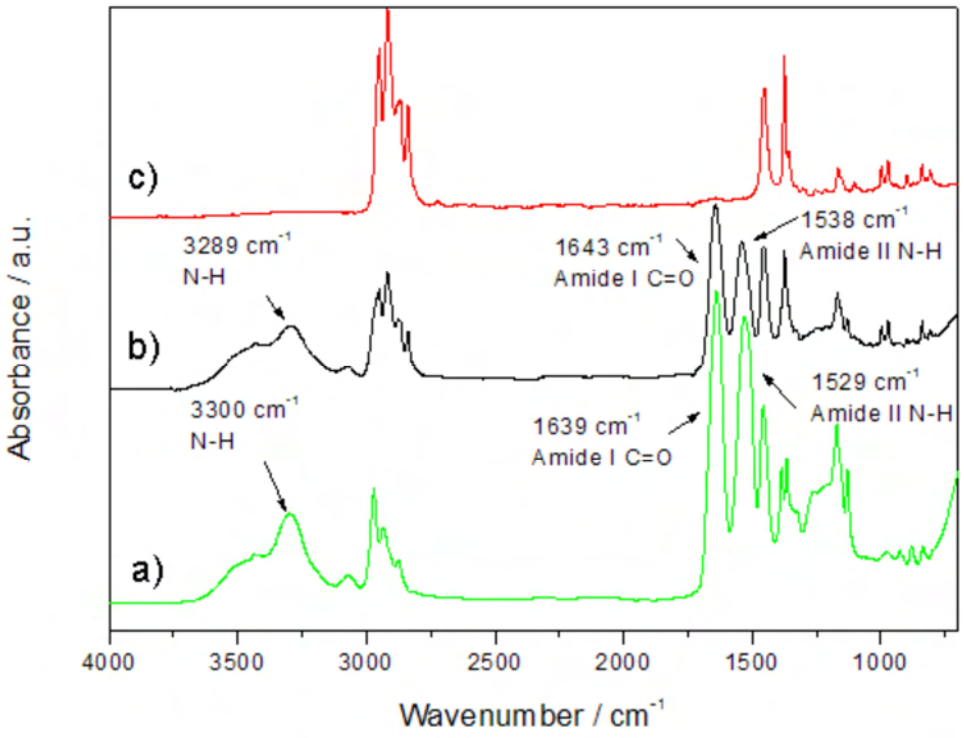

Figure 5.17: ATR-FTIR spectra of (a) PNIPAAm control; and PP-*g*-PNIPAAm NWF scaffolds when graft polymerisation was without initiator and grafting was performed on (b) oxyfluorinated PP NWF; and c) direct fluorinated PP NWF.

However using both oxyfluorinated PET and nylon NWF scaffolds, PNIPAAm could not be detected on the grafted surfaces by ATR-FTIR, using this method, which indicates that peroxy groups or trapped peroxy radicals were absent on these surfaces or were insufficient to induce a significant amount of graft chains on the polymer backbone. Also as we observed previously when graft polymerisation was performed on oxyfluorinated PP, the new functional groups following oxyfluorination (i.e. C=O, O-H, C-F) were reduced after graft

polymerisation. Seeing that grafting could not be confirmed on the nylon NWF scaffolds using ATR-FTIR, it can be assumed that C-F and C=O functional groups (which were also reduced for nylon) do not play a role in initiating graft polymerisation, and these bonds are not the active sites for grafting.

6) Graft yield determination from ATR-FTIR

To determine the graft yield of PNIPAAm onto PP NWF, a semi-quantitative calibration graph was constructed based on the peak area ratios of the C=O peak (at 1644 cm^{-1}) to the C-H peak on PP (at 1455 cm^{-1}). Flat disks were incubated in a series of PNIPAAm solutions of known concentrations in polytops. PNIPAAm of a known mass was precipitated on the PP disks, and the peak area ratios were measured. The difference in intensity of the peaks was attributed to the concentration or mass of the PNIPAAm layer. Anova single factor statistical test was conducted to determine the statistical significance of the results. Accurate results could not be obtained when the NWF scaffolds were used for determining the calibration graph due to the porous structure of the NWF scaffolds. The calibration graph is given in **Figure 5.18**.

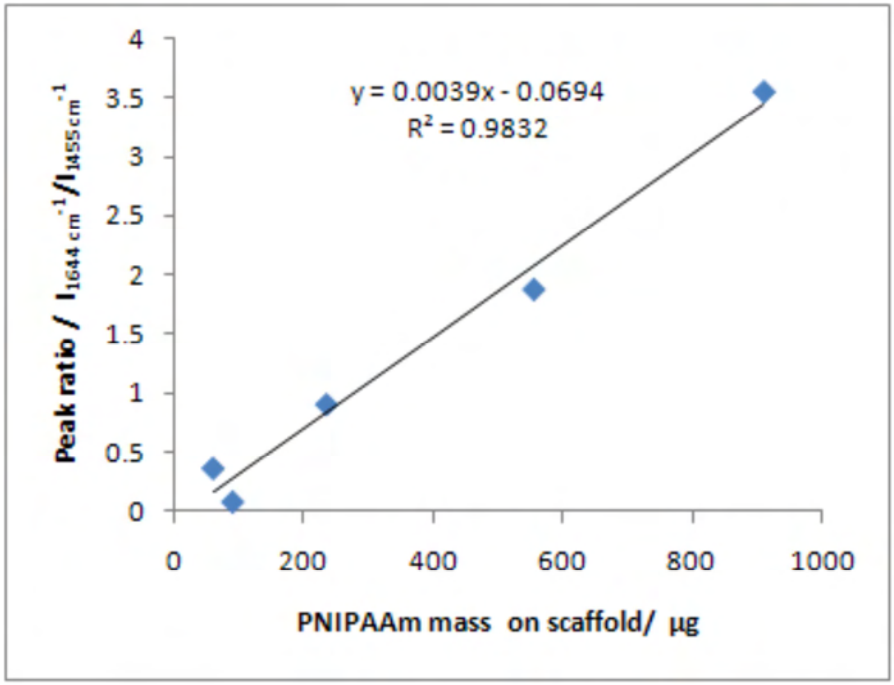

Figure 5.18: Calibration graph showing relationship between PNIPAAm mass on scaffolds and intensity of the peak area ratios of the C=O peak (at 1644 cm^{-1}) to the CH_3 peak in PP (at 1455 cm^{-1}).

From the equation of the graph, parameter x (i.e. PNIPAAm mass) was calculated as follows:

x=(y + 0.0694) / 0.0039 (Eq 5.5)

Where y is the peak area ratios and x is the PNIPAAm mass.

The graft yield was expressed as PNIPAAm mass/ total surface area of the NWF disks. The total surface area of the NWF disks (**Equation 5.13**) was derived for PP (T4-N13) using the NWF physical properties as follows:

- NWF disk area (A_{NWF}):

  $$A_{NWF} = \pi r^2$$ (Eq 5.6)

  Where r is the radius of the NWF disk (0.075 cm), and π = 3.14159.

- NWF weight (M_{NWF}):

  The mass of the NWF could be determined by weighting the sample or alternatively it could be calculated from the A_{NWF} (m^2) and the mean area weight M/A_{NWF} (g/m^2) as follows:

  $$M_{NWF} = A_{NWF} * M/A_{NWF}$$ (Eq 5.7)

- NWF volume (V_{NWF})

  The volume of the NWF (V_{NWF}) was calculated using the M_{NWF} (g) and the density of PP (ρ) (g/cm^3) as follows:

  $$V_{NWF} = \frac{M_{NWF}}{\rho_{NWF}}$$ (Eq 5.8)

  ρPP was taken as 0.903 g/cm^3

- Total surface area of NWF(A_{Total})

  The total surface area of the NWF can be determined using the volume of a fibre as follows:

  $$A_{total} = \pi dl$$ (Eq. 5.9)

  Where π = 3.14159, d is the diameter of a fibre, and l is the length of a fibre. The Volume of a fibre (V_{fibre}) is as follows:

  $$V_{fibre} = \frac{\pi}{4} d^2 l$$ (Eq 5.10)

  Where $l = \frac{4 * V_{fibre}}{\pi d^2}$ (Eq 5.11)

  $$A_{NWF} = \pi d * \frac{4 * V_{fibre}}{\pi d^2}$$ (Eq 5.12)

A_{total} (cm^2) was then derived as: $A_{NWF} = \frac{4V_{NWF}}{d_{fibre}}$ (Eq. 5.13)

By dividing by the mass of the NWF the total surface area per 1 g of NWF could be determined.

The total surface area of the PP NWF disks with mean flow pores of 200 µm (T3-N13) was determined to be ~25 cm^2 i.e. ~1400 cm^2/g. This compares relatively well to some of the 3D scaffolds on the market (**Table 5.7**). It should be noted that the total surface area available for cell culture in the bioreactor can be increased substantially by stacking a number of NWF disks onto each other.

Table 5.7: Relative surface areas of currently available 3D scaffolds versus NWF scaffold of present study (Fibra-Cel ® disks, 2012; GE Healthcare, 2012).

Competing 3D scaffolds	**Surface area (cm^2/g)**
Fibra-Cell disks	1200
Cytodex 1	4400
Cytodex3	2700
PP NWF scaffold of present study	~1440

Using the graft yield and a density of PNIPAAm of 1.1 $g.cm^3$, the graft thickness could also be calculated by **Equation 5.14** as follows:

$$\text{Graft thickness (nm)} = \frac{\text{Graft yeild (g/cm}^2\text{)}}{\rho_{\text{PNIPAAm}}\left(\frac{\text{g}}{\text{cm}^3}\right)} * 10^7 \quad \text{(Eq 5.14)}$$

The graft yield for PP-*g*-PNIPAAm NWF scaffolds when grafting was on oxyfluorinated and pure PP NWF appear in **Figure 5.19**. PNIPAAm graft yield on the PP NWF was ~24 ± 6 µg/cm^2 on grafted pre-oxyfluorinated NWF when APS was used; which was found to be significantly higher compared to when pre-oxyfluorinated NWF was used without initiator (9 ± 6 µg/cm^2, p= 1.7x10^{-7}); or when grafting was on pure PP with APS (2 ± 0.3 µg/cm^2, p = 8.4x10^{-12}). This corresponded to an average PNIPAAm layer thickness of ~220 ± 54 nm; 92 ± 60 nm; and 19 ± 3 nm respectively. For the pure PP NWF scaffolds, it is postulated that PNIPAAm homopolymer formed on the PP surface rather than grafting. When grafting was performed on the oxyfluorinated PP without initiator, large deviations were observed between samples, which may be attributed to the instability of the peroxide groups and/or the trapped radicals on the PP surface upon storage.

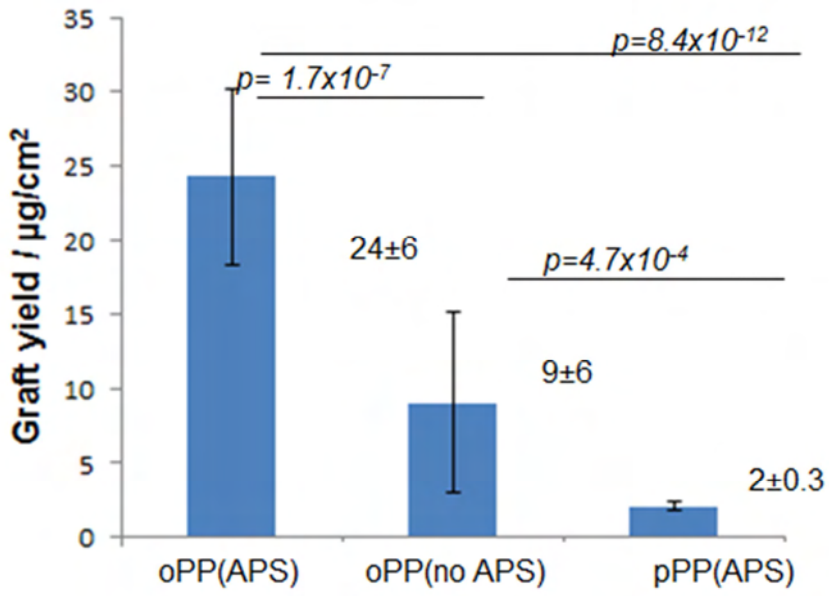

Figure 5.19: Graft yield determination for PP-*g*-PNIPAAm whereby grafting was performed on oxyfluorinated PP with APS treatment [oPP(APS)]; oxyfluorinated PP without APS treatment [oPP(no APS)], and pure PP with APS treatment [pPP(APS)].

PNIPAAm surfaces with various graft thickness have been developed previously for cell culture. Studies conducted by Akiyama *et al* have demonstrated that endothelial cells only attached onto PNIPAAm TCPS trays of graft thickness 15.5 nm ± 7.2 nm (1.4 ± 0.1 µg/cm^2), whereas no cells attached on surfaces when the graft layer was thicker (29.3 nm ± 8.4 nm, i.e. 2.9 ± 0.1 µg/cm^2) (Akiyama et al., 2004). An optimum PNIPAAm graft thickness of ~15-20 nm was reported for optimal cell attachment/release (Akiyama et al., 2004). In the present study, the graft thickness reported is relatively high. However as discussed in **Chapter 2**, discrepancy exists in the literature with regards to the optimum graft thickness (Kumashiro et al., 2010). Also it should be noted that the morphology of the NWF of the current study differs substantially to that of 2D TCPS on which most of the previous studies are based. Hence the dehydration/hydration of the PNIPAAm layer to enable cell attachment/release will also be different. Refer to **Chapter 6** for the cell culture studies using the PP-*g*-PNIPAAm NWF scaffolds.

5.3.3 XPS analysis

Since graft polymerisation on PP gave the most promising results, XPS analysis was only performed on the PP NWF scaffolds.

5.3.3.1 XPS analysis of functionalised NWF scaffolds

To investigate the changes to the chemical functionality of the NWF scaffold surfaces after fluorination, XPS studies were also conducted. The wide XPS spectra for pure PP NWF, direct fluorinated PP NWF, and oxyfluorinated PP NWF appear in **Figure 5.20**.

For the pure PP NWF, mainly C (and a small amount of oxygen) was detected, however for the direct fluorinated and oxyfluorinated PP, various functional groups including oxygen, fluorine, and nitrogen formed on the surface of PP. The new functional groups display high electronegativity and could be responsible for increasing the hydrophilicity of the direct fluorinated and oxyfluorinated PP (Woo et al., 2005).

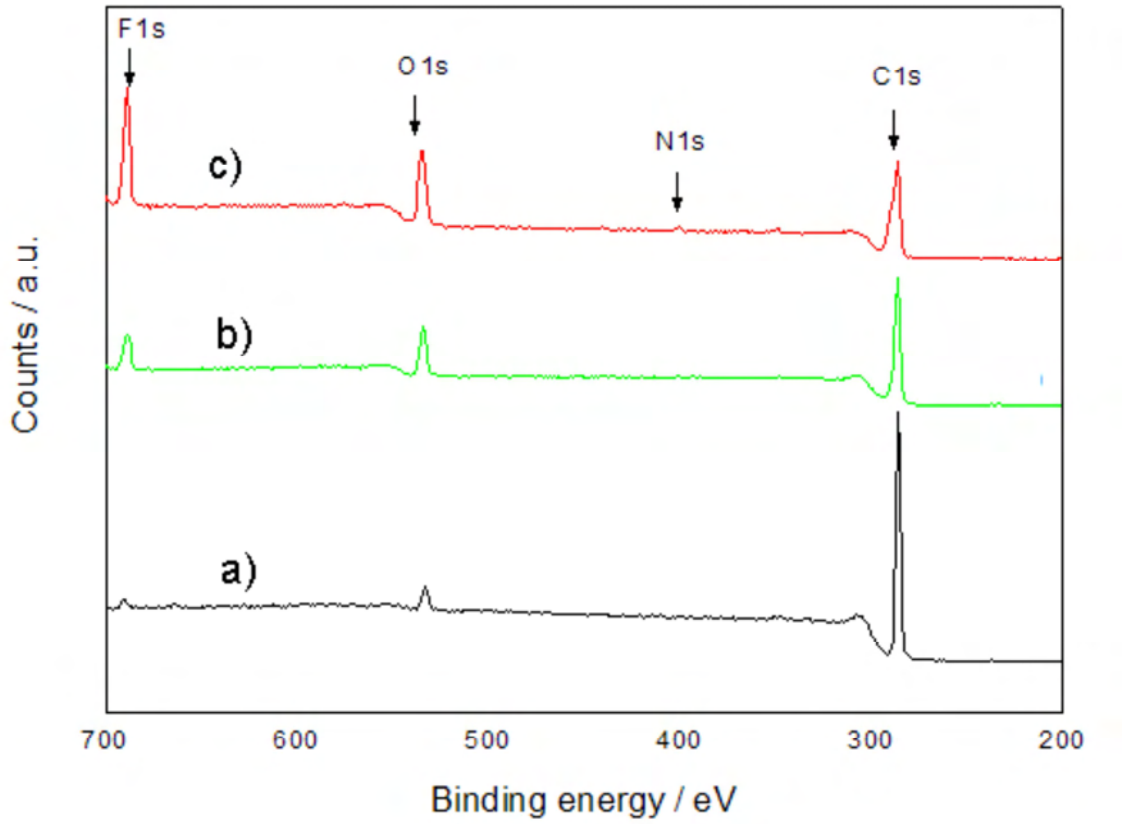

Figure 5.20: Wide XPS spectra of (a) pure PP NWF; (b) direct fluorinated PP NWF; and (c) oxyfluorinated PP NWF.

The high resolution C1s spectra for pure PP, fluorinated PP, and oxyfluorinated PP is given in **Figure 5.21**. From the C1s spectra, only one symmetric peak was measured for the pure PP NWF at 284.8 eV (with 100 % peak area), which represents the C-H of the PP backbone (Lee et al., 2003). For the direct fluorinated and oxyfluorinated PP, asymmetric C1s spectra

were observed which were fitted with multiple peaks due to new fluorine and oxygen functionality.

For the direct fluorinated PP the following peaks were identified: 284.8 eV (C-H); 286.5 eV (C-O), and 287.9 eV (CHF-CH_2, CHF-CHF); while for the oxfluorinated PP, peaks were assigned as follows: 284.7 eV (C-H); 286.4 eV (C-O); 287.8 eV (CHF-CH_2, CHF-CHF), and 288.9 eV (C=O) (Lee et al., 2003; Park et al., 2005).

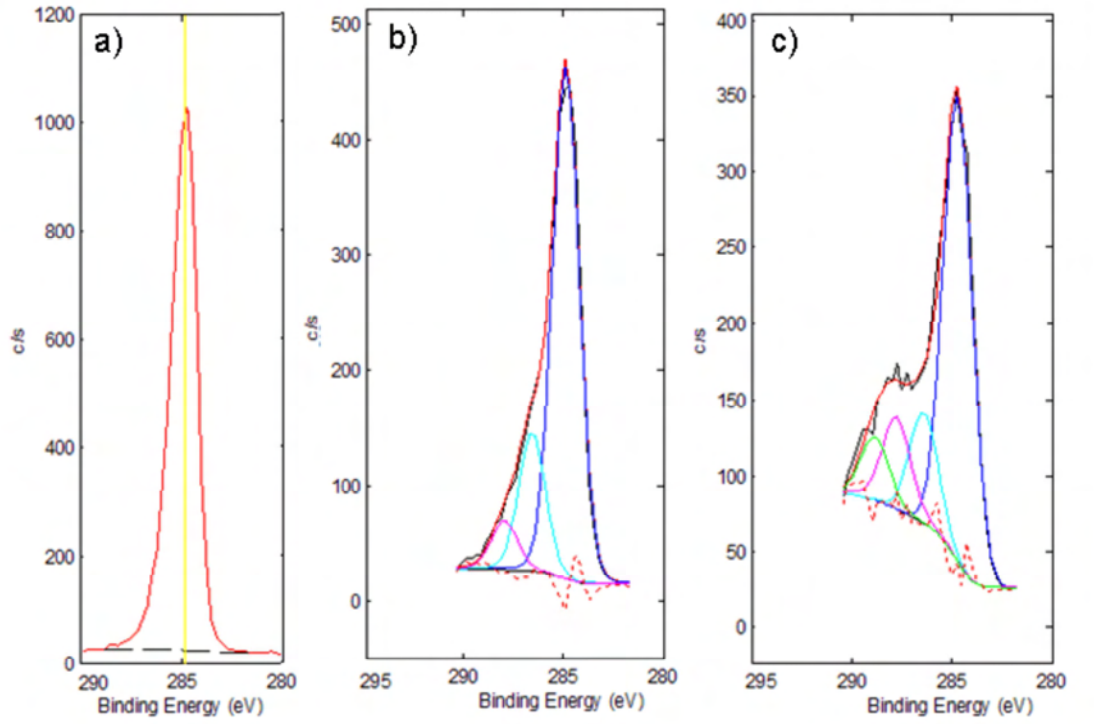

Figure 5.21: Narrow C1s for (a) pure PP NWF; (b) direct fluorinated PP NWF; and (c) oxyfluorinated PP NWF.

From the binding energies in **Table 5.8**, it can be seen that some of the hydrogen's of the C-H group of the PP backbone was substituted with either F or O atoms following the fluorination treatment. The relative amount of the C-H group at 284 eV decreased from 100% for pure PP to 72.69% and 63.12% for direct fluorinated and oxyfluorinated PP respectively. The O1s peak increased from 4.2 % (atomic) for pure PP NWF, to 14.8 % (atomic) and 18.2 % (atomic) for direct fluorinated and oxyfluorinated PP respectively, while F1s peak almost doubled from 9.1 % (atomic) for direct fluorinated PP to 17.9 % (atomic) for the oxyfluorinated sample. These results indicate that the extent of modification was the highest for the oxyfluorination process compared to direct fluorination, and corroborates with the ATR-FTIR data.

Table 5.8: Atomic percent of C, O, F, and N present on the surface of pure and functionalised PP NWF and probable peak assignments (Lee et al., 2003; Park et al., 2005 ; Woo et al., 2005).

Element	Atomic concentration / %	Binding energy / eV	Area %	Assignment
C1s				
Pure PP	94.8	284.8	100	CH
Direct fluorinated PP	76.1	284.8 286.5 287.9	72.69 20.00 7.31	CH C-O CHF-CH_2;CHF-CHF
Oxyfluorinated PP	62.5	284.7 286.4 287.8 288.9	63.12 14.95 13.45 8.49	CH C-O CHF-CH_2;CHF-CHF C=O
O1s				
Pure PP	4.2	532.2	100	C-O
Direct fluorinated PP	14.8	532.6	100	C-O
Oxyfluorinated PP	18.2	533.3	100	C-O-C
F1s				
Pure PP	-	-	-	-
Direct fluorinated PP	9.1	686.9	100	C-F
Oxyfluorinated PP	17.9	687.4	100	C-F
N1s				
Pure PP	-	-	-	-
Direct fluorinated PP	-	-	-	-
Oxyfluorinated PP	1.4	389.8	100	N-H

On pure PP, ~4.2 at% of elemental oxygen was detected from the O1s spectra at 532.2 eV. The presence of a small amount of oxygen on pure PP was reported previously and was attributed to the impurities incorporated in PP as a result of degradation occurring during processing in air (Kranz et al., 1994). Oxygen was also detected on the direct fluorinated PP by XPS, even though O was not directly introduced into the reactor during this process.

It is known that commercial fluorine contains trace amounts of oxygen, and other authors have indicated that fluorination always accompanies oxyfluorination (du Toit and Sanderson, 1999). According to Kranz *et al* even a small O_2 content of 1 vol% during fluorination can still result in significant changes to the oxygen functionality (C=O, COF) (Kranz et al., 1994). The oxygen present in the reactor during the oxyfluorination treatment was mainly from air which was introduced during both the partial evacuation and the cycle purging steps in air.

The high-resolution O1s and F1s spectra for the direct fluorinated and oxyfluorinated PP NWF scaffolds, showed single peaks at 532.2 eV & 533.3 eV and 686.9 eV & 687.4 eV which were assigned to the presence of C-O, and C-F respectively (Park et al., 2005). Formation of fluorinated groups such as -C-F, $-CF_2$, and/or $-CF_3$ are preferential due to the higher energy of the C-F bond compared to C-H (Kharitonov, 2008). Some nitrogen was also detected on oxyfluorinated PP, which may be due to the high N_2 content used during oxyfluorination.

The F/C, O/C, and F/O ratios were higher for the oxyfluorination process compared to direct fluorination (**Table 5.9**). Since the oxyfluorination treatment demonstrated superior performance, oxyfluorinated PP underwent further analysis.

Table 5.9: Atomic ratios for F, C, and O present on pure, direct fluorinated and oxyfluorinated PP surfaces.

Atomic ratios	**F /C**	**O / C**	**F /O**
Pure PP	-	0.04	-
Direct fluorinated PP	0.6	0.2	0.1
Oxyfluorinated PP	1.0	0.3	0.3

5.3.3.2 XPS analysis of PP-*g*-PNIPAAm NWF scaffolds

The C1s XPS spectra for the PP-*g*-PNIPAAm NWF scaffolds, when graft polymerisation was conducted on oxyfluorinated, direct fluorinated and pure NWF scaffolds appear in **Figure 5.22.** In each case, the C1s spectra were fitted with three peaks and peak assignments were as follows: C1s: 284.8-284.9 eV (CH_3, CH_2, CH); 286.5-286.6 eV (CH-NH); 287.9-288 eV (C=O: 10.47). The amide group on the grafted PP NWF was confirmed by the O1s and N1s spectra which displayed single peaks at 531.2 eV(C=O) and 399,6 eV (N-H) respectively (Akiyama et al., 2007).

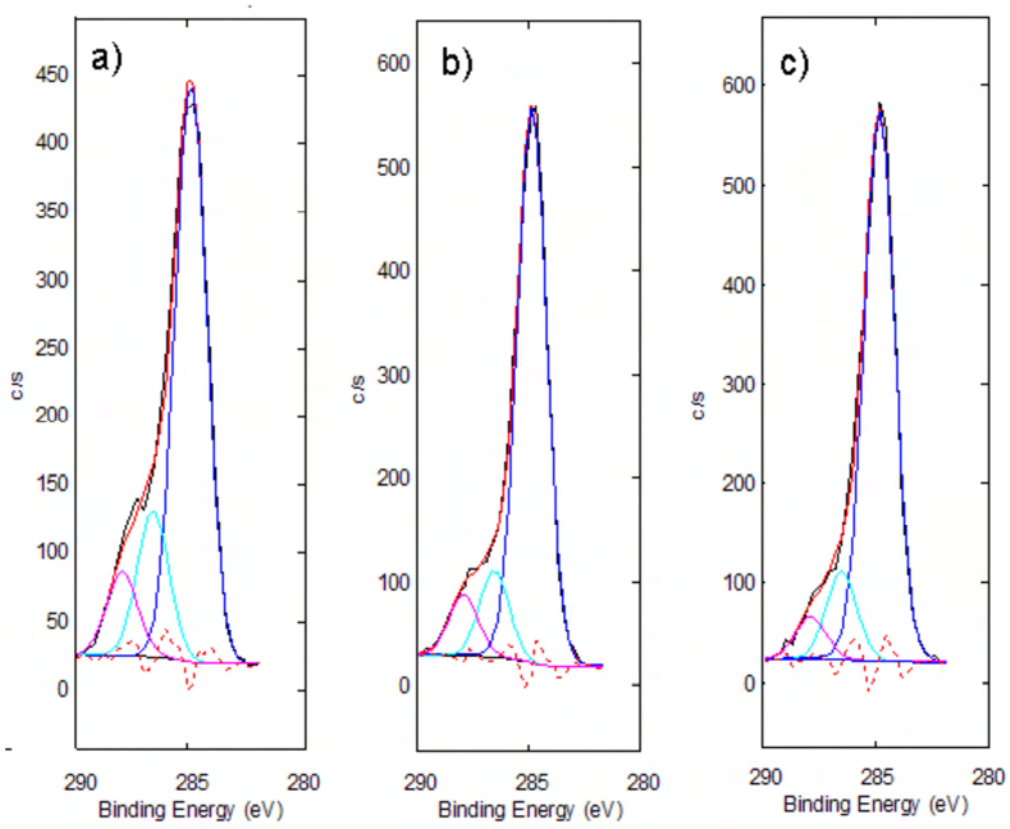

Figure 5.22: Narrow C1s for PP-*g*-PNIPAAm when graft polymerisation was conducted on (a) oxyfluorinated PP NWF; (b) direct fluorinated PP NWF; and (c) pure PP NWF.

The composition of the elements appear in **Table 5.10**. The degree of grafting was estimated from XPS and was based on the N atomic concentration present on the grafted surface as compared to the theoretical N atomic content in PNIPAAm (Akiyama et al., 2007).

Table 5.10: Atomic % of C, N, O, F present on the surface of the PP NWF scaffolds when graft polymerisation was conducted on oxyfluorinated (gNWF1-2), direct fluorinated (gNWF3) and pure NWF (gNWF4) scaffolds.

PP-*g*-PNIPAAm	Functionalisation	APS	Heat	C	N	O	F	Degree of grafting (%)
gNWF1	Oxyfluorination	+	+	74.9	10.4	13.1	1.6	84
gNWF2	Oxyfluorination	-	+	76.8	6.4	13.5	2.8	52
gNWF3	Direct fluorination	+	+	76.6	8.5	13.0	1,5	69
gNWF4	None	+	+	82.6	7.1	10.3	-	57
PNIPAAm calculated				75	12.5	12.5	-	-

The theoretical N content on pure PNIPAAm was calculated to be 12.5% (Akiyama et al., 2007). When graft polymerisation was performed on oxyfluorinated PP NWF surfaces (with APS and heat), the N content was ~10.4 (%) (atomic) which corresponded to a PNIPAAm graft yield was ~84%. This implies that ~84% of the surface was covered by PNIPAAm chains. However more measurements are required per sample, for statistical significance.

5.3.4 SEM analysis

5.3.4.1 Morphology of pure and oxyfluorinated NWF surfaces

SEM images of the pure and oxyfluorinated NWF scaffolds are given in **Figures 5.23-5.24** respectively. The NWF scaffolds were highly porous and displayed open and interconnected pores. All of the NWF displayed a smooth fibre surface. However some artefacts were observed on the surface of the control fibres for all of the NWF scaffolds which could be as a result of accumulation of dust or debris during the non-woven manufacturing process. Furthermore the fibres used in the NWF manufacture may have been treated with a spin finish for commercial applications. Hence the artefacts observed could be due to this treatment process. From **Figure 5.24**, significant surface changes were detectable on the oxyfluorinated PP NWF compared to pure PP. The oxyfluorinated PP surface displayed increased roughness compared to the control and the oxyfluorinated surface contained numerous vein-like cracks which appeared to run across the fibre length. Other authors have also reported an increase in surface roughness on PP and PE following fluorination (Kranz et al., 1994).

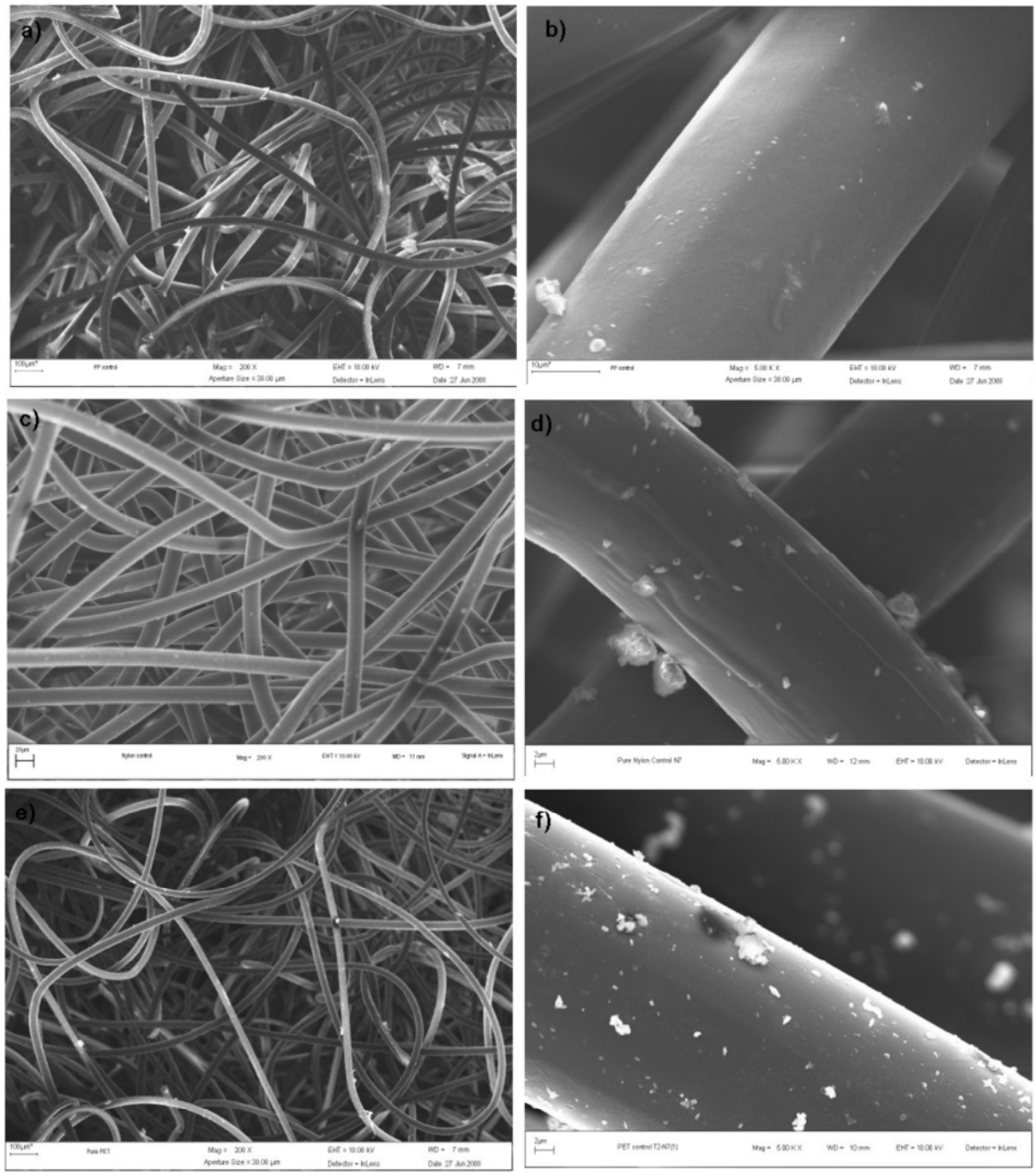

Figure 5.23: SEM images showing the highly porous structures of (a-b) PP NWF (T2-N6 (1)); (c-d) nylon (T3-N7 NWF) and (e-f) PET NWF (T2-N7).

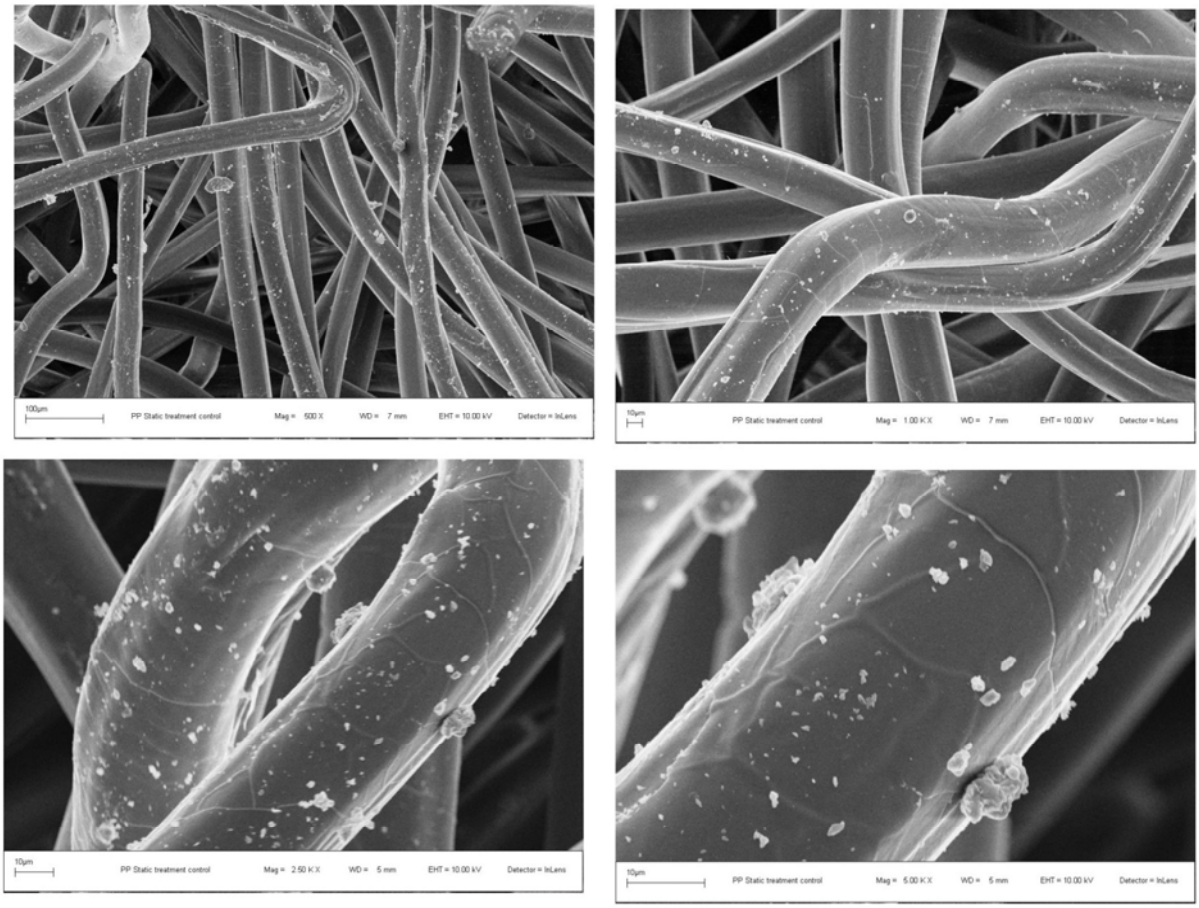

Figure 5.24: SEM images of PP NWF T2-N6 (1) after oxyfluorination.

Fluorination was performed at Pelchem Ltd. Pelchem operates an industrial fluorination plants and due to the large size of the reactor, our samples had to be processed together with other commercial samples during normal operation. All effort was made to ensure that similar processing conditions were maintained for all the samples during oxyfluorination; however we did observe some batch to batch variation amongst samples. The lack of surface functionality on the NWF following direct fluorination was corroborated by the SEM analysis where no significant changes were observed to the surfaces for any of the NWF scaffolds (images not shown).

5.3.4.2 Morphology of PNIPAAm grafted NWF

The SEM images of the PP surface when graft polymerisation was performed on the oxyfluorinated and pure PP NWF scaffolds appear in **Figures 5.25-5.26** respectively. From the SEM analysis, the PP-*g*-PNIPAAm NWF scaffolds prepared by the OAGP method displayed increased roughness and a surface layer was clearly discernible for both methods. The graft layer appeared as node-like structures on the PP surface for the pre-oxyfluorinated

NWF scaffolds (**Figure 5.25**), which was intimately attached on to the fibre surface. The node like structures on the grafted PP surface may have formed at active sites on the polymer backbone. Also the graft layer appeared to be homogenously distributed throughout the sample. This however was in direct contrast to when graft polymerisation was performed on the pure PP NWF scaffolds.

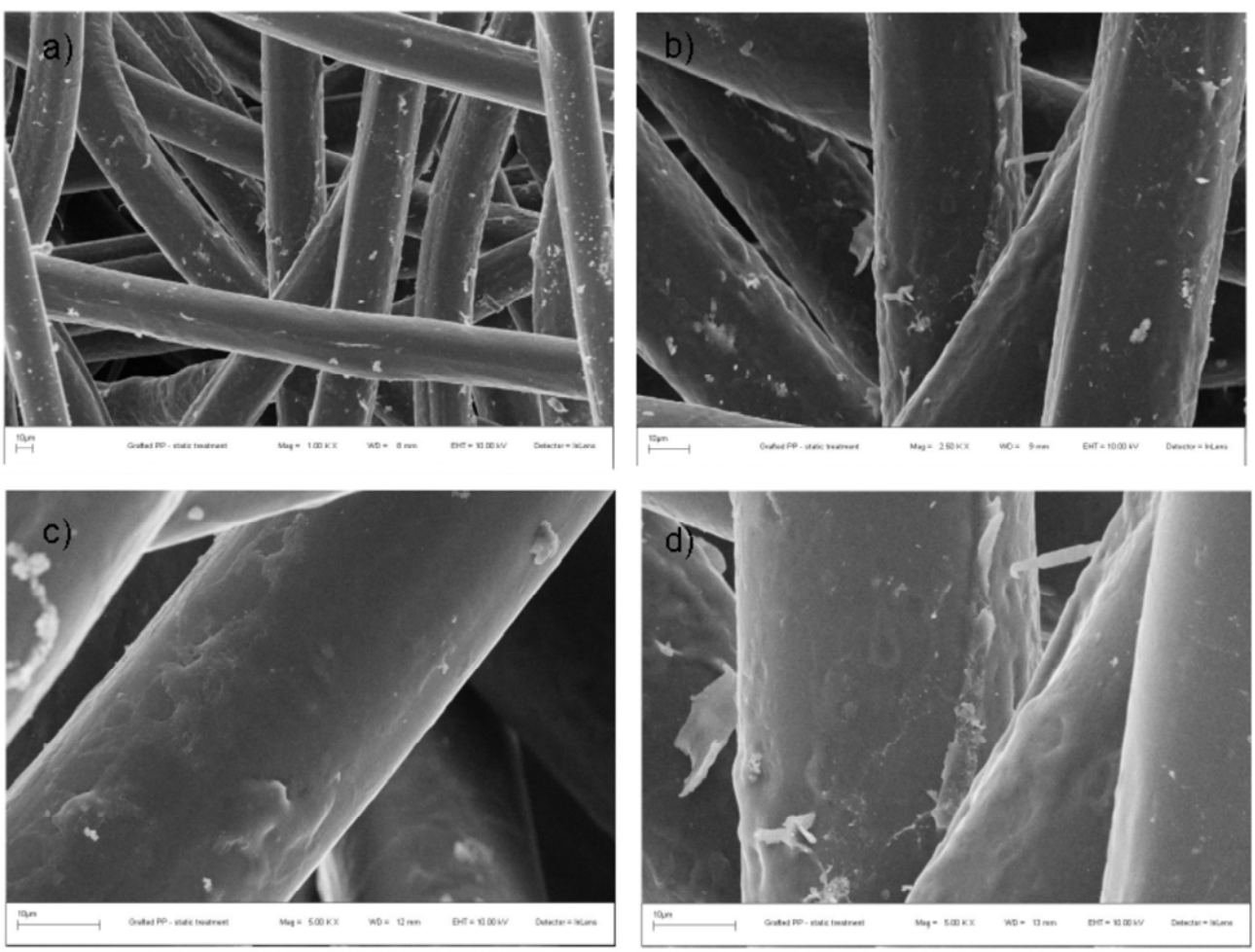

Figure 5.25: SEM images of PP-*g*-PNIPAAm NWF scaffolds at (a) 1000x; (b) 2500x and (c-d) 5000x magnification, where NWF were pre-treated by oxyfluorination and grafting was with an initiator.

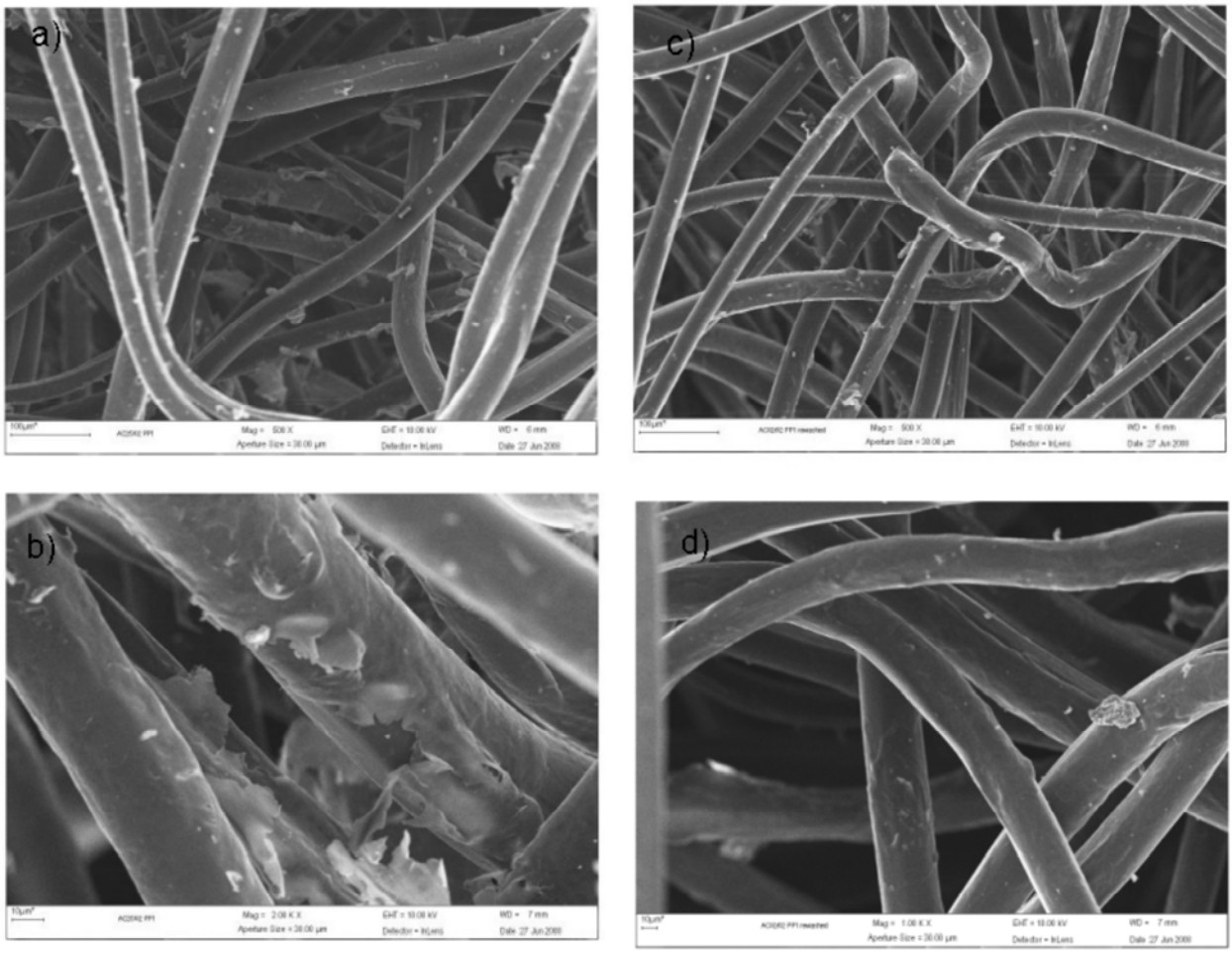

Figure 5.26: SEM images of PP-*g*-PNIPAAm NWF scaffolds when graft polymerisation was conducted on pure NWF, (a-b) shows the surface of the grafted NWF after three days of washing in water; (c-d) shows the same grafted NWF after a second washing cycle of three days.

From **Figure 5.26** it can be seen that when pure non-functionalised PP NWF were used, the PNIPAAm layer appeared to be loosely bound to the fibre surface, and appeared to be "peeling" off the surface. This was attributed to excessive PNIPAAm homopolymer which precipitated and adsorbed onto the pure PP surface during polymerisation. When graft polymerisation was conducted on the pure PP at 70 °C which is above the LCST of PNIPAAm, PNIPAAm is hydrophobic, and will preferentially precipitate onto the pure hydrophobic PP NWF matrix rather than remain in the aqueous solution which may have contributed to the high homopolymerisation seen on the surface of the pure grafted NWF scaffolds. Homopolymer could also be seen within the 3D structure of the NWF scaffolds. This was undesired since the original morphology of the NWF was compromised. To investigate if the layer was covalently attached, a second wash step was conducted on the

PP-*g*-PNIPAAm scaffolds (**Figure 5.26 c-d**). As can be seen after further washing of the PP-*g*-PNIPAAm, the PNIPAAm layer was significantly reduced indicating the presence of PNIPAAm homopolymer on the NWF surface. Due to the elevated temperature, it is possible that the homopolymer becomes entrapped in the PP polymer chains, which would then require prolonged periods of washing to be completely removed.

For the nylon-*g*–PNIPAAm NWF (**Figure 5.27-5.28**), the surface appeared rough, and the PNIPAAm graft layer was clearly visible. When the pre-oxyfluorinated PP NWF surface was used, the PNIPAAm layer was bound on to the fibre surface. Again for the pure nylon surface, homopolymerisation was clearly visible. However the extent of modification was reduced compared to the PP-*g*-PNIPAAm surface.

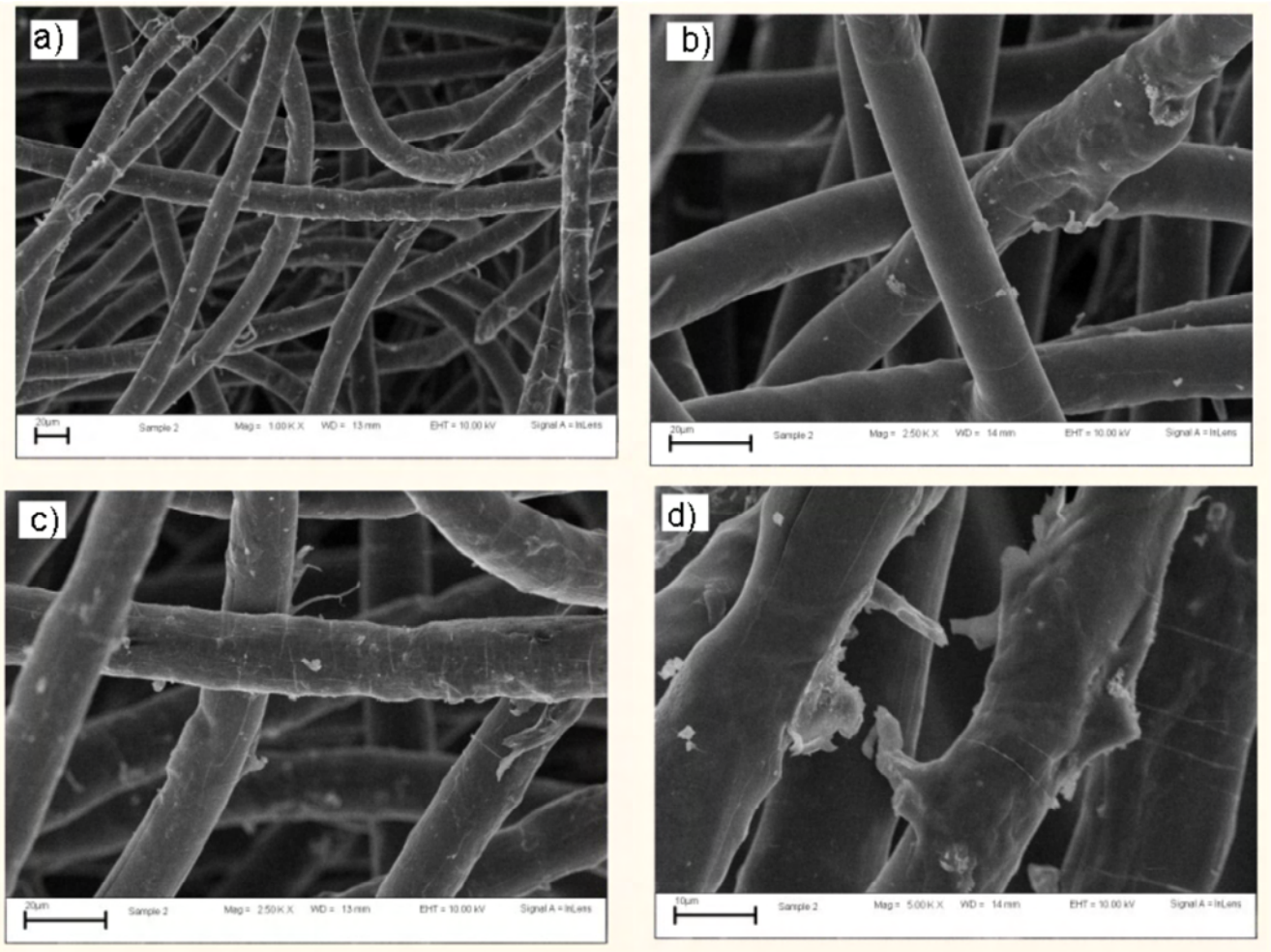

Figure 5.27: SEM images of nylon-*g*-PNIPAAm NWF scaffolds at (a) 1000x; (b-c) 2500x; and (d) 5000x magnification, when grafting was on the oxyfluorinated nylon NWF.

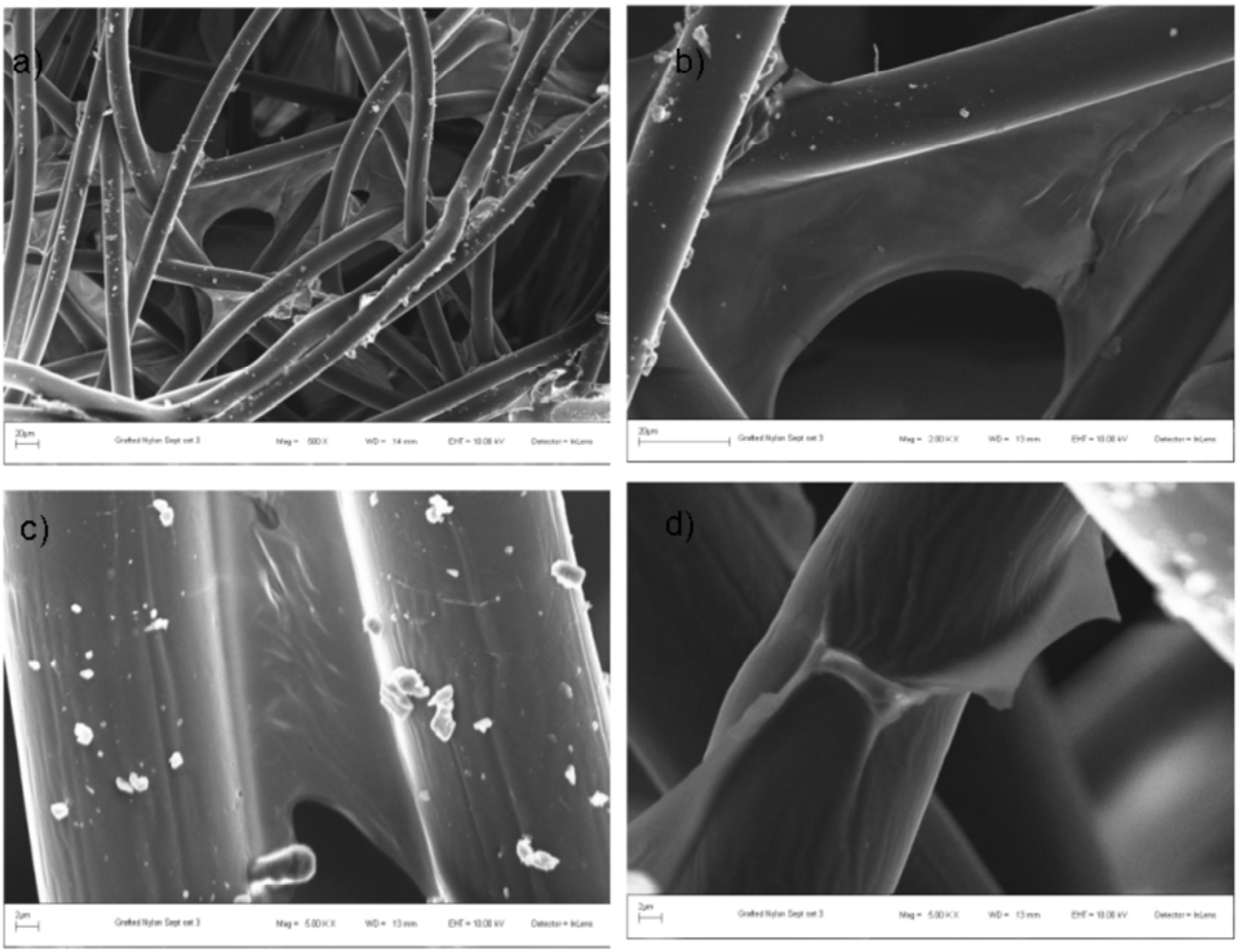

Figure 5.28: SEM images of nylon-*g*-PNIPAAm NWF scaffolds at (a) 500x; (b) 2000x; and (c-d) 5000x magnification when graft polymerisation was conducted on pure NWF.

A further observation made for the nylon-*g*-PNIPAAm surfaces, is that cracks appeared on the fibre surfaces which indicates fibre damage due to the heat treatment during graft polymerisation. For the PET-*g*-PNIPAAm scaffolds (**Figure 5.29-5.30**), ribbon-like structures were observed emanating from some of the fibre surfaces however the occurrence of these structures was very limited, indicating that graft polymerisation was very limited on the PET surface. From the morphological changes it appeared that graft polymerisation was largest for PP, followed by nylon, and then PET.

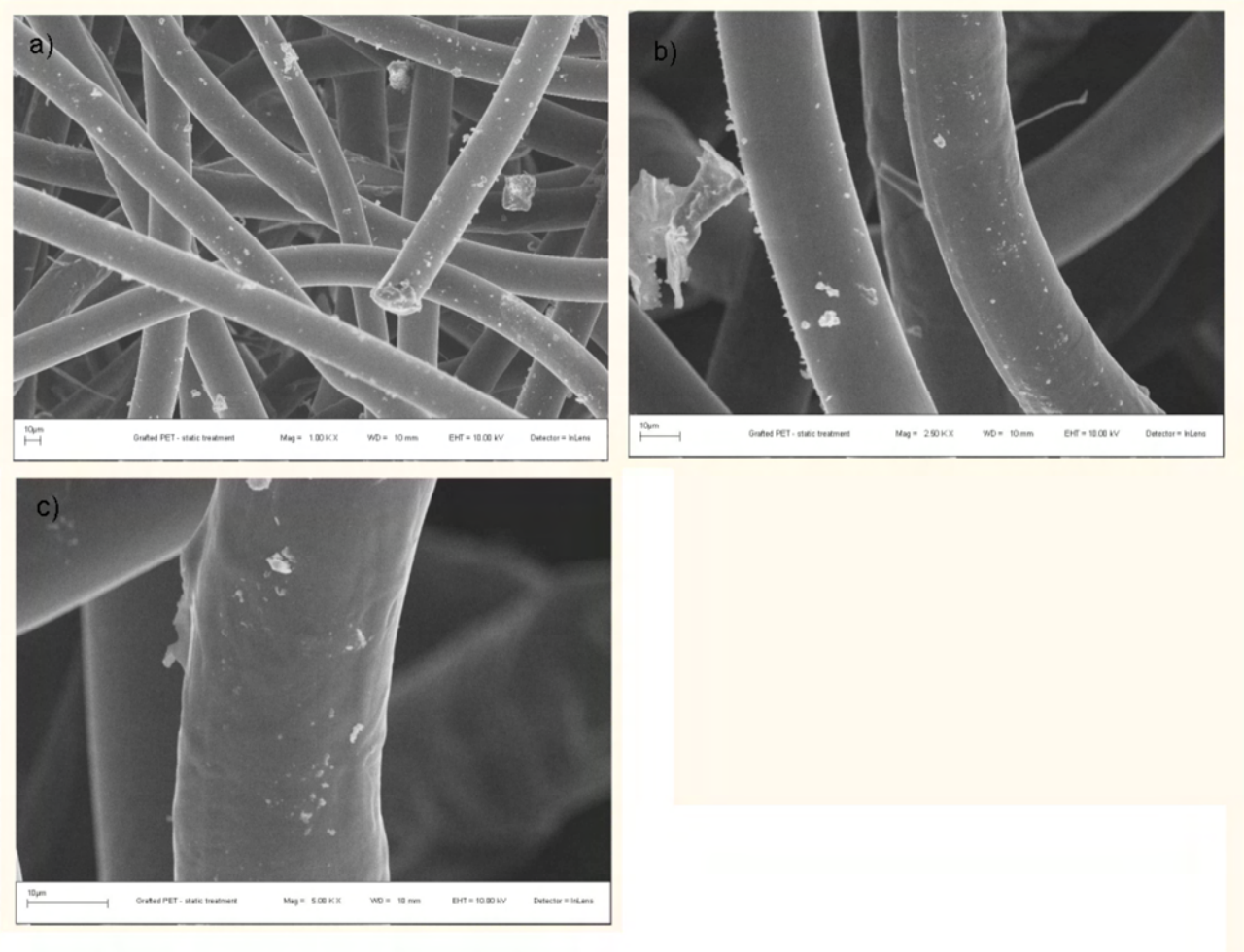

Figure 5.29: SEM images of PET-*g*-PNIPAAm NWF scaffolds at (a) 1000x; (b) 2500x and (c) 5000x magnification when grafting was on oxyfluorinated PET.

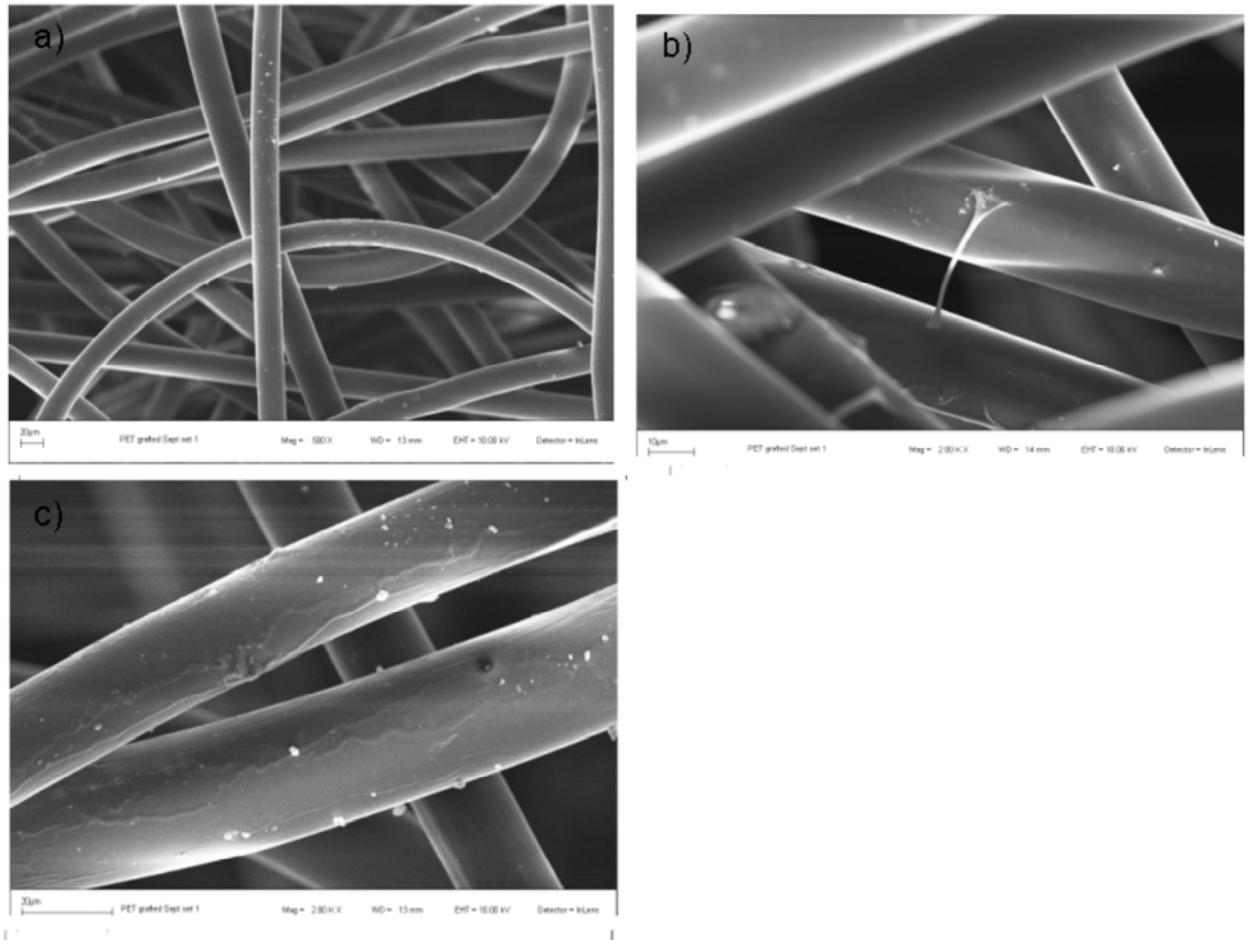

Figure 5.30: SEM images of PET-*g*-PNIPAAm NWF scaffolds at (a) 500x and b-c) 2000x magnification when graft polymerisation was conducted on pure NWF after 1st washing.

The SEM images of PP-*g*-PNIPAAm synthesised by the OAGP but without the chemical initiator appear in **Figures 5.31**. The PNIPAAm layer was reduced compared to when APS was used. Hence this indicates that peroxyradicals from the oxyfluorinated PP as well as the APS contributes to free radical sites on the polymer backbone and the monomer respectively, both of which are required for grafting.

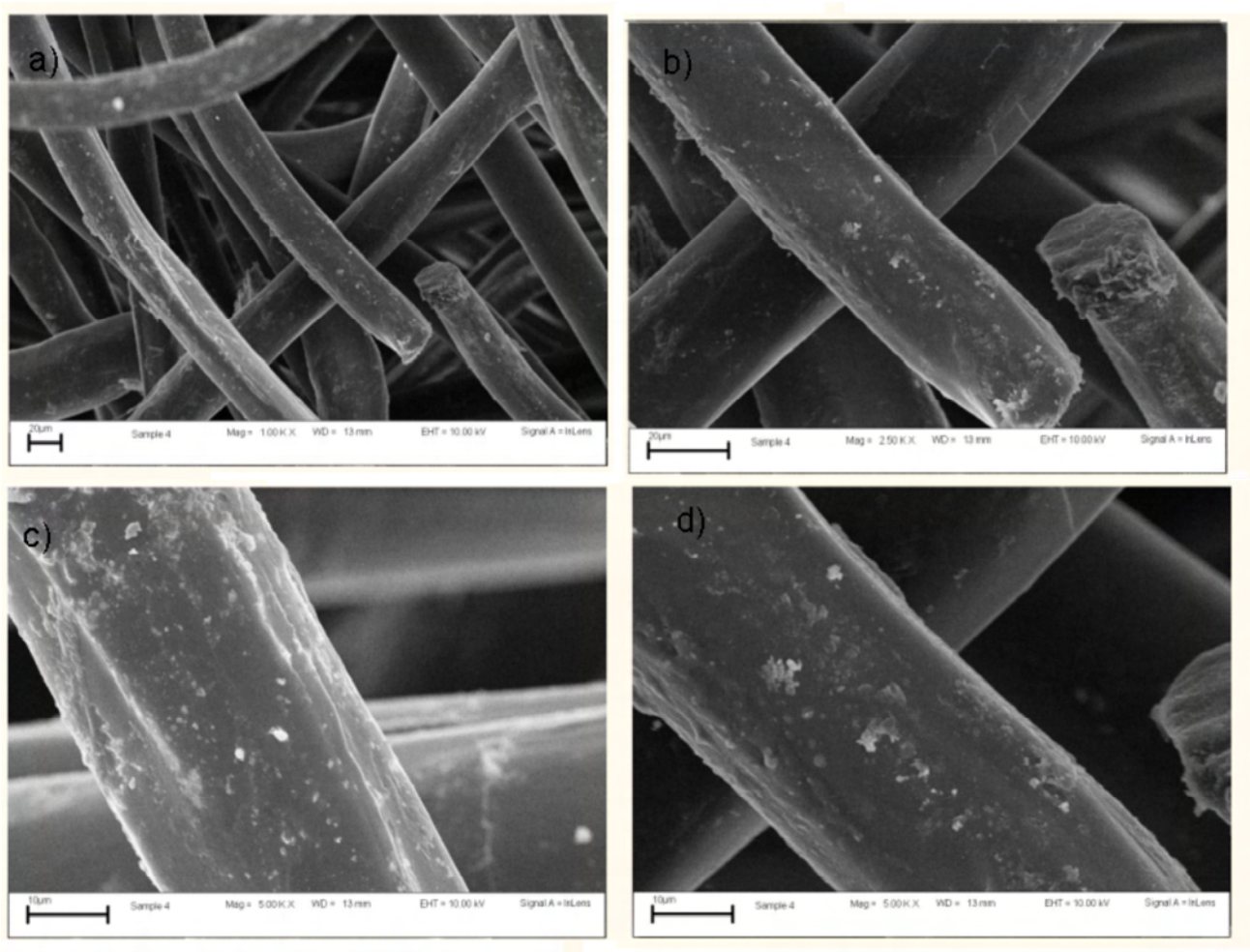

Figure 5.31: SEM images of PP-*g*-PNIPAAm NWF scaffolds at (a) 1000x; (b) 2500x; and (c-d) 5000x magnification when PP NWF scaffolds were pre-treated by oxyfluorination and graft polymerisation is by heat activation only without an initiator.

5.3.5 Water contact angle and swelling of NWF scaffolds in water

It is known that graft polymerisation is highly dependent on the monomer permeability into the polymer bulk, and monomer availability to the graft sites (Anjum et al., 2006). Good wetting would ensure that the monomer and the monomer radicals can easily access the backbone polymer to induce graft polymerisation. Since NIPAAm and PNIPAAm are water soluble, water was preferred as the graft medium over the use of toxic solvents. It has been reported previously that oxyfluorination increases the hydrophilicity, and surface energy of polymers thereby improving wetting (Kharitonov and Kharitonova, 2009). To assess the wettability of the NWF scaffolds in water, water contact angle and swelling studies were performed.

5.3.5.1 Water contact angle studies

Water contact angle studies were performed on pure PP, oxyfluorinated PP and PP-*g*-PNIPAAm NWF scaffolds (**Figure 5.32).** Improved wetting was observed particularly on the PP-*g*-PNIPAAm surfaces compared to the pure or oxyfluorinated PP surfaces. The water contact angles were quantified over an ageing period of 10 seconds (**Figure 5.33**).

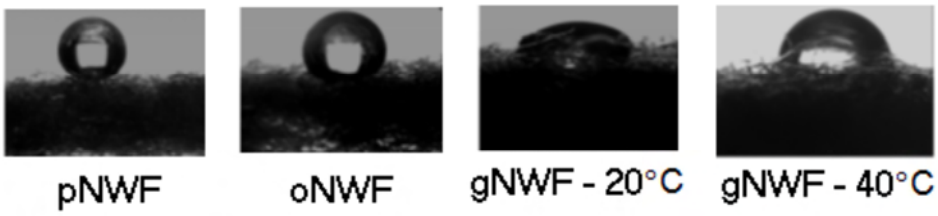

Figure 5.32: Images showing a representative water drop on the surface of pure PP NWF (pNWF), oxyfluorinated NWF (oNWF); PP-*g*-PNIPAAm NWF (gNWF) at 20°C, and gNWF at 40°C. For pNWF and oNWF similar images were obtained at both temperatures. Images were taken a few seconds after the drop contacted the surface.

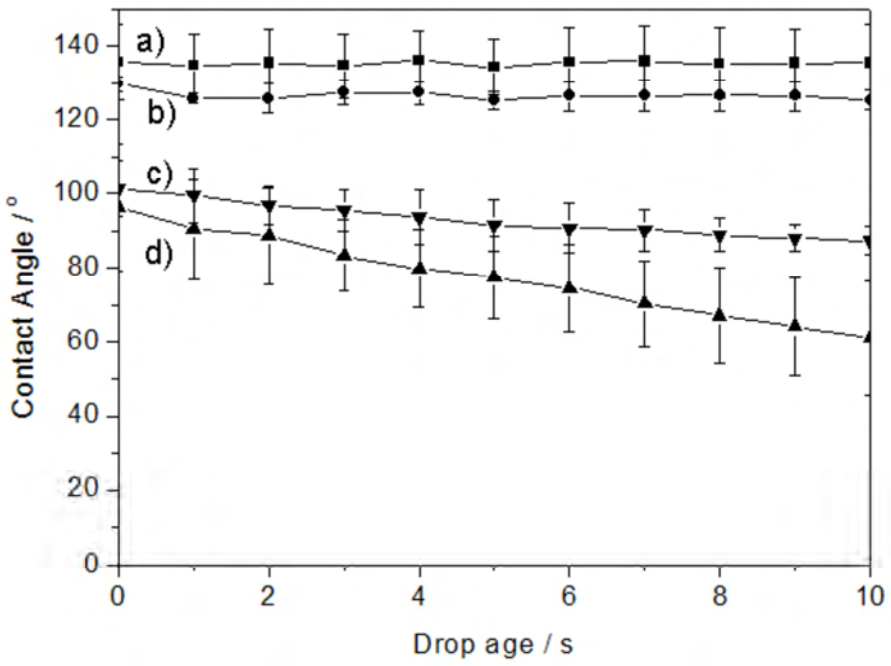

Figure 5.33: Static water contact angle on the surface of (a) pure PP NWF at 20 °C, (b) oxyfluorinated NWF at 20 °C, (c) PP-*g*-PNIPAAm at 40 ℃; and (d) PP- *g*-PNIPAAm at 20 ℃ as a function of the drop age. The average of three drops per time point was taken.

Pure PP NWF as expected displayed an intrinsically hydrophobic surface with a relatively stable water contact angle at ~135 ± 6° at 20℃, while for the oxyfluorinated PP NWF th e contact angle was reduced to ~127 ± 3° at 20 ℃, indicating improved wetting for the l atter. The contact angle for the PP-*g*-PNIPAAm NWF was found to be temperature-dependent showing a relatively hydrophobic surface at 40 ℃ w ith improved hydrophilicity at 20 ℃, confirming the presence of PNIPAAm in the graft layer. For the grafted NWF scaffolds, stable water drops could not be obtained at each time point within the 10 second ageing period (hence the large standard deviations reported here). This was attributed to rapid wetting due to intramolecular hydrogen bond formation between the C=O and N-H groups in the PNIPAAm chain and water molecules (Gu et al, 2012). The contact angles for both the pure and oxyfluorinated PP NWF however was independent of temperature and similar contact angle values were obtained at 20 ℃ and at 40 ℃ (data not shown).

Although the contact angle measurements for oxyfluorinated PP decreased compared to pure PP at 20 ℃, it was also observed that the dif ference in contact angle between the pure PP NWF and the oxyfluorinated PP NWF was relatively small, which was unexpected, and in contrast to other reported studies (Lee et al, 2003). Lee *et al* reports on the oxyfluorination of PP films, and in that study when the F_2: O_2 content varied from 9:1 to 1:9 the contact angle decreased from 103.3 for pure PP film, to 98.7 and 80.8 respectively for the oxyfluorinated PP surfaces at a reaction pressure of 5 kPa (Lee et al, 2003). Although in the present study the oxygen used for the oxyfluorination process was not directly introduced in the reactor as O_2 gas but was due to O_2 present in air, it can be argued that the O_2 content was insufficient to improve surface wetting. However this finding is contradictory to the ATR-FTIR and XPS data reported previously where we have shown a relatively high oxygen content on the surface of the NWF after oxyfluorination i.e. 4.2% (atomic) for pure PP compared to 18.2% (atomic) for oxyfluorinated PP.

It has been reported that morphology of surfaces can also influence contact angle. It has been reported that porous surfaces are non-ideal for contact angle measurements using the Young equation due to the heterogeneity, roughness, capillary forces within pores, contraction of the polymer in the dry state, and restructuring of the surfaces (Kou et al., 2003). While it is acknowledged that the NWF scaffolds used in the present study is non-ideal for contact angle measurements using the DSA due to the highly porous structures, and hence comparisons with other reported studies cannot be directly made, this method is still valuable in providing a quantitative tool for accessing the wetting and comparing data between the different NWF samples under investigation.

A possible explanation for the relatively high contact angle on the oxyfluorinated PP surface in comparison to pure PP may be due to a physical surface rearrangement process. Hruska *et al* have reported that the contact angle and surface energy of oxyfluorinated PP increases significantly with storage time due to re-orientation of the new polar functional groups away from the polymer surface into the polymer bulk in order to minimise the interfacial free energy at the surface (Hruska and Lepot, 2000). Since freshly oxyfluorinated NWF was unavailable during the contact angle studies, aged oxyfluorinated NWF which had been stored for several months were used, hence surface restructuring could have been possible. Also it should be noted that contact angle provides information about the outermost 5-10 Å of a solid surface whereas for ATR-FTIR for example the depth of analysis is substantially higher.

Thus, although the contact angle of the oxyfluorinated PP surface was only marginally lower than that of pure PP, the oxygen functionality was still present in the oxyfluorinated surface which we have already confirmed by ATR-FTIR and SXPS. To further confirm if the "relatively poor wetting" observed from the contact angle measurements was just a surface phenomenon, swelling studies were conducted in water.

5.3.5.2 Swelling studies

Swelling studies were performed in water for pure and oxyfluorinated PP and PET NWF scaffolds, and the mass of wet samples were recorded to determine the water uptake with time (**Figure 5.34**). It can be seen that pure PP and pure PET displayed very poor swelling in water, while substantial improvements to swelling were observed for the oxyfluorinated samples. Oxyfluorinated PP displayed the highest swelling response and after only 2 hours, more than 60% increase in its dry weight was observed. To further visualise swelling of the scaffolds, optical images were taken of the pure and oxyfluorinated PP NWF scaffolds immediately upon submersion in water (**Figure 5.35**). For the pure PP NWF almost no wetting could be detected, however when oxyfluorinated PP NWF was immersed in water, wetting was instantaneous (**Figure 5.35**). The improved swelling of the oxyfluorinated NWF can be attributed to the presence of new polar functional groups on the oxyfluorinated surfaces which we have previously confirmed.

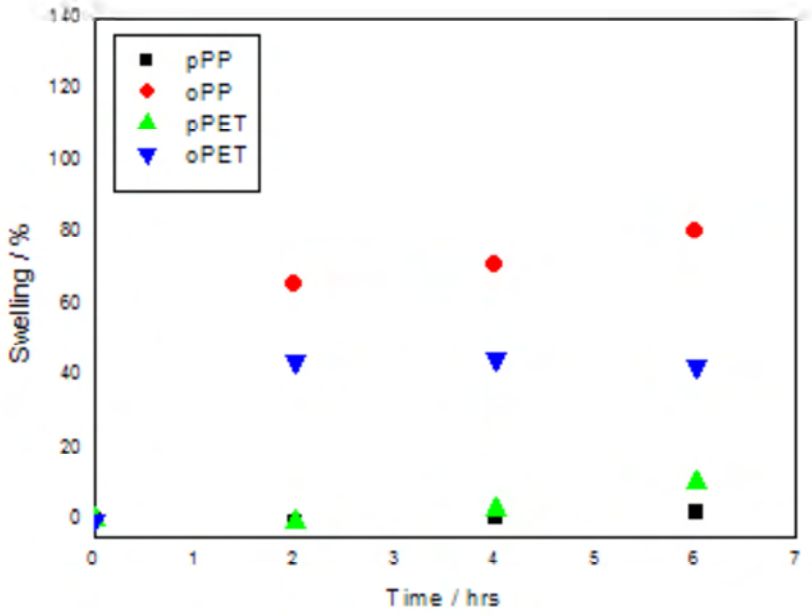

Figure 5.34: Percent swelling based on mass % for pure PP (pPP); oxyfluorinated PP (oPP), pure PET (pPET), and oxyfluorinated PET (oPET).

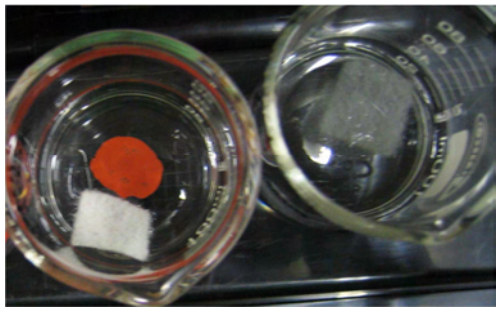

Figure 5.35: Visual observation of wettability of (a) pure PP NWF (indicated by red dot); and b) oxyfluorinated PP NWF in water (right). Images were taken immediately after immersion in water.

5.3.6 Determination of peroxides on NWF

In this study the DPPH – UV-VIS method and ESR was used to detect peroxy radicals on the oxyfluorinated PP NWF scaffolds.

5.3.6.1 DPPH radical-scavenger method

It is well-known that DPPH is a free-radical scavenger which can be used to react with other free radical species in solution (Fargere et al., 1995; Ionita, 2005; Jeong et al., 2011). DPPH exists as a stable free radical in solution because it delocalises its unpaired electron over the whole molecule. Three types of DPPH free radicals are possible as shown in **Figure 5.36**.

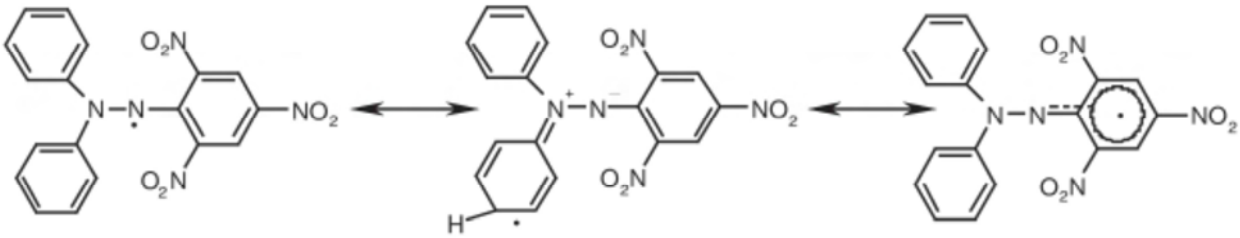

Figure 5.36: Scheme showing electron delocalisation in DPPH (Ionita, 2005).

DPPH is intensely violet in colour and it is known as a good hydrogen abstractor forming DPPH-H which has an orange-yellow colour (Ionita, 2005). The reduction of DPPH to DPPH-H can be easily monitored both visually and also by UV-VIS spectroscopy due to a high λ-shift in the visible spectra from 520 nm (for DPPH) to 330 nm (for DPPH-H) (Ionita, 2005). DPPH has been shown to react with a number of species including hydrogen peroxide, hydroxyl radical, and superoxide anion radical species. Reaction of DPPH with peroxides leads to chain scission as shown below (Fargere et al., 1994):

$$R - O - O - R + 2X \rightarrow 2R - OX \qquad \text{(Eq. 5.15)}$$

Where R-O-O-R and X refers to the peroxide and DPPH respectively.

According to Ionita *et al*, reaction of DPPH with oxygen species (such as hydrogen peroxide, tert-butyl peroxide, tert-butyl hydroperoxide, sodium peroxide, hydroxyl radical etc.) yield DPPH-H as the main product and not an oxy-derivative of DPPH. Jeong *et al* have reported the use of DPPH for detection of hydroperoxide species on oxyfluorinated LDPE films by monitoring the absorbance at 520 nm (Jeong et al., 2011).

In this study, both oxyfluorinated and pure PP were incubated in DPPH solution for 7 hrs at 70 ℃ and colour was detected visually (**Figure 5.36**) as well as using UV-VIS absorbance. However when compared to the oxyfluorinated PP NWF samples, a clear colour difference of the DPPH solution could be seen. The blank DPPH solution, and the sample containing

the pure NWF, displayed a violet colour as expected, however for the sample containing the oxyfluorinated PP the solution turned light pink as can be seen in **Figure 5.36**.

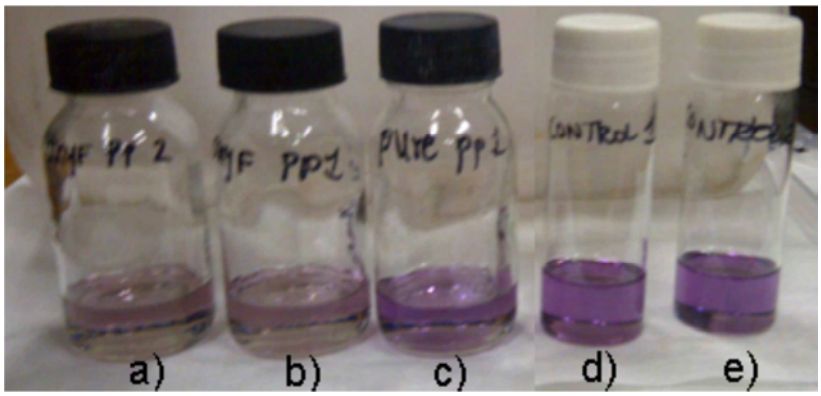

Figure 5.37: Colour observation after reaction with DPPH at 70 ℃ for 7 hours for (a-b) oxyfluorinated PP NWF; (c) pure PP NWF; and (d-e) DPPH blank.

The UV-VIS absorbance spectrum for each solution measured at 520 nm appears in **Figure 5.37**. For the oxyfluorinated NWF sample, a reduction in the 520 nm peak was observed, as compared to the blank and pure PP control.

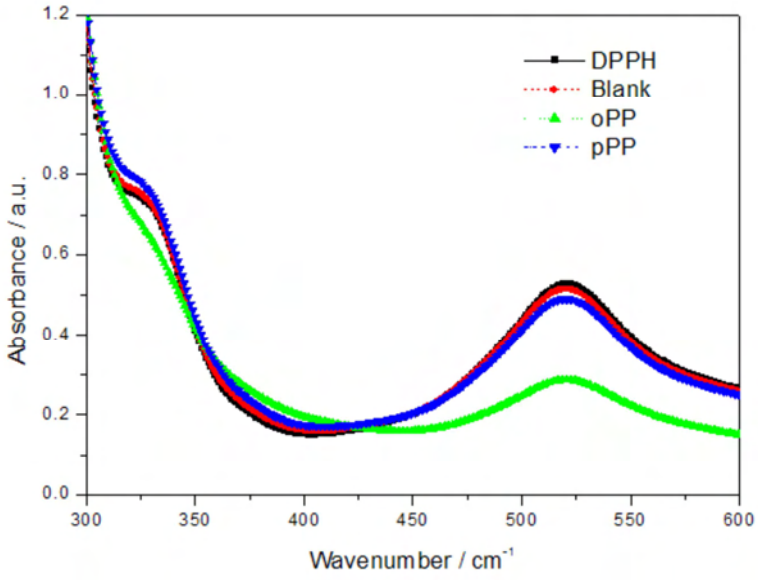

Figure 5.38: UV-VIS absorbance of DPPH solution at 520 nm prior to treatment (DPPH), and the DPPH blank (Blank), oxyfluorinated PP (oPP), and pure PP (pPP) which were all treated at 70℃ for 7 hours.

To determine the amount of hydroperoxides present on the scaffold surface, a calibration graph was determined using DPPH concentrations from 1-10 ppm (**Figure 5.39**).

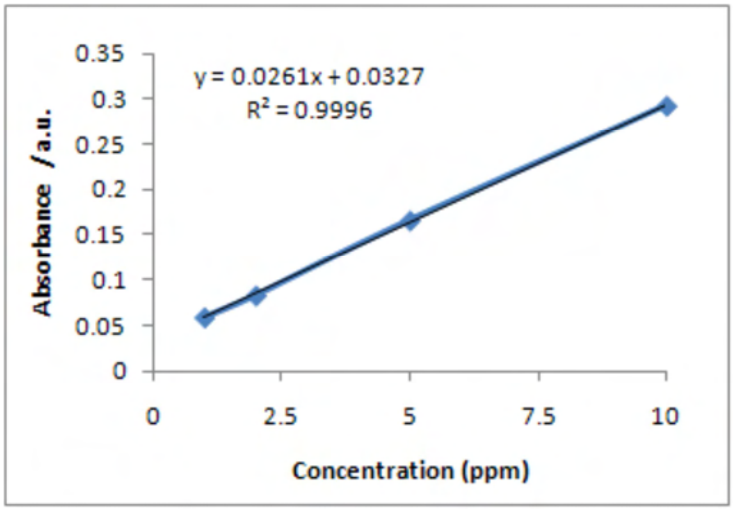

Figure 5.39: Calibration graph relating absorbance and DPPH concentration.

From **Figure 5.39**, the DPPH present in solution after reaction with the oxyfluorinated PP NWF was determined by: x = (y – 0.037) /0.0261, where x is the DPPH concentration (ppm), and y is the absorbance. The moles hydroperoxide per surface area of NWF was then calculated using **Equation 5.15** given previously and the results appear in **Table 5.11,** and are also shown graphically in **Figure 5.40.**

Table 5.11: Moles peroxides on oxyfluorinated NWF (oPP) using DPPH method. Controls included pure NWF (pPP), and a blank DPPH sample containing no NWF.

Sample	A_{520nm}	C_{DPPH} (solution)/ppm	$(Co\text{-}C)_{DPPH}$ (consumed) /ppm	Moles DPPH consumed/Mol	Moles peroxides/ Mol	Moles peroxides per surface area/ Mol/cm^2
oPP	0.286	9.7	8.72	2.21×10^{-7}	1.11×10^{-7}	4.34×10^{-9}
oPP	0.286	9.7	8.72	2.21×10^{-7}	1.11×10^{-7}	4.34×10^{-9}
pPP	0.490	17.5	0.90	2.28×10^{-8}	1.14×10^{-8}	4.49×10^{-10}
Blank	0.513	18.4	-	-	-	-
Blank	0.514	18.4	-	-	-	-

Interestingly for pure PP NWF a slight decrease in absorbance was observed compared to the blank. This perhaps may be due to some active oxygen species entrapped in the PP surface as a result of oxidation due to ageing of PP. From XPS, we also observed a small oxygen content on the pure PP. Alternatively the decrease in DPPH, could be due to

adsorption of some DPPH molecules onto the PP surface. However the moles of peroxide on the oxyfluorinated PP surface increased by a factor compared to the pure PP which can be attributed to the oxyfluorination treatment. The amount of hydroperoxides present on the oxyfluorinated PP is relatively low compared to other studies (Jeong et al., 2011). The yield of hydroperoxides can be improved by varying the O_2 content during oxyfluorination.

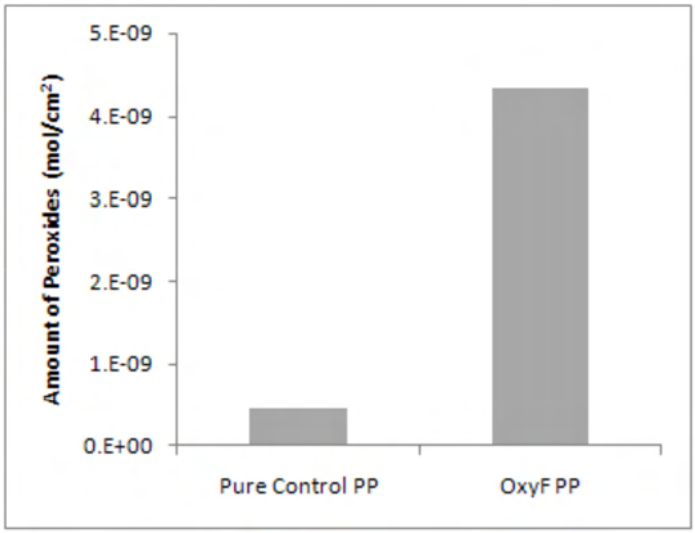

Figure 5.40: Comparison of peroxides or free radicals on pure PP and oxyfluorinated PP.

5.3.6.2 ESR

ESR was also used to detect peroxy radicals on the PP oxyfluorinated NWF. The ESR analysis was performed by Prof László Korecz at the Chemical Research Centre of the Hungarian Academy of Sciences in Hungary. ESR studies were conducted at room temperature and at 70°C. The ESR spectra for the oxyfluorinated PP NWF at room temperature appear in **Figure 5.41.** A weak asymmetric singlet absorption peak was detected for the oxyfluorinated NWF, indicating the presence of long-lived free radicals in the polymer structure. To interpret the ESR spectrum, the experimental results were compared to a simulated spectrum. Excellent agreement with the experimental data was obtained in case of g factor $g_{\perp}$=2.0022 and $g_{||}$=2.0054 where $g_{\perp}$ and $g_{||}$ refers to the electrons perpendicular and parallel to the magnetic field respectively. This indicates anisotropy, i.e. the g factor differs for all orientations of the free electron in the magnetic field. The g-factor refers to the intrinsic magnetic moment of the electron, and the g-factor for a free electron is

2.0023 (Bovet, 2009). The $g_{\perp}$ and $g_{||}$ values observed for the oxyfluorinated PP correspond to mid chain peroxyradicals (Schlick and Mcgarvey, 1983).

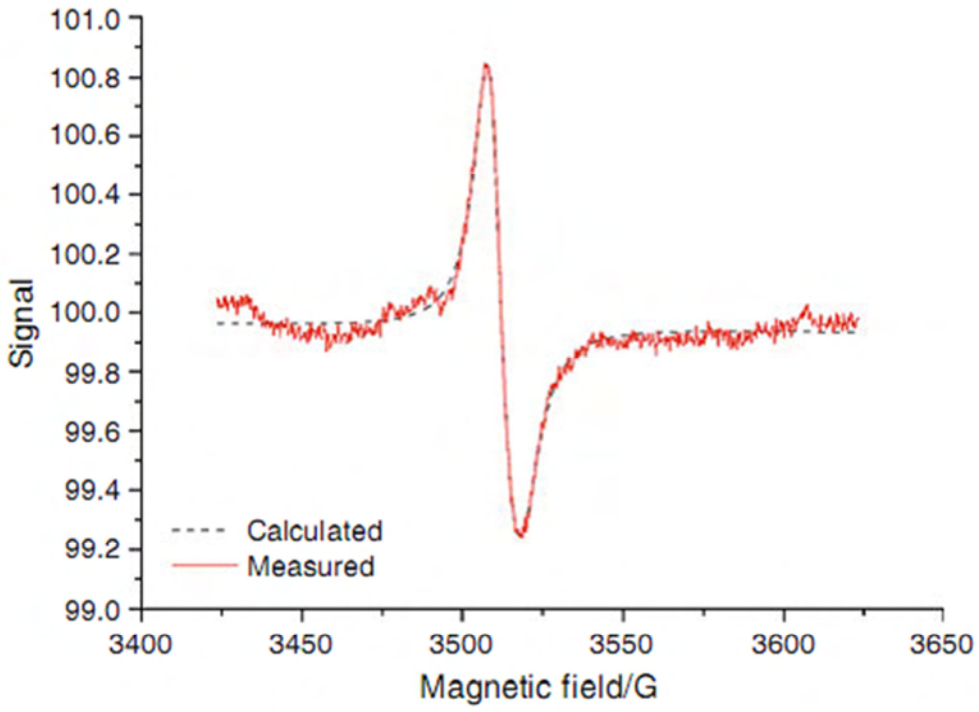

Figure 5.41: Experimental (measured) and simulated (calculated) ESR spectra of PP oxyfluorinated NWF at ambient temperature.

In polymers treated with fluorine–oxygen mixtures, a controlled amount of long-lived peroxyradicals are generated (Kharitonov et al., 2005). The radicals formed in fluorinated polymers are long-lived ones; their amount is decreased by a factor 2 in several hours at room temperature from 1 to 15 hrs depending on the polymer nature (Kharitonov et al., 2005). Although the oxyfluorinated NWF scaffolds were tested several weeks after the oxyfluorination process, long-lived radicals could still be detected on the surfaces of the NWF scaffolds as mid chain peroxyradicals. It has been reported previously that peroxy radicals are more stable in the crystalline phase of polymers (Kharitonov et al., 2005). This may indicate that the radicals were entrapped in the crystalline structure of the NWF scaffolds during the oxyfluorination process, and slowly diffuse to the surface with time. Long-lived peroxyradicals will be very useful for inducing graft polymerisation for attachment of PNIPAAm on to the NWF scaffolds.

Further measurements were carried out at 70°C, to follow the change in radical concentration with time at the temperature of grafting (**Figure 5.42**).

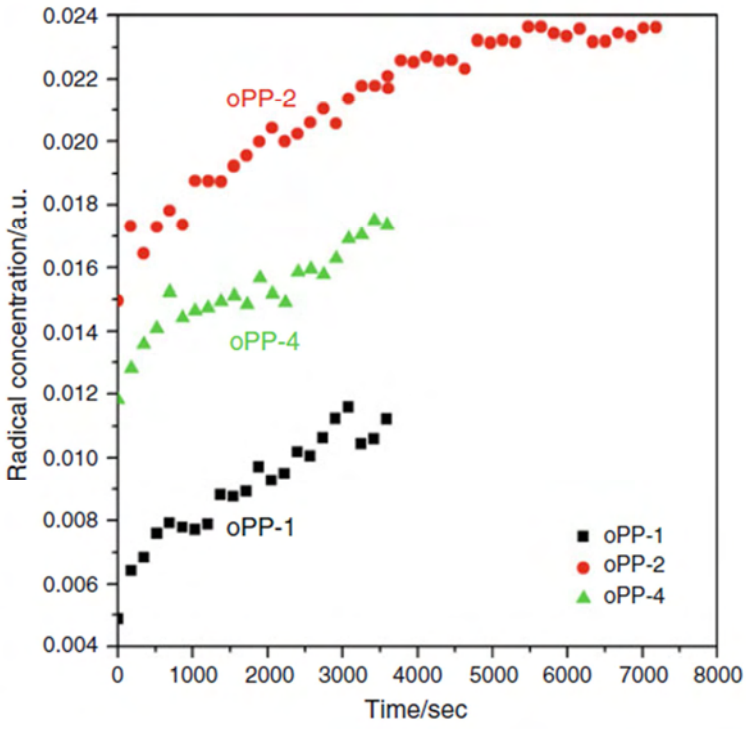

Figure 5.42: Typical change in radical concentration with time at 70°C for the oxyfluorinated PP NWF scaffolds.

Three oxyfluorinated PP NWF samples were analysed (i.e. oPP-2, oPP-3, and oPP-4). The concentration scale was not calibrated, although the samples were normalised to 1 mg, so that they could be compared. The absolute radical concentrations were found to be very small, and the background noise was rather high. However sample oPP-2 was the easiest to measure the time dependence of radical concentration at 70 °C. It can be seen that the radical concentration on the oxyfluorinated PP, at first increased, and after some time the concentration of the radicals remained constant. This result indicates that peroxide groups may be present on the oxyfluorinated PP surface, which upon heat activation at 70°C, leads to the formation of peroxy radicals, the concentration of which increases with time, until maximum peroxy radicals are formed.

5.3.7 Proposed mechanism for OAGP

In this study OAGP was used to graft PNIPAAm onto NWF scaffolds as shown in **Scheme 5.1**. It is known that graft polymerisation is highly dependent on the monomer permeability into the polymer bulk, and monomer availability to the graft sites (Anjum et al, 2005). This was enabled by ensuring that the fluorinated scaffolds were highly swollen prior to grafting to

ensure diffusion of the monomer molecules into the amorphous regions of the PP. NWF scaffolds were swollen in the APS initiator solution such that the initiator molecules were localised on the fibres to aid in graft polymerisation. An advantage of the OAGP method used here is that graft polymerisation was carried out in an aqueous medium under mild conditions.

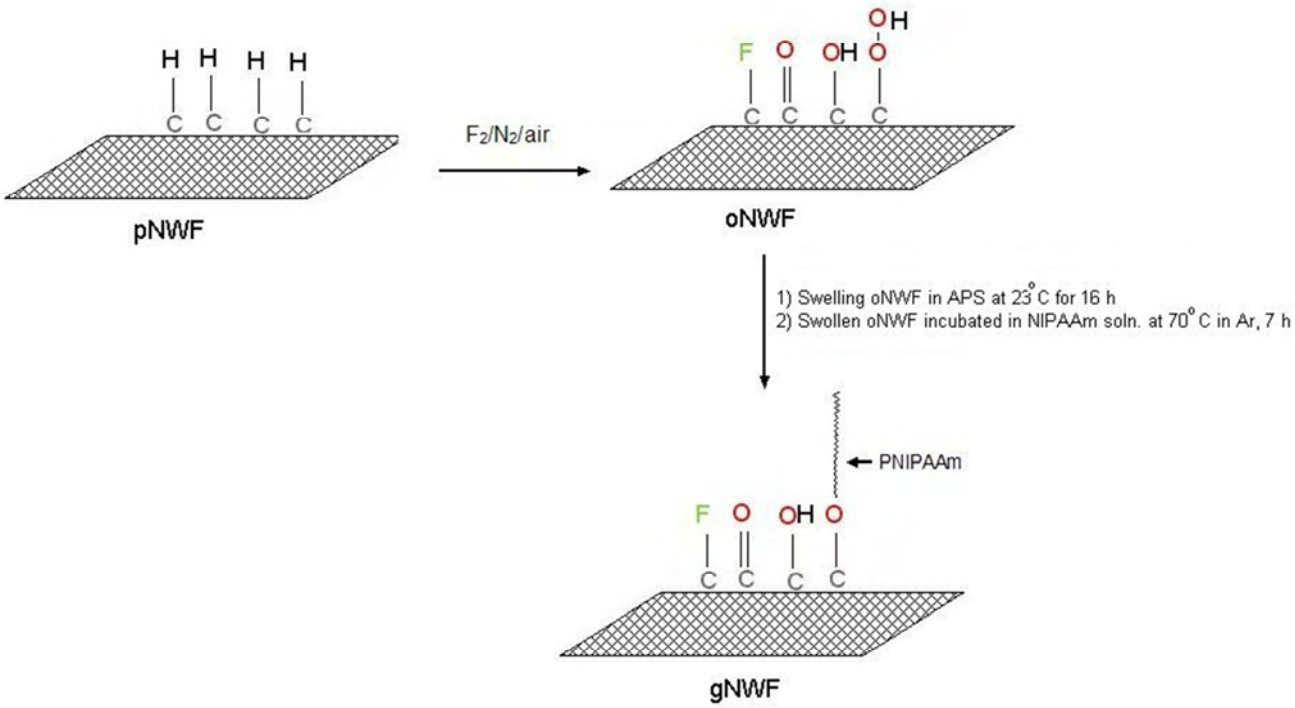

Scheme 5.1: Schematic representation showing OAGP of PNIPAAm on to NWF scaffolds.

The OAGP method of the present study proceeds via a free-radical mechanism which is diffusion driven (Woo et al., 2005). The reaction mechanism for the OAGP method is shown in **Scheme 5.2.**

$F_2 + RH \rightarrow R^{\cdot} + HF + F^{\cdot}$ ΔG=+4.1 kcal/mol

$R^{\cdot} + F^{\cdot} \rightarrow RF$ ΔG=-34 kcal/mol

$R^{\cdot} + F_2 \rightarrow RF + F^{\cdot}$ ΔG=-68 kcal/mol

$R^{\cdot} + O_2 \rightarrow R-O-O^{\cdot}$

$R-O-O^{\cdot} + H_2O \rightarrow R-O-OH$

$-C(=O)F + H_2O \rightarrow -COOH + HF$

Scheme 5.2: Reaction mechanism for fluorination of NWF scaffolds (Woo et al, 2005).

During fluorination, F_2 gas reacts exothermically with the surface of the polymer to form free radicals (du Toit and Sanderson, 1999). Fluorine, due to its high electronegativity, partially replaces the hydrogen on the polymer back bone to form alkyl free radicals ($R^{\bullet}$), fluorine free radicals ($F^{\bullet}$), as well as hydrogen fluoride (Woo et al., 2005). The formed alkyl and fluorine free radicals then react to form the fluorocarbon backbone (RF). Initiation via dissociation of molecular fluorine is not possible since homolysis of fluorine is too endothermic (ΔH=157.88 kJ/mol) to proceed at room or relatively low temperatures (Pryor, 1966). Since the bond energies of F_2 (157.88 kJ/mol) and C-H (410 kJ/mol) are relatively low compared with the bonding energy of C-F (456 kJ/mol) and H-F (569 kJ/mol), the formation of C-F and HF is preferred and the reaction is spontaneous (Woo et al., 2005). Also the Gibbs energy for the reactions indicates that the reactions proceed rapidly. Elemental oxygen and fluorine are introduced into the PP molecular chain to partially replace the H atoms. During oxyfluorination, molecular oxygen reacts spontaneously with the alkyl and fluorine radicals and oxygen functional groups are formed (Kharitonov, 2000). It has been reported that by reactions with R•, O_2, and F_2, peroxyradicals (RO_2•), acid fluorides (COF), and carboxylic acid (COOH) form on the oxyfluorinated surface (Jeong et al., 2011; Kharitonov, 2008; Park et al., 2005). According to Tu *et al*, oxidation of PP during oxyfluorination preferably occurs at the pendant methyl group (Tu et al., 1997). Many authors have reported that acid fluoride is hydrolysed to the highly polar carboxylic acid group (du Toit and Sanderson, 1999; Kharitonov et al., 2005; Lee et al., 2003).

The formation of reactive peroxide groups and long-lived trapped peroxy radicals on oxyfluorinated polymer surfaces is well-known (du Toit and Sanderson, 1999; Jeong et al., 2011; Kharitonov, 2000; Kharitonov et al., 2004). Kharitonov *et al* have reported middle (–$CH(OO^{\bullet})$– or –$CF(OO)^{\bullet}$-) and “end” peroxy groups (–$CH_2OO^{\bullet}$ or –$CHFOO^{\bullet}$ or –$CF_2OO^{\bullet}$) on oxyfluorinated LDPE (Kharitonov et al., 2005). It has been reported that the amount of peroxyradicals exceeds the amount of fluororadicals (Tressaud et al., 2007). Since the reactivity of peroxyradicals is much slower than alkyl radicals, peroxyradicals can exist as long-loved radicals (Woo et al., 2005). Using the DPPH UV-VIS method and electron-spin resonance we have detected peroxy radicals on the oxyfluorinated PP NWF. For graft polymerisation of PNIPAAm onto the oxyfluorinated NWF scaffolds, there exists two sources of initiators i.e. the peroxide groups on the oxyfluorinated NWF scaffolds as well as from the chemical initiator APS (**Scheme 5.3**).

Radical formation:

$$ROOH \xrightarrow{\Delta} RO^{\cdot} + OH^{\cdot}$$

$$S_2O_8^{2-} \xrightarrow{\Delta} 2SO_4^{-\cdot}$$

$$SO_4^{-\cdot} + H_2O \rightarrow HSO_4^{-} + OH^{\cdot}$$

Initiation of monomer:

$$SO_4^{-\cdot} + M \rightarrow M^{\cdot}$$

$$OH^{\cdot} + M \rightarrow M^{\cdot}$$

$$RO^{\cdot} + M \rightarrow R - OM^{\cdot}$$

Propagation:

$$M^{\cdot} \xrightarrow{nM} (M)_nM^{\cdot}$$

$$R - OM^{\cdot} \xrightarrow{nM} R - O(M)_nM^{\cdot}$$

Termination:

$(M)_nM^{\cdot} + M^{\cdot}(M)_n \rightarrow (M)_x$ (PNIPAAm homopolymer) [I]

$R - OM^{\cdot} + M^{\cdot}(M)_n \rightarrow R - O(M)_x$ (Grafted PNIPAAm) [II]

$R - O(M)_nM^{\cdot} + M^{\cdot}(M)_n OR \rightarrow R - O(M)_x - O - R$ (Grafted PNIPAAm) [III]

Scheme 5.3: Possible mechanism for graft polymerisation during synthesis of PNIPAAm grafted NWF scaffolds.

At elevated temperatures, the peroxide on the polymer backbone can be homolytically cleaved due to the low bond dissociation energy of the O-O bond to form alkoxy radicals ($RO^{\bullet}$) on the NWF surface which serve as active sites for grafting (Kildal et al, 2007). Conversely the APS initiator, which is also a peroxide, undergoes thermal decomposition to form sulphate radical ions ($SO_4^{\bullet-}$) and hydroxyl radicals ($OH^{\bullet}$), which are capable of initiating polymerisation by adding to the unsaturated double bond of the NIPAAm monomer (Riggs and Rodriguez, 1967). The alkoxy radicals ($RO^{\bullet}$) on the NWF is also capable of forming a free radical on the NIPAAm monomer. Propagation then pursues and a number of growing radicals are possible. Termination of the growing radicals involves formation of the PNIPAAm homopolymer as well as PNIPAAm graft chains which proceed via coupling of the growing NIPAAm chains [I] and the polymer radical and the propagating NIPAAm chains [II-III] respectively.

The method of graft polymerisation employed in the present study can be described as a combination “grafting from” the NWF surface as well as “grafting to” the NWF surface. For the former, oxyfluorination was used to form peroxide radicals on the NWF which then

enabled attachment of a propogating NIPAAm radical chain, leading to grafting and polymerisation of PNIPAAm from the PP surface (Grafted PNIPAAm [III]). However when APS was used as the initiator, PNIPAAm homopolymerisation occurred and it is possible that the growing PNIPAAm chain can terminate by reaction with the alkoxy radical on the PP surface, implying that “grafting to” the PP surface will also occur (Grafted PNIPAAm [II]). We have also shown that graft yeilds are significantly higher when APS is used, implying that a combination of both graft methods contribute to improving the graft efficiency.

5.3.8 XRD

The XRD patterns for pure PP NWF, oxyfluorinated PP NWF, and PP-*g*-PNIPAAm NWF appear in **Figure 5.43**. The diffractogram patterns for all the pure and modified PP NWF were similar displaying three relatively strong bands and three less-intense bands at 2θ between 13-28° indicating a semi-crystalline materi al, while PNIPAAm displayed 2 broad peaks indicating an amorphous material.

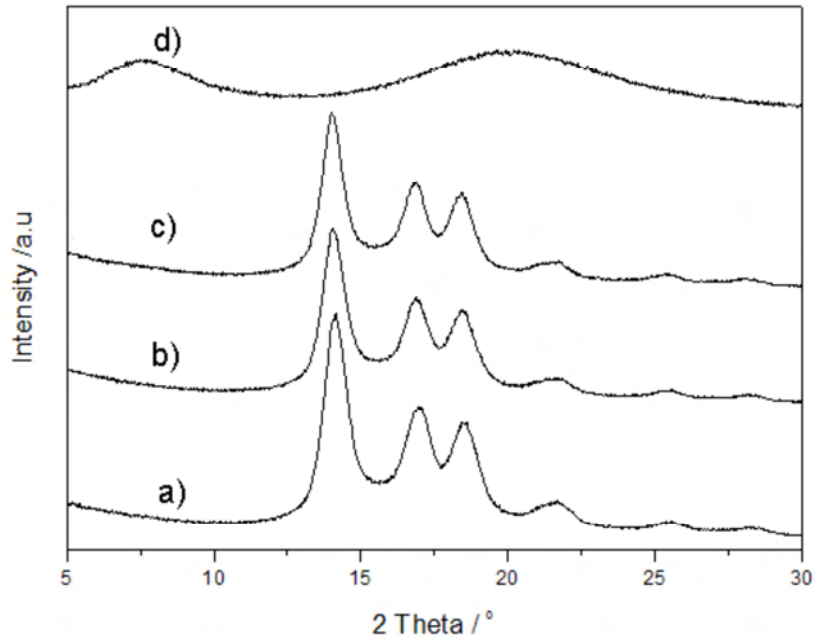

Figure 5.43: XRD diffractograms of (a) pure PP NWF; (b) oxyfluorinated PP NWF; (c) PP-*g*-PNIPAAm NWF; and (d) PNIPAAm (control).

To determine which isomer of PP was present, a matching was done using the X’Pert Prodatabase, and it was confirmed that the PP was isotactic. It is known in literature that isotactic PP can have three different polymorphs i.e. α, β, γ forms which corresponds to the monoclinic, trigonal, and orthorhombic crystal systems respectively, and can be identified by

characteristic reflections (Krache et al., 2007). The monoclinic α form is the most common and stable modification of isotactic PP. The trigonal β form is a metastable phase, the formation of which can be promoted by using specific nucleating agents while the orthorhombic γ form is favoured when there are stereo and / or region defects present in the structure interrupting the isotactic segments (Krache et al., 2007).

The XRD patterns for the pure PP NWF; oxyfluorinated PP NWF; and PP-*g*-PNIPAAm NWF in all cases matched to monoclinic α-form of polypropylene (a = 6.65Å; b = 20.8Å; c = 6.5Å) (a,b,c represents the lattice parameters). The results indicate that after OAGP treatment the crystal structure of PP was not affected, i.e. the arrangement of the atoms in the crystal lattice remained in the monoclinic form despite the introduction of randomly spaced functional groups.

5.3.9 DSC

The DSC thermograms for crystallisation and melting of the PP NWF appear in **Figures 5.44 - 5.45** respectively, and the results are summarised in **Table 5.12**. Two melting cycles were performed in this study, since 1st melting eliminates the material's thermal history, and 2nd melting after crystallisation is more accurate due to sample purity and thermal transitions are free from artefacts. During crystallisation, a sharp symmetric crystallisation peak was observed for the pure PP NWF at Tc_{max} of 111.6 ℃ indicating a relatively pure semi-crystalline material, however for the oxyfluorinated PP and PP-*g*-PNIPAAm, the crystallisation peaks appeared somewhat broader, and was shifted to a higher temperature (Tc_{max} 117.66 ℃ and 115.08 ℃ respectively). During melti ng, pure PP NWF displayed a single melting peak at 160.42 ℃ indicating one sta ble crystalline form in PP, while strikingly for the oxyfluorinated and grafted PP, twin melting peaks were observed at T_{m1}:147.24 ℃ & T_{m2}:161.66 ℃ and T_{m1}:148.63 ℃ & T_{m2}:165.22 ℃ respectively. Peak multiplication behaviour has been observed previously for isotactic PP (Horváth et al., 2010; Huda et al., 1985). Peak multiplication may be due to a number of different factors such as changes in the crystalline structure or crystal phases; crystal defects and irregularities; crystals of different sizes whereby the smaller and imperfect crystals will melt at lower temperatures compared to the perfect crystals; or re-crystallisation phenomena whereby during the slow melting process some of the melted crystals recrystallise (Horváth et al., 2010).

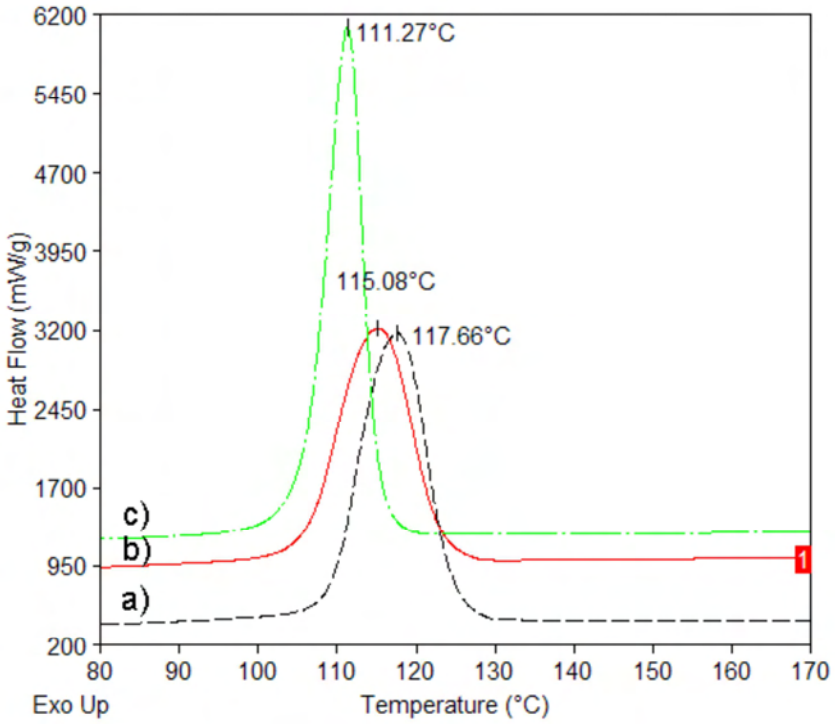

Figure 5.44: DSC thermograms showing 1st cooling for (a) oxfluorinated PP NWF; (b) PP-*g*-PNIPAAm NWF; and (c) pure PP NWF (Exothermic is up).

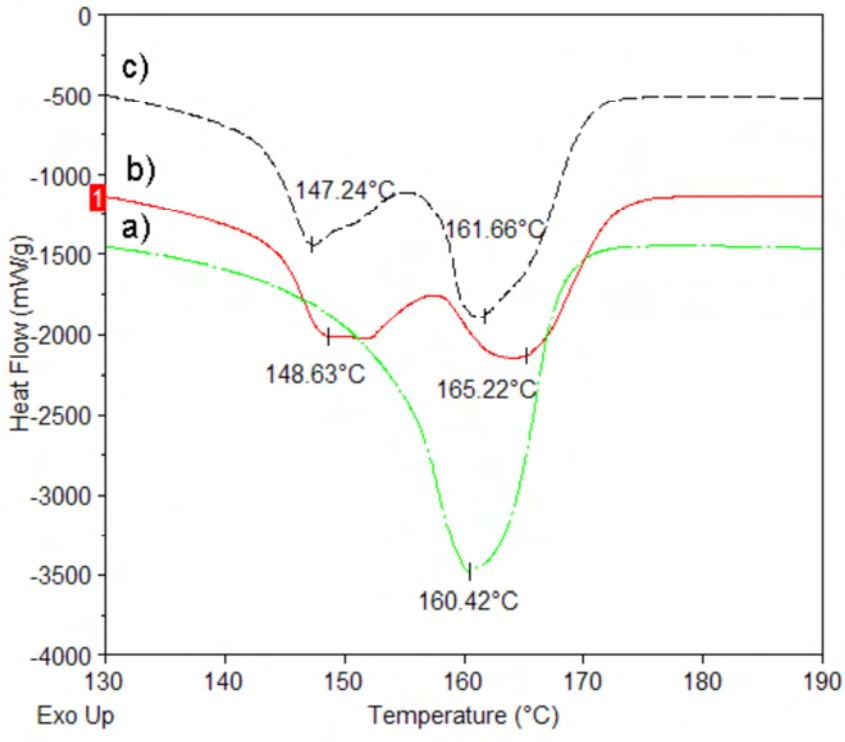

Figure 5.45: DSC thermograms showing 2nd heating for (a) pure PP NWF; (b) PP-*g*-PNIPAAm NWF and (c) oxyfluorinated PP NWF (Exothermic is up).

Table 5.12: Crystallisation and melting DSC data for pure and oxyfluorinated PP NWF scaffolds.

NWF	*Crystallisation*		*Melting*					ΔT
	T_{onset}/℃	T_c/℃	T_{onset}/℃	T_{m1}/℃	T_{m2}/℃	ΔH/J.g^{-1}	% crystall-isation	
Pure PP	106.51	111.27	142.38	-	160.42	74.26	50.69	49.15
Oxyfluorinated PP	109.54	117.66	152.71	147.24	161.66	72.92	49.78	44
PP-*g*-PNIPAAm	106.41	115.08	144.17	148.63	165.22	68.39	46.68	50.14

According to XRD (**see Section 5.3.8**) oxyfluorination and grafting did not affect the crystal structure of PP, i.e. even after the modification only the monoclinic α-form of isotactic polypropylene was present. It can be assumed that even though the crystal phases in oxyfluorinated and grafted PP are the same, it is possible that crystal defects may exist in the modified PP due to the presence of the new functional groups which lower the stereo regularity of the PP chains causing irregular packing and thereby creating defects in the crystal lattice structure. This would result in a combination of impure irregular crystals (due to the functional groups) which are less stable and which would melt first, and pure well-ordered crystals (due to the pure PP repeat units-which may have not been modified) which melt at a higher temperature. Additionally crystals of two sizes may be present due to the modification, which would melt at different rates.

The higher melting peak temperature (T_m) for the oxyfluorinated NWF and grafted NWF scaffolds compared to the pure NWF indicate improved structural stability for the modified NWF scaffolds (Horváth et al., 2010). This may be attributed to enhanced inter-/intramolecular forces in the modified polymers due to hydrogen bonding between adjacent positively charged hydrogen atoms and the electronegative atoms in the oxyfluorinated scaffolds (such as F and O), and between the N-H and C=O groups in the grafted NWF scaffolds. The improved inter-/intramolecular forces within the structure, may result in a more stable material with a higher T_m and T_c compared to pure untreated PP.

Crystallinity

The degree of crystallisation based on the heat of fusion was calculated from the enthalpy of melting as shown in **Table 5.13**. From the heat of fusion calculations it was determined that the degree of crystallinity of pure PP was 50.69% indicating a semi-crystalline material. After oxyfluorination and graft polymerisation, the crystallisation percent of the NWF decreased slightly to 49.78% and 46.68% respectively. Since the method used to determine crystallinity based on heat of fusion calculation from peak areas is only an approximate calculation, the difference observed here is negligible. It can be concluded that the degree of crystallinity of pure PP is unaffected by the OAGP method. This means that during oxyfluorination and grafting, new functional groups attack the amorphous domains in PP, with negligible modification to the crystalline regions.

Undercoolability

Another interesting observation which was made was that for all of the PP NWF scaffolds the Tc appeared at a lower temperature than T_m for both cycles. This may be due to the supercooling / undercooling effect, i.e. lowering of the liquid melt below the freezing point without the material solidifying. Undercooling is required to overcome the surface Gibbs energy barrier for the formation of the crystal phase (Horváth et al., 2010). The undercooling may be represented by ΔT, and it is the difference between the peak maximum for the melting and cooling.

According to Horváth et al., the lower the undercoolability the higher is the inclination for crystallisation. Oxyfluorinated PP NWF scaffolds displayed lower ΔT values compared to pure and grafted PP indicating a higher ability to crystallise for the functionalised polymers which could be due to the functional groups increasing the chain mobility (due to electrostatic attraction) which allows the molecules to more quickly rearrange into a crystalline structure compared to pure PP.

Determination of the LCST

To identify the LCST of PNIPAAm, DSC was also conducted on wet PP-*g*-PNIPAAm NWF scaffolds as shown in **Figure 5.46**. A LCST was detected at Tp of 33.4 ℃ which confir med the presence of PNIPAAm in the grafted PP NWF, and also indicated that the OAGP method did not modify the LCST of PNIPAAm.

\

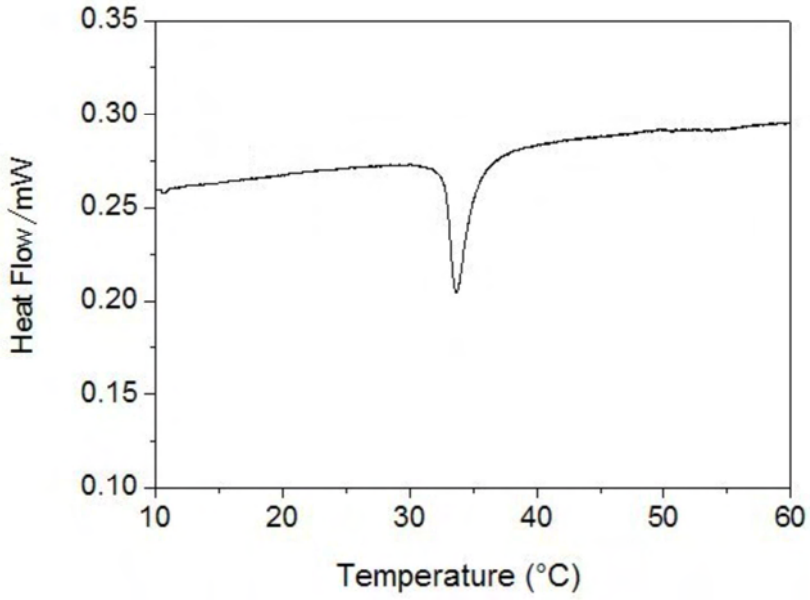

Figure 5.46: Heating DSC thermogram of PP-*g*-PNIPAAm NWF showing a LCST at ~33.4 ℃ using wet samples.

5.4 Conclusions

We have succeeded in grafting PNIPAAm onto PP, PET, and nylon NWF scaffolds using an OAGP two-step method which first involved fluorination, followed by free radical induced graft polymerisation. PP, PET, and nylon NWF scaffolds were manufactured using the needle-punching technology. PP and PET NWF scaffold displayed mean flow pores which was suitable for cell culturing while the MFP on the nylon NWF scaffold was below the required pore size range due to the lower linear density of the fibres used.

The PP, PET, and nylon were functionalised by direct fluorination and oxyfluorination. New functional groups formed on the surface of the NWF scaffolds included C-OH, C=O, CH_2-CHF and CHF-CHF. PP and nylon displaying the largest modification, while for PET very little changes were observed on the fibre surface. The high surface functionalisation on oxyfluorinated PP was attributed to the tertiary carbon in the polymer backbone. In the case of PET, the low surface modification was attributed to the resonance effect of the aromatic ring. Improved wetting and swelling in water was observed for the oxyfluorinated PP compared to pure PP, which is an important requirement for graft polymerisation in aqueous media. However the new functional groups on oxyfluorinated PP were significantly reduced after hydrolysis post-treatment. Water contact angle values showed reduced hydrophobicity

of the oxyfluorinated PP surface in comparison to pure PP, however the small reduction in contact angle value was attributed to a surface rearrangement process.

PNIPAAm on the grafted NWF surface was confirmed using a variety of techniques including ATR-FTIR, XPS, contact angle, and SEM. Additionally the LCST of PNIPAAm was preserved in PP-*g*-PNIPAAm NWF scaffolds. Oxyfluorinated PP NWF showed the highest graft yield when grafting was with the chemical initiator APS. Using the DPPH UV-VIS method and ESR, we have identified peroxide groups and trapped long-lived peroxy radicals on the surface of the oxyfluorinated PP NWF, which are believed to be involved in graft initiation. On the pure NWF scaffolds, excessive homopolymerisation was observed due to adsorption of the PNIPAAm homopolymer onto the NWF surfaces. The OAGP method did not affect the crystalline phase of bulk PP; however, twin-melting thermal peaks were detected for the oxyfluorinated and grafted PP NWF indicating crystal defects.

A free radical mechanism was proposed for the OAGP method with initiation via $SO_4^{\bullet -}$, $OH^{\bullet}$ and $RO^{\bullet}$ radicals. An advantage of this method is that no organic solvents, or toxic chemcials are used, and graft polymerisation is carried out in an aqueous medium under mild conditions. This method presents an attractive alternative to other more expensive graft polymerisation technologies such as gamma radiation, plasma-radiation etc.

5.5 References

Akiyama Y, Kushida A, Yamato M, Kikuchi A, Okano T. 2007. Surface characteristics of poly(*N*-isopropylacrylamide) grafted tissue culture polystyrene by electron-beam irradiation using atomic force microscopy and X-ray photoelectron spectroscopy. Journal of Nanoscience and Nanotechnology 7:796-802.

Anjum N, Moreau O, Riquet AM. 2006. Surface designing of polypropylene by critical monitoring of the grafting conditions. Journal of Applied Polymer Science 100:546–553.

Boguslavsky L. 2008. Needle-punched nonwovens from PP fibres for Scaffolds Application (Trial 4). unpublished report. 9 p.

Boguslavsky L. High efficiency particulate air (HEPA) filters from polyester and polypropylene-nonwovens. FILTREX; 2010; Cologne, Germany.1-15.

Boguslavsky L, Anandjiwala R. 2007. Needle-punched non-woven for scaffolds applications - 2nd trial. unpublished report. 1-12.

Boguslavsky L, Tsheloane C, Whitebooi H, Anandjiwala R. 2008. Needle-punched non-wovens for scaffold applications from nylon 6.6 (3rd Trial). unpublished. 1-9.

Bovet C, Barron AR. 2009. EPR Spectroscopy: An overview, http://cnx.org/content/m22370/latest/, Date accessed: 16 August 2012.

Bucio E, Burillo GA, E. , Coqueret X. 2005. Temperature sensitive behaviour of Poly(*N*-isopropylacrylamide) grafted onto electron beam-irradiated poly(propylene). Macromolecular Materials Engineering 290: 745-752.

Chang H, Wang Y. 2011. Cell Responses to Surface and Architecture of Tissue Engineering Scaffolds, Regenerative Medicine and Tissue Engineering - Cells and Biomaterials, Prof. Daniel Eberli (Ed.),ISBN: 978-953-307-663-8, InTech, 27: 570-588.

Clough RL. 2001. High-energy radiation and polymers: A review of commercial processes and emerging applications. Nuclear Instruments and Methods in Physics Research B 185: 8-33.

Contreras-Garcıa A, Burillo G, Aliev R, Bucio E. 2008. Radiation grafting of N,N-dimethylacrylamide and N-isopropylacrylamide onto polypropylene films by two-step method. Radiation Physics and Chemistry 77 936–940.

du Toit FJ, Sanderson RD. 1999. Surface fluorination of polypropylene 1. Characterisation of surface properties. Journal of Fluorine Chemistry 98:107-114.

Fargere T, Abdennadher M, Delmas M, Boutevin B. 1995. Determination of peroxides and hydroperoxides with 2,2-diphenyl-1-picrylhydrazyl (DPPH). Application to ozonized ethylene vinyl acetate copolymers (EVA) European Polymer Journal 31(5):489-497.

Geuskens G, Nedelkos G. 1993. The post-irradiation oxidation of poly(propylene), Radical decay and oxygen absorption. Makromolekulare Chemie 194:3349-3355.

Gu SY, Wang ZM, Li JB, Ren J. 2010. Swichability wettability of thermo-responsive biocompatible nanofibrous films created by electrospinning. Macromolecular Materials and Engineering 295: 32-36.

Horváth Z, Sajó IE, Stoll K, Menyhárd A, Varga J. 2010. The effect of molecular mass on the polymorphism and crystalline structure of isotactic polypropylene. Express Polymer Letters 4(2):101–114.

Hruska Z, Lepot X. 2000. Ageing of the oxyfluorinated polypropylene surface: evolution of the acid-base surface characteristics with time. Journal of Fluorine Chemistry 105:87-93.

Huda MN, Dragaun H, Bauer S, Muschik H, Skalicky P. 1985. A study of the crystallinity index of polypropylene fibres. Colloidal Polymer Science 263(9):730-737.

Ionita P. 2005. Is DPPH stable free radical a good scavenger for oxygen active species? Chemical Papers 59(1):11—16

Jaganathan S, Tafreshi HV, Shim E, Pourdeyhimi B. 2009. A study on compression-induced morphological changes of nonwoven fibrous materials. Colloids and Surfaces A: Physicochemical and Engineering Aspects 337:173-179.

Jeong E, Bae TS, Yun SM, Woo SW, Lee YS. 2011. Surface characteristics of low-density polyethylene films modified by oxyfluorination-assisted graft polymerization. Colloids and Surfaces A: Physicochemical and Engineering Aspects 373:36-41.

Justice BA, Badr NA, Felder RA. 2009. 3D cell culture opens new dimensions in cell-based assays. Drug Discovery Today 14(1/2):102-107.

Kharitonov AP. 2000. Practical applications of the direct fluorination of polymers. Journal of Fluorine Chemistry 103:123-127.

Kharitonov AP. 2008. Direct fluorination of polymers – From fundamental research to industrial application. Progress in Organic Coatings 61:192-204.

Kharitonov AP, Kharitonova LN. 2009. Surface modification of polymers by direct fluorination: A convenient approach to improve commercial properties of polymeric articles. Pure and Applied Chemistry 81(3):451-471.

Kharitonov AP, Moskvin YL, Syrtsova DA, Starov VM, Teplyakov VV. 2004. Direct fluorination of the polyimide matrimid® 5218: The formation kinetics and physicochemical properties of the fluorinated layers. Journal of Applied Polymer Science 92:6–17.

Kharitonov AP, Taege R, Ferrier G, Teplyakov VV, Syrtsova DA, Koops GH. 2005. Direct fluorination—Useful tool to enhance commercial properties of polymer articles. Journal of Fluorine Chemistry, 126:251–263.

Kildal K., Olafsen K, Stori A. 1992. Peroxide-initiated grafting of acrylamide onto polyethylene surfaces. Journal of Applied Polymer Science 44:1893-1898.

Kou RQ, Xu ZK, Deng HT, Liu ZM, Seta P, Xu Y. 2003. Surface modification of microporous polypropylene membranes by plasma-induced graft polymerization of a-Allyl glucoside. Langmuir 19:6869-6875.

Krache R, Benavente R, López-Majada JM, Pereña JM, Cerrada ML, Pèrez E. 2007. Competition between α, β, γ polymorphs in a – β nucleated metallocenic isotactic polypropylene. Macromolecules 40:6871-6878.

Kranz G, Luschen R, Gesang T, Schlett V, Hennemann OD, Stohrer WD. 1994. The effect of fluorination on the surface characteristics and adhesive properties of polyethylene and polypropylene. International Journal of Adhesion and Adhesives 14(4):243-253.

Kumashiro Y, Yamato M, Okano T. 2010. Cell attachment–detachment control on temperature-responsive thin surfaces for novel tissue engineering. Annals of Biomedical Engineering 38(6):1977–1988.

László K, Kosik K, Geissler E. 2004. High-sensitivity isothermal and scanning microcalorimetry in PNIPA hydrogels around the volume phase transition. Macromolecules 37:10067-10072.

Lee BK, Lee YS, Chong YB, Choi JB, Rho JR. 2003. Hydrophilic modification of polypropylene film by oxyfluorination. Journal of Industrial and Engineering Chemistry 9(4):426-432.

Liu M, Fengling B, Fenling S. 2005. FTIR study on molecular structure of poly(*N*-isopropylacrylamide) in mixed solvent of methanol and water. European Polymer Journal 41:283–291.

Louw IdV, Carstens PAB. 2006. Oxyfluorination. US patent PCT/IB03/04701.

Mark JE. 1999. Polymer data handbook: Oxford University Press. pg 1012.

Okano T, Yamada N, Okuhara M, Sakai H, Sakurai Y. 1995. Mechanism of cell detachment from temperature-modulated, hydrophilic-hydrophobic polymer surfaces. Biomaterials 16:297-303.

Park SJ, Song SY, Shin JS, J.M. R. 2005 Effect of surface oxyfluorination on the dyeability of polyethylene film. Journal of Colloid Interface Science 283:190–195.

Pryor WA. 1966. Introduction to free radical chemistry. Prentice-hall foundations of modern organic chemistry series. London: Prentice-Hall Inc. p 61.

Riggs IP, Rodriguez F. 1967. Persulfate-initiated polymerisation of acrylamide. Journal of Polymer Science Part A-1: Polymer Chemistry 5:3151-3165.

Schild H. 1992. Poly(*N*-isopropylacrylamide): Experiment, theory, and application. Progress in Polymer Science 17:163-249.

Schlick S, Mcgarvey BR. 1983. Motion of midchain peroxy-radicals in poly(tetrafluoroethylene). Journal of Physical Chemistry 87(2):352-352.

Singha K, Maity S, Singha M, Paul P, Gon DP. 2012. Effects of fiber diameter distribution of non-woven fabrics on its properties. International Journal of Textile Science 1(1): 7-14.

Skoog DA, West DM, Holler FJ. 1996. Fundamentals of analytical chemistry: Saunders College Publishing.

Socrates G. 2001. Infrared and raman characteristic group frequencies: tables and charts: John Wiley & Sons Ltd. 347 p.

Tressaud A, Durand E, Labruge`re C, Kharitonov AP, and Kharitonova LN. 2007. Modification of surface properties of carbon-based and polymeric materials through fluorination routes: From fundamental research to industrial applications. Journal of Fluorine Chemistry 128:378–391.

Tu L, Kruger D, Wagener JB, Carstens PAB. 1997. Wettability of surface oxyfluorinated polypropylene fibres and its effect on interfacial bonding with cementitious matrix. Journal of Adhesion 62:187-211.

Uchimaru A, Kutsuna S, Chandra AK, Sugie M, Sekiya A. 2003. Effect of fluorine substitution on the rate for ester hydrolysis: estimation of the hydrolysis rate of perfluoroalkyl esters. Journal of Molecular Structure (Theochem) 635:83–89.

Wan L-S, Yang Y-F, Tian J, Hu M-X, Xu Z-K. 2009. Construction of comb-like poly(*N*-isopropylacrylamide) layers on microporous polypropylene membrane by surface-initiated atom transfer radical polymerization. Journal of Membrane Science 327:174–181.

Wang X, McCord MG. 2007. Grafting of poly(N-isopropylacrylamide) onto nylon and polystyrene surfaces by atmospheric plasma treatment followed with free radical graft copolymerization. Journal of Applied Polymer Science 104:3614-3621.

Woo SW, Song MY, Rho JS, Lee YS. 2005. The effect of oxyfluorination on the surface characteristics of low-density polyethylene films. Journal of Industrial and Engineering Chemistry 11(1):55-61.

Yamato M, Akiyama Y, Kobayashi J, Yang J, Kikuchi A, Okano T. 2007. Temperature-responsive cell culture surfaces for regenerative medicine with cell sheet engineering. Progress in Polymer Science 32:1123–1133